Wind Stress Analysis Over the Western Equatorial Pacific and North Atlantic Oceans Based on ECMWF Operational Wind Products 1985-1989

Le Ngoc Ly
Institute for Naval Oceanography

John C. Kindle
and
J. Dana Thompson
Naval Research Laboratory

Wesley J. Youtsey
Sverdrup Technology, Inc.
Stennis Space Center, MS 39529

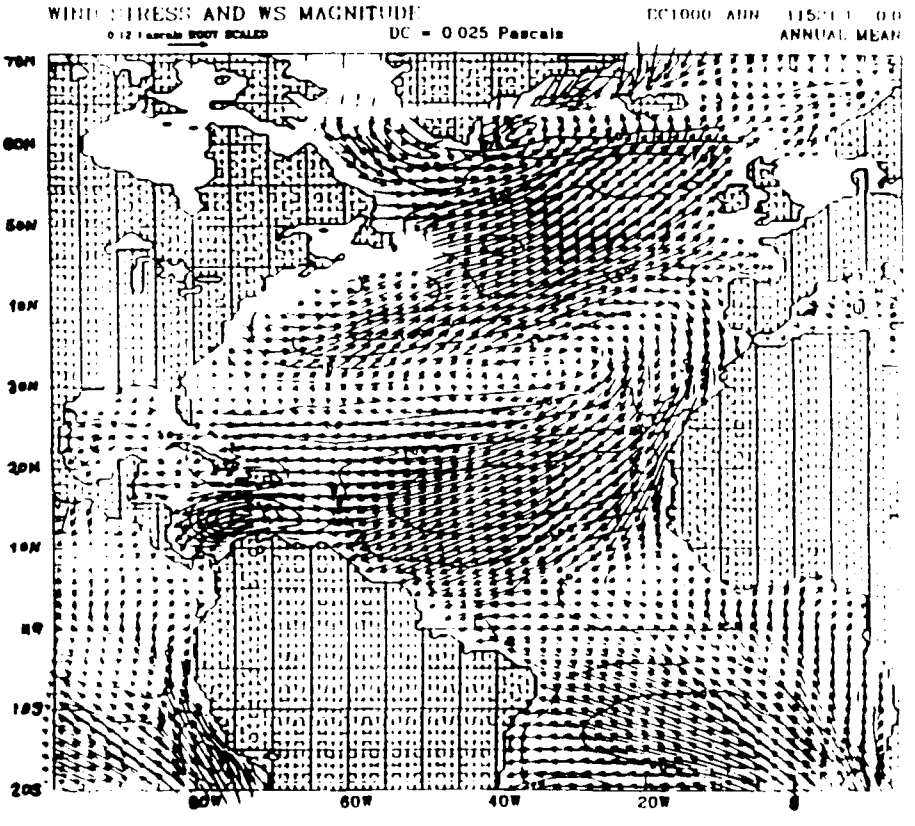

Approved for public release; distribution is unlimited.
Institute for Naval Oceanography,
Stennis Space Center, MS

The Institute for Naval Oceanography is operated by the University Corporation for Atmospheric Research (UCAR) under sponsorship of the Naval Research Laboratory (NRL). Any opinions, findings and conclusions or recommendations expressed in this publication are those of the author(s) and do not necessarily reflect the views of NRL.

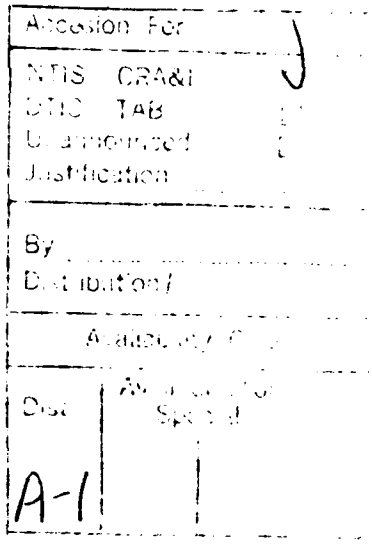

TECHNICAL REPORT

Wind Stress Analysis over the Western Equatorial Pacific and North Atlantic Oceans Based on ECMWF Operational Wind Products 1985-1989

Le Ngoc Ly
Institute for Naval Oceanography

John C. Kindle
and
J. Dana Thompson
Naval Research Laboratory

Wesley J. Youtsey
Sverdrup Technology, Inc.
Stennis Space Center, MS 39529 USA

August 1992

TABLE OF CONTENTS

Acknowledgments

The authors express thanks to Mr. Robert Peloquin of the Navy Ocean Modeling and Prediction Program (NOMP) of the Office of Naval Research (ONR) for his support. The authors would like to express special thanks to Mr. E. Joseph Metzger of the Naval Research Laboratory (NRL, Code 323) for his help in supplying ECMWF winds and sharing his experience in wind stress computations. Special thanks also go to Dr. Harley E. Hurlburt and the NRL (Stennis Space Center, SSC) Ocean Modeling Group for friendly group meeting discussions, encouragement, and interest in the study. One of us (LNL) acknowledges the support of the Institute for Naval Oceanography (INO), funded by the Office of Naval Research (ONR) and managed by the University Corporation for Atmospheric Research (UCAR). We also express thanks to INO computer staff and Mr. Monty Peffley of NRL (Code 323) who helped with computer connections between NRL (SSC) and INO. We also want to thank Ms. Lydia Harper for her help in technical preparation. The comments of three reviewers were helpful. Funding for this study was also provided by the NRL Air-Ocean Coupled Dynamics Project under program element 61153N (sponsored by ONR and NOMP under program elements 62435N and 63207N). The NRL contribution number is CR 021:92.

Abstract

The mean annual and monthly mean wind stress and wind stress curl over the ocean have been computed for 1985-1989 from European Centre for Medium-Range Weather Forecasting (ECMWF) 12-hourly operational 1000 mb, 10 m winds, and direct surface stresses. Both linear and non-linear drag coefficient formulations were employed. The analyses focused on wind stress and curl fields over the Western Equatorial Pacific and the North Atlantic Basin. The wind stress and curl fields of the various ECMWF and Hellerman and Rosenstein wind products are compared.

The study shows that the wind stresses have similar large-scale patterns. There are wind stress curl differences in some particularly important regions for ocean modeling, such as the Gulf Stream separation region, the Caribbean, and the region of maximum northeast and southeast trades. The monthly mean climatological wind stresses in January and July show strong seasonal variability. Over the Gulf Stream separation region all wind stress curls of the various datasets show a region of positive curl with stronger magnitudes in January than July. The comparison also shows that 1000 mb and 10 m nonlinear drag coefficient wind stress magnitudes are the largest and smallest percent of wind stress from ECMWF wind products. The individual wind stress products from ECMWF (i.e., those formed from the 10 m winds, the 1000 mb winds, and the direct surface stresses) were normalized by a global average from 40°N to 40°S. The temporal variability of the normalized products are virtually identical. The Naval Research Laboratory (NRL) global non-eddy resolving model was run to study the sensitivity of the model to ECMWF operational wind forcing. The study shows that the model transports through the Yucatan Straits and between the Pacific and Indian Oceans are not sensitive to small differences in 1000 mb normalized and 10 m wind stresses.

1 Introduction

Atmospheric forcing is an important component of the atmosphere-ocean system. The understanding of the response of the ocean to atmospheric forcing is one of the primary goals in the thermal and dynamical coupling between the atmosphère and ocean. The momentum flux or wind stress is the most important atmospheric forcing for the oceans. The wind stress drives the ocean currents and generates surface gravity waves. Ocean circulation models require the surface wind stress as a surface boundary condition. Climatological wind stress is used to force ocean circulation models to yield an estimate of the mean state of the oceans. Higher space-time resolution of wind forcing is needed for many studies, such as interannual variability, ocean model response to atmospheric forcing, and prediction of future ocean states.

The surface stress is commonly computed by a bulk aerodynamic formula

$$\vec{\tau} = (\tau_x, \tau_y) = \rho\, C_D\, \vec{V}\, |\vec{V}| \qquad (1)$$

where the surface wind vector $\vec{V}$ (accepted as 1000 mb, or 10 m height wind) is assumed to be parallel to the surface stress vector. The surface wind has components u and v and magnitude $|\vec{V}|$. The density of surface air is ρ, and the drag coefficient C_D depends on the height at which the wind is measured and is a function of wind speed and of the near-surface atmospheric stability.

Wind stress fields have been estimated by different investigators using various methods and a wide variety of drag coefficients. It is always difficult to obtain adequate spatial and temporal sampling of the surface winds when estimating reliable wind stress.

Several wind stress climatological estimates have been made based on wind data. Hellerman (1967) used wind rose data to estimate climatological wind stress fields. Bunker (1976) used the individual observations of the Voluntary Observing Ship (VOS) Program to compute monthly mean wind stress distributions for the North Atlantic Ocean for the period 1941-1972. The drag coefficient used by Bunker was dependent on wind speed and atmospheric stability. The Hellerman and Rosenstein (1983, hereafter HR) climatology is popular in the ocean science community, and has become the standard climatological wind stress dataset for ocean modeling. They calculated monthly mean surface wind stresses for 2° x 2° boxes for the world ocean based on the surface marine dataset for the period 1870-1976. HR used the same drag

coefficient as Bunker. Recently, Isemer and Hasse (1987) presented a new air-sea flux climatology for the North Atlantic Ocean. They used Bunker's original dataset with a 21 percent smaller drag coefficient for all wind speed and stability categories (Böning et al., 1991). They also revised the Beaufort equivalent scale for wind estimation and took the influence of humidity on the atmospheric stability into account. More recently, Harrison (1989) calculated a new global climatology based on a similar wind dataset of HR but used the Large and Pond (1982, hereafter LP) drag coefficient. The LP drag coefficient is smaller than Bunker's by about 20 percent (Harrison, 1989).

At present there are several operational centers that produce wind products. For example, ECMWF, the Fleet Numerical Oceanography Center (FNOC), the National Meteorological Center (NMC), and the United Kingdom Meteorological Office (UKMO), among others produce global surface wind and wind stresses. It is important to know how sensitive ocean models are to these different datasets from the various operational centers. It is not well known to what extent the spatial and temporal resolution of the atmospheric forcing affects the ocean model results. The above questions must be taken into account in large-scale atmosphere-ocean coupling.

Operational wind stress is also important in climate change studies. Presently our knowledge of the mean atmospheric climate over the oceans is largely based on VOS data. Unfortunately, data quality and sampling density are not adequate for determining the surface fluxes on a wide range of time scales. If all data observed for the global ocean up to the present time were collected and used to estimate mean surface fluxes, rather accurate climatological mean fluxes might be obtained because of the large amount of data. However, long-term mean values contain relatively little information, and for the purpose of studying climate change, time series of momentum and heat fluxes are needed. Furthermore, even using all available collected data, there are some regions of the globe where there are only a few observations, as in the Southern Hemisphere. An example is given in Figure 1, which shows the January 1977 distribution of VOS data locations over the Pacific.

Trenberth, Olson and Large (1989, here after TOL) have generated a global ocean wind stress climatology based on the 1980-1986 ECMWF 1000 mb, 12-hourly global wind fields from a four-dimensional data assimilation system. This has the advantages of global coverage and regular 12-hour sampling. It has the disadvantage of depending entirely on the accuracy of the data assimilation system in reproducing the true wind fields (Trenberth et al., 1989).

Our report focuses on the surface momentum flux, or surface wind stress, based on the ECMWF operational wind products of 1000 mb, 10 m wind, direct surface stress (1985-1989), and HR wind stress for the Western Equatorial Pacific and North Atlantic Oceans. We are interested in the properties of datasets and the sensitivity of ocean models to the various wind stress products.

2 ECMWF Wind

We have computed five years (1985-1989) of monthly mean and annual mean surface wind stresses and wind stress curls on a 2.5° x 2.5° grid based on ECMWF 12-hour, 1000 mb, and 10 m height wind analyses. These surface stresses will be compared with the direct surface wind stress computed by the ECMWF atmospheric model. The above analyses are World Meteorological Organization (WMO) Global Analysis datasets which do not have sea-surface temperatures and surface fluxes. The ECMWF wind datasets provide much better coverage and temporal sampling than ship observations over much of the world's oceans, especially in the Southern Hemisphere. The ECMWF model uses four-dimensional data assimilation in the surface wind analysis to incorporate all available observed data and information of the numerical weather prediction model. Comparing the ECMWF and NMC analyses, Trenberth and Olson (1988a, b, c) have shown that the ECMWF fields have better and more complete analyses (less missing data). More details on comparisons between ECMWF and NMC analyses can be found in Trenberth and Olson (1988 a, b, c).

Here we used 1000 mb and 10 m height wind to generate surface wind stresses. It is noted that the wind vector in equation (1) must be the surface wind. Ship wind observations are often assumed to be 10 m winds. The 1000 mb and 10 m height winds are generally accepted in oceanography as surface winds, but should not be expected to be equal to those at the surface. There was a major change in the ECMWF analysis on 9 September 1986. Before that date the analysis was on standard pressure levels, and afterward it has been on model sigma levels. It is also noted that in the ECMWF analysis prior to the above date the ship wind observations were effectively assigned to the 1000 mb level, and 1000 mb winds are considered to be the most appropriate ECMWF "surface" wind product. The 10 m height winds were derived from the 30 m winds (lowest model level) assuming a neutral atmospheric stratification until 7 April 1987, and after that by assuming a stability dependent boundary layer with the stratification determined by the model (see Trenberth et al., 1989). There was a major change in the model in September 1986, and so subsequent data was not included in the climatology of Trenberth et al. (1989) and did not include wind data in their climatology.

3 The Drag Coefficient C_D

Although there are some uncertainties associated with flux estimates made using bulk aerodynamic formulae, the bulk parameterizations are commonly used to derive surface air-sea fluxes. There have been many estimates of C_D. Data from a variety of locations have provided estimates of C_D that vary by as much as a factor of three (Geernaert, 1987). Theoretical and observational studies show that the drag coefficient is dependent on wind speed, surface atmospheric stratification (Large and Pond, 1981, 1982), and ocean surface gravity waves (Geernaert, 1987; Ly, 1990). The first two factors are better understood than the third. An example of variations of observed neutral drag coefficients by different investigators can be seen in Figure 2. These differences between C_D are thought to be primarily due to the various sea states under which measurements were taken. Although there are large discrepancies between the curves, most (except curve 1 by Amorocho and De Vries, 1981, and curve 7 by LP, 1981) increase with 10 m height wind for speeds less than 10 ms^{-1}. The C_D values of LP are smaller (except Kondo for wind greater than 17 ms^{-1}) than those in Figure 2 for the winds greater than 7 ms^{-1}. The drag coefficients vary greatly as the wind speed increases above 10 ms^{-1}.

A workshop on atmospheric forcing of ocean circulation (Scoggins and Mooers, 1988) recommended that ocean modelers adopt a particular set of bulk coefficients and continue to use them for years. Harrison (1989) and TOL (1989) chose the LP drag coefficient to generate surface wind stresses. TOL computed a stability dependent C_D. They used the Comprehensive Ocean-Atmosphere Data Set (COADS) to compute climatological mean spatially varied monthly values of air-sea temperature and humidity differences. TOL showed that the LP drag coefficient is sensitive to atmospheric stratification only at wind speeds less than 5 ms^{-1}, but the contribution of these winds to the total stress is small. Taking this into account, both the neutral LP and linear drag coefficients were used to generate surface wind stresses from 1000 mb and 10 m winds. The neutral linear C_D (hereafter LCD) is taken in this study as $C_D = 1.5 \times 10^{-3}$. The LP (1982) neutral drag coefficient (hereafter LPCD) has the following form:

$$
\begin{aligned}
C_{DN} \times 10^3 &= 0.49 + 0.065\,V \quad \text{for } V > 10\ ms^{-1} \\
&= 1.14 \qquad\quad \text{for } 3 \le V \le 10\ ms^{-1} \\
&= 0.62 + 1.56\,V^{-1} \quad \text{for } V \le 3\ ms^{-1}.
\end{aligned} \tag{2}
$$

It is clear that the selection of the drag coefficient is important in surface wind stress calculation.

4 Annual Wind Stress and Wind Stress Curls

4.1 Annual Mean Wind Stress

4.1.1 Western Equatorial Pacific

We are interested in studying the response of the Western Equatorial Pacific (WEP) from 20°S to 20°N and from 120°E to 160°W to operational wind forcing functions. The annual mean wind stress vectors are shown in Figure 3 for 1000 mb, 10 m winds, and direct surface stress. Here we used a linear drag coefficient (C_D = 1.5 x 10^{-3}) for 1000 mb and 10 m winds (Figures 3a and 3b). Figure 3c shows the annual mean wind stress generated from 10 m winds by using the LP drag coefficient. Figure 3d shows the annual mean of the direct surface stress from the atmospheric model. In Figure 3e the HR annual mean wind stress is shown. The main feature of 1000 mb, 10 m, and HR winds is the strong trade winds in the northeastern and southwestern parts of the region. The maxima of wind stresses for 1000 mb and 10 m winds are 1.3 dyn cm^{-2} and 0.93 dyn cm^{-2}, respectively (1 Pa = 1 N m^{-2} = 10 dyn cm^{-2}). The wind stress of 10 m winds using the LP C_D is the smallest value with a maximum of 0.77 dyn cm^{-2}. The HR wind stress in this region has a maximum of 1.3 dyn cm^{-2}. All wind stress maxima of the above datasets are located in the region of maximum northeast trades. These figures show that over most of the area between 10°S to 10°N the LP 10 m wind stress is less than 0.25 dyn cm^{-2}. This is because the LP drag coefficient is smaller than the linear and HR C_D for winds less than 15 ms^{-1} and greater than 1.5 ms^{-1} (see Figure 2). It can be seen from these figures that in this region wind stress patterns generated from 1000 mb, 10 m, and HR winds are generally similar. A comparison of different wind stress magnitudes at the global scale will be given later. The individual components of surface stress generated by both the LCD (Figures 4a, b) and LPCD (Figures 4c, d) for 10 m winds are shown in contour form. The trade winds have strong activity with stronger zonal components over the northern and southwestern (off Australia and New Guinea) regions, with strong horizontal gradients both in the zonal and meridional components. It is clear again that the LP wind stress has smaller magnitudes.

4.1.2 North Atlantic Basin

The North Atlantic Basin (NAB) from 20°S to 70°N and 100°W to 15°E is another region to study the ocean response to operational wind forcing functions. The annual mean wind stress vectors and magnitudes of 1000 mb, 10 m with LCD

and LPCD, direct surface stress, and HR winds for NAB are shown in Figures 5abcde, respectively. The wind stresses were generated from 1000 mb (Figure 5a) and 10 m winds by using LCD (Figure 5b) and LPCD (Figure 5c). Figures 5d and 5e show the annual mean wind stresses and their magnitudes for direct surface wind stress and HR wind stress. The main feature in the NAB is the subtropical anticyclonic circulation in the central part which is related to the subtropical high pressure cell centered near 30°N and 30°W. Another feature that can be clearly seen in Figures 5abcd is the intertropical convergence zone (ITCZ). The 1000 mb wind stress is the strongest with a maximum magnitude of over 2 dyn cm^{-2}. The maxima of wind stresses for 10 m with LCD, LPCD, and HR are 1.4, 1.6, and 1.5 dyn cm^{-2}, respectively. The direct surface wind stress has a maximum of 2.28 dyn cm^{-2}. It is noted that all the maxima of various datasets over the NAB are located over the Caribbean. There are three important latitudes which we will discuss later: ψ = 52°N (maximum westerlies), ψ = 14°N (maximum northeast trades), and ψ = 6-8°N which characterizes the annual cycle associated with the meridional shift of the ITCZ (Böning et al., 1991).

It is interesting to see the zonal and meridional components of annual mean wind stress over the NAB. Figure 6 shows two components of wind stress of 10 m winds with LCD (Figures 6ab) and LPCD (Figures 6cd) and HR wind (Figures 6ef). From these figures the three regions with maximum westerlies, maximum northeast trades, and the ITCZ are clearly apparent. We can see from Figures 6ace that the regions of maximum westerlies have maximum x-components. The regions of maximum northeast trades and the ITCZ are easy to recognize by the negative x-components of wind stress. For the NAB the maxima and minima of the x-components of 10 m and HR wind stresses have similar absolute values. HR wind stress has the largest positive value of the x-component (over 1.5 dyn cm^{-2}) in comparison with the x-component of 10 m wind stresses. In Figures 6bdf where the y-components of 10 m and HR wind stress are shown, a specific region of maximum westerlies with maximum northern y-component wind stress near 52°N can be seen easily. The region of maximum northeast trades (14°N) is recognized as a region with strong y-components.

4.2 Annual Mean Wind Stress Curl

The curl of the wind stress, $\mathrm{curl}_z\vec{\tau}$, is an important forcing component of the vertically integrated mass transport of the mean ocean circulation. The Sverdrup equation which relates surface wind stress and the north-south mass transport over the depth of the ocean can be obtained by taking the integration over the ocean depth with some simplifying assumptions.

$$M_y = \frac{1}{\beta}(\nabla \times \vec{\tau})_z = \frac{1}{\beta}\,\mathrm{curl}_z(\vec{\tau}) \qquad (3)$$

where $My = \int_{-H}^{o} \rho_w \upsilon_w dz$; H is ocean depth; ρ_w is seawater density; υ_w is north-south seawater velocity; and β is the change of the Coriolis parameter with latitude. This equation shows that the basin scale, inviscid mass transport is established only by the horizontal gradients of the surface wind stress, i.e., $\mathrm{curl}_z(\vec{\tau})$.

Figures 7abcde show the annual average wind stress curl fields from 1000 mb (Figure 7a), 10 m with LCD (Figure 7b) and LPCD (Figure 7c), direct surface stress (Figure 7d), and HR winds (Figure 7e) for the WEP. It can be seen from these figures that the curl fields of various datasets are similar. The main features that can be seen from these figures are the large bands of positive curl between 15°N and just south of the equator, and the area of the negative curl in the southern part (between the equator and 20°N) of the WEP. The 1000 mb wind stress curl has largest absolute magnitudes in the WEP with a maximum of 4.2 x 10^{-8} dyn cm^{-3} and a minimum of -4.1 x 10^{-8} dyn cm^{-3}. HR wind stress curl has smallest absolute values in the WEP with a maximum of 1.8 x 10^{-8} dyn cm^{-3} and a minimum of -1.3 x 10^{-8} dyn cm^{-3}.

The annual average wind stress curls over the NAB for 1000 mb, 10 m with LCD and LPCD, direct surface stress, and HR winds are shown in Figures 8abcde. The annual wind stress curls over NAB for different datasets have different values but similar patterns. Substantial spatial curl differences are found in the Gulf Stream Region where it separates from the coast, off Gibraltar, and over the Caribbean Sea. Over the Gulf Stream Separation Region (GSSR) the wind stress curls are positive. The GSSR has a wind stress curl maximum of ~ 1.25 x 10^{-8} dyn cm^{-3} for 1000 mb wind stress (Figure 8a), ~ 1.0 x 10^{-8} dyn cm^{-3} for LCD (Figure 8b) and LPCD (Figure 8c) 10 m wind stress, and ~ 0.75 x 10^{-8} dyn cm^{-3} for HR wind stress. Harrison (1989) indicated that because the separation physics of western boundary currents involves a delicate balance of forcing, inertial, and frictional effects, the differences in wind stress curls over the GSSR may help explain why it has been so difficult to get realistic boundary current separation in ocean circulation model simulations. Over NAB the 1000 mb wind stress curl has the largest spatial change with a maximum of 7.5 x 10^{-8} dyn cm^{-3} and a minimum of -8.3 x 10^{-8} dyn cm^{-3}; HR wind stress curl has the smallest spatial change with a maximum of 3.1 x 10^{-8} dyn cm^{-3} and a minimum of -1.4 x 10^{-8} dyn cm^{-3}. This is primarily due to the strong gradient of $\nabla \times \vec{\tau}$ near

certain coastal regions for the ECMWF products. For curl in the basin interior, the HR dataset is second only to 1000 mb.

5 Climatological Monthly Mean Wind Stress and Curls

5.1 Monthly Mean Wind Stress

5.1.1 Western Equatorial Pacific

Figures 9 and 10 show a five year climatology of 1000 mb, 10 m, direct surface stress, and HR wind stresses over the WEP for January (Figure 9) and July (Figure 10). These wind stresses have similar patterns but different magnitudes. As for the case of the annual mean in Figure 3, the 1000 mb wind stress has the largest magnitude of 2.76 dyn cm^{-2}, and the 10 m wind stress with LP C_D has the smallest magnitude of 1.64 dyn cm^{-2}. Comparing these wind stresses over the WEP for January, the 1000 mb wind stress (9a) is closer to the HR wind stress (9e) than the others, both in magnitude (maximum wind stress of HR is 2.3 dyn cm^{-2}) and in pattern. Both 1000 mb and HR wind stresses have more "noise" than other ECMWF wind products. Figures 9bcd show that the 10 m wind stress with LCD (Figure 9b) and LPCD (Figure 9c) and direct surface stress (Figure 9d) are close to each other both in magnitude and in pattern.

Figures 10abcde show climatological monthly means of wind stress in July over the WEP for 1000 mb (Figure 10a), 10 m with LCD (Figure 10b) and LPCD (Figure 10c), direct surface stress (Figure 10d), and HR winds. As for January, wind stresses of 1000 mb and 10 m winds with LP C_D in July have the largest (2.52 dyn cm^{-2}) and smallest (1.25 dyn cm^{-2}) magnitudes, respectively. Comparing Figures 9 and 10, there is a strong seasonal variation in wind stress between January and July. This can be seen, for example, in Figures 9a and 10a where 1000 mb wind stresses in January and July are shown. In winter (January, Figure 9a) strong northeast trade winds occupied the whole northern part of WEP (from the equator to 20°N), but there is almost no activity of the southeastern trades at this time of the year. However, in July both northeast and southeast trades are strong. The especially strong southeast trades at this time of year are related to the strong monsoon activity in summer. One of the main features of the wind stress over WEP in summer is the strong convergence zone in the northwestern part. In general, winter wind stresses have the largest magnitudes.

5.1.2 North Atlantic Basin

The monthly mean wind stresses of the five year climatology for 1000 mb, 10 m, direct surface stress, and HR winds over the North Atlantic Basin (NAB) for January and July are shown in Figures 11 and 12, respectively. One of the main features over NAB in winter for 1000 mb (Figure 11a), 10 m with LCD (Figure 11b) and LPCD (Figure 11c), direct surface (Figure 11d), and HR (Figure 11e) wind stresses is the strong westerlies at about 50°N. The HR wind stress over NAB has the largest westerly magnitudes of 2.75 dyn cm^{-2}, and has another region with high values at 40°N with magnitudes of 2.25 dyn cm^{-2}. The strong westerlies occur in connection with the strong subpolar cyclonic circulation in the NAB in winter. Figures 11abcde show the region of strong northeast trades at around 14°N. The direct surface wind stress (Figure 11d) has the largest magnitude of 3.44 dyn cm^{-2} over the Caribbean. This is also the largest magnitude for wind stresses of the above datasets over both NAB and WEP in January. Another common feature of these datasets over NAB is the intertropical convergence zone (ITCZ). In winter the ITCZ is shifted south of the equator in comparison with the ITCZ of the annual fields (Figures 5abcde). This results from the seasonality of the northeast trades which are strongest in winter as a result of the winter subtropical anticyclonic circulation. The 1000 mb wind stress has a maximum of 1.25 dyn cm^{-2} (Figure 11a) in the region of the southeast trades.

Wind stress vectors and magnitudes of 1000 mb, 10 m with LCD and LPCD, direct surface stress, and HR winds for July over NAB are presented in Figures 12abcde. These figures reveal the seasonality of the atmospheric circulation primarily in the Northern Hemisphere due to the greatly expanded subtropical high in the northern summer in comparison with winter (Figures 11abcde). Summer wind stress fields, in general, of all datasets over the Northern Hemisphere of NAB are weaker than in winter. The only exception is for July wind stresses over the Caribbean, which are 10 percent greater than those in January for both 1000 mb and 10 m with LCD wind stresses. It is noted that the maxima of wind stresses in this region are also maxima of wind stress fields for all datasets over the whole NAB. The region of maximum northeast trades shifts northward in summer in connection with the subtropical anticyclone shifting northward. In this region the ratios of maximum wind stress values in July to January are ~ 86 percent for 1000 mb, ~ 80 percent for 10 m with LCD, 75 percent for 10 m with LPCD, ~ 60 percent for direct surface stress, and ~ 84 percent for HR winds. In July the maximum westerlies of all datasets are smaller than in winter. The maximum westerlies of 1000 mb wind stresses in July is 50 percent of that in January. Comparing the maximum westerlies in July to those in January, the ratios are ~ 38 percent for LCD 10 m wind stress, ~ 25 percent for 10 m wind

stress with the LPCD, ~ 34 percent for the direct surface stress, and ~ 27 percent for HR wind stress. The reason for the weak westerlies over NAB in summer is the weak summer subpolar cyclonic circulation. Unlike the northern part of NAB, in the southern equatorial region of NAB the southeastern trades dominate and strengthen in July in comparison with those in January. This occurs because the monsoon in summer has a strong influence on the southeast trades. The maxima of southeast trades in July are greater than those in January by ~ 25 percent for 1000 mb, 100 percent for 10 m with LCD, 50 percent for 10 m with LPCD, 50 percent for direct surface stress, and 100 percent for HR.

The zonal and meridional components of 10 m wind stresses with LCD are shown in Figures 13ab for January and Figures 13cd for July. The important regions of maximum westerlies, maximum northeast trades, ITCZ, and maximum southeast trades are clear in these figures for both 10 m wind stress components. The positive zonal component of wind stress in July is ~ 40 percent of that in January, but the negative zonal component is ~ 32 percent greater in July than those in January. The picture is different for the meridional components in January and July. Both positive and negative magnitudes of meridional component have not only similar patterns, but also nearly equal maximum and minimum magnitudes. The maximum and minimum of both months are ~ 1.2 dyn cm^{-2} and ~ -1.6 dyn cm^{-2}, respectively.

5.2 Monthly Mean Wind Stress Curl

Section 4.2 has shown the annual average wind stress curl fields for WEP and NAB. In this section we study the monthly variation of the curl fields of 1000 mb, 10 m with LCD and LPCD, direct surface stress, and HR wind stresses over WEP and NAB for January and July.

5.2.1 Western Equatorial Pacific

It is known that annual variation of curl forces large seasonal changes in parts of the tropics, particularly in the Pacific and Atlantic north equatorial counter currents (Harrison, 1989). Wind stress curl fields of 1000 mb, 10 m with LCD and LPCD, direct surface stress, and HR for January and July are shown in Figures 14abcde and 15abcde, respectively. In general the wind stress curl fields of these datasets over WEP for both January and July are similar in pattern but different in magnitude. The main features for both January and July wind stress curl fields are strong bands of positive curl in the northern part of WEP, and areas of negative curl in the southern part (south of the equator). These curl changes probably are associated with movement of the convergence zones, such as the

South Pacific convergence zone (Harrison, 1989). The big difference in the curl fields of January and July is that the zero curl line shifts far north in July in comparison with January. This zero line in January is between 5°S and 12°S, while in July it is between 3°S and 13°N. It results from strong southeast trades which are associated with the monsoon in July (see Figures 10abcde). Figures 14abcde show that 1000 mb curls have the largest positive magnitude of ~ 8 x 10^{-8} dyn cm^{-3} of all datasets in January, while direct surface stress has the largest negative curl with a minimum of -5.7 x 10^{-8} dyn cm^{-3}. But, as explained in Section 4.2, the large minimum in the direct surface stress curl is presumably due to the strong near coastal gradients. The wind stress curl of the direct surface stress in July (Figure 15d) has largest and smallest magnitudes of 8.2 x 10^{-8} dyn cm^{-3} and -9.0 x 10^{-8} dyn cm^{-3} of all datasets. Next we will study seasonal variations of climatological wind stress curls of the above mentioned datasets over NAB.

5.2.2 North Atlantic Basin

The curl fields of 1000 mb, 10 m with LCD and LPCD, direct surface stress, and HR wind stresses for January and July over NAB are shown in Figures 16abcde and 17abcde, respectively. Wind stress curls of the above datasets for January and July have similar patterns but different magnitudes. The substantial differences in monthly mean wind stress curls, as for the annual average curls (Figures 8abcde), are found in the Gulf Stream Region, off Greenland, off Gibraltar, over the Caribbean, and over the region of maximum northeast trades. In general, both maximum and minimum January curl fields are 10 percent to 20 percent greater than those in July, except that the minimum of the direct surface wind stress in July is 12 percent greater than that in January. Over the GSSR all wind stress curl of different datasets are shown as a region of positive curl with stronger magnitudes in January than in July. The maximum 1000 mb curl is 3.0 x 10^{-8} dyn cm^{-3} in January, but only 1.25 x 10^{-8} dyn cm^{-3} in July. In this region the January maxima are 2.0 x 10^{-8} dyn cm^{-3} for 10 m with LCD wind stress curl; 2.25 x 10^{-8} dyn cm^{-3} for 10 m with LPCD wind stress curl; 1.75 x 10^{8} dyn cm^{-3} for direct surface stress curl; and 1.5 x 10^{-8} dyn cm^{-3} for HR curl. The maxima of these curls for those datasets in July are 1.25 x 10^{-8} dyn cm^{-3}, 1.0 x 10^{-8} dyn cm^{-3}, 0.75 x 10^{-8} dyn cm^{-3}, 0.75 x 10^{-8} dyn cm^{-3}, and 0.75 x 10^{8} dyn cm^{-3}, respectively. It is noted that the positive curl of GSSR is believed to be connected with Gulf Stream separation (Harrison, 1989). The other important region of wind stress curl is the region of maximum northeast trades (around 10°N). The wind stress curl over this region is believed to be connected to transports in the Florida Straits (Schott et al., 1988). The positive curl magnitudes of all datasets in January are almost the same as those in July. It is clear that the zero curl lines in all datasets in this region are shifted northward to

between 5°N and 10°N in July, while these lines are near the equator in January. This may be the result of strong monsoon activity in July.

6 Some Wind Stress Vector Comparisons

The discussion in the previous sections shows that wind stresses of various ECMWF and HR winds have similar patterns but different magnitudes. In this section we will discuss the relative magnitudes of these datasets.

The vector differences of monthly climatological mean wind stresses for January and July over WEP are presented in Figures 18abc and 19abc, respectively. Figure 18a shows the vector subtraction of 10 m with LCD from 1000 mb wind stresses over WEP in January. The maximum difference is 0.85 dyn cm^{-2}. The major difference between these fields is an enhanced magnitude of 1000 mb wind stress in the trade wind regions. In July the differences between the above two datasets are larger with a maximum of over 1.0 dyn cm^{-2} in the southeast trade wind region (Figure 19a). This is because the southeast trades are enhanced in July during the summer monsoon.

The differences in wind stress vectors and magnitudes between 10 m with LCD and the LPCD for January and July are shown in Figures 18b and 19b. Again, this is a large difference in wind stress fields in the northern equatorial trades in January with a maximum of 0.29 dyn cm^{-2}. In July the southern trades are stronger and the difference between 10 m with LCD and the LPCD wind stress values has a maximum of 0.34 dyn cm^{-2} in this region. In both months the LPCD wind stress has larger magnitudes than the LP wind stress. This is because the LCD has larger magnitudes than LP for winds between 3 and 15 ms^{-1} (see Figure 2).

Figures 18c and 19c show the differences of HR wind stress and 10 m LCD wind stress in January and July. The HR wind stress is enhanced strongly in the northwestern region of WEP with a maximum of deference of 0.83 dy cm^{-2} in January. In July HR wind stress is enhanced strongly in the region off Australia with a maximum of 0.76 dy cm^{-2}.

Examples of the differences in HR and 10 m LCD wind stress fields over NAB in January and July are shown in Figures 20a and 20b. The major differences between the fields are a substantially enhanced magnitude of the HR wind stresses in the northwestern region in January with a difference maximum of 1.47 dyn cm^{-2} in January (Figure 20a), and the trade wind region in July with a maximum difference of 0.9 dyn cm^{-2} (Figure 20b). The differences

between these fields is a spatial structure with smaller scale and stronger extrema north of 60°N. This may be regarded as an effect of the different spatial sampling and smoothing procedures in an area of poor data coverage.

7 Global Mean Wind Stress Comparison and Ocean Response

The global monthly mean wind stress magnitudes of various datasets for each year are averaged spatially from 40°N to 40°S. The results are plotted in Figure 21. The 1000 mb wind stress magnitudes are largest for the period of 1985-1989 for the different ECMWF wind products. The 10 m with the LPCD wind stress has the smallest magnitudes for that period. The 1000 mb monthly global mean wind stress also has the largest variations with a wind stress maximum of 0.85 dyn cm^{-2} in August 1985 and a minimum of 0.5 dyn cm^{-2} in March 1989. The 10 m with LCD and LPCD and direct surface stresses vary in magnitude from 0.29 to 0.55 dyn cm^{-2}. It is noted that the direct surface wind stress curve follows closely the 10 m with LCD wind stress for January 1985 to April 1987. The curve changes the trend in April 1987 to follow the 10 m LPCD wind stress curve. It is evident that some changes in the ECMWF atmospheric model occurred at this time. This may be connected with a change in model boundary layer parameterization in April 1987. Before April 1987 the 10 m wind was derived from the 30 m wind assuming a neutral boundary layer, and after that date the stratification was dependent on the boundary layer model stability (Trenberth et al., 1989). It is interesting to note that a major change in the ECMWF model in September 1986, mentioned by Trenberth et al. (1989), did not appear in our results. This may suggest that the boundary layer stratification has more effect on surface winds than changing from standard pressure levels to model sigma levels.

For the purpose of better comparing time series of globally averaged wind stress magnitudes, a normalization procedure is introduced. The normalized factor is obtained by dividing the globally spatially averaged (from 40°S to 40°N) monthly mean 1000 mb wind stress by the globally spatially averaged monthly mean 10 m wind stress. Wind stress calibration values of 1000 mb, 10 m with LCD, and a normalized 1000 mb with the normalizing factor $C_N = 1.06 \times 10^{-3}$ for 1985 to 1989 are shown in Figure 22. The figure shows that the normalized 1000 mb and 10 m wind stresses are almost exactly the same in magnitude. This means that globally 1000 mb ECMWF wind stress is different from the 10 m wind stress only by a constant multiple, but this could be different regionally.

The NRL global non-eddy resolving model was used to study model sensitivity to ECMWF operational wind forcing. This 1.5 layer, global reduced

gravity model has a grid resolution of 0.5 degree. The model domain extends from 72°S to 71°N. The model includes the effects of realistic coastline geometry and thermodynamics based on a relaxation to a mean density climatology based on Levitus (1982).

Examples are shown for model transports at two locations using normalized 1000 mb and 10 m LCD wind stresses as forcing. The wind-driven model transports through the Yucatan Straits (22.0°N, 87.75°W -84.23°W) and between the Pacific and Indian Oceans (114.05°E, 22.0°S -8.5°S) are shown in Figures 23ab and 24ab, respectively. The model transport variations through the Yucatan Straits from 1985-1989 for the 1000 mb normalized and 10 m wind stresses are shown in Figures 23a and 23b, respectively. These figures show that the two transport variations are almost the same. Another example can be seen in Figures 24a and 24b for the same atmospheric forcing except for model transports between the Pacific and Indian Oceans. Again, they are similar. The model transports through the Yucatan Straits and between the Pacific and Indian Oceans are not sensitive to small differences in 1000 mb normalized and 10 m wind stresses.

8 Summary and Remarks

The annual mean and climatological mean surface wind stress and wind stress curl over the ocean for 1985-1989 have been generated from ECMWF 12-hourly operational 1000 mb, 10 m winds, and direct surface stress by using the LCD and LPCD. The analyses are made for various wind stresses over WEP and NAB. The comparisons of wind stress and wind stress curl fields of various ECMWF wind products and HR are made with a focus on WEP and NAB. The main interest of the study of the above mentioned datasets is the sensitivity study of the ocean models to operational atmospheric forcing.

The study of the wind stress fields from various ECMWF and HR winds over WEP and NAB shows that the wind stresses have similar large-scale patterns. There are some wind stress curl differences in some particularly important regions for ocean modeling, such as the Gulf Stream separation region, the Caribbean, and the region of maximum northeast and southeast trades. The annual means of 1000 mb and HR wind stresses have the largest maxima of 1.3 dyn cm^{-2} over the WEP. The 10 m with LPCD wind stress is the smallest with a maximum of 0.77 dyn cm^{-2} over WEP. All the wind stress maxima of the above datasets are located in the region of maximum northeast trades. Over NAB the 1000 mb wind stress is the largest with a maximum of 2 dyn cm^{-2}, and 10 m with LCD is the

smallest with a maximum of 1.4 dyn cm^{-2}. All the maxima are located over the Caribbean.

In general the large-scale annual mean wind stress curl fields of the above datasets over WEP and NAB have similar patterns. The main features of the curl fields are the large bands of positive curl between 15°N and somewhat south of the equator, and the movements of the negative curl in the southern parts of WEP. Over the GSSR of NAB, the wind stress curls have maxima of ~ 1.25 x 10^{-8} dyn cm^{-3} for 1000 mb wind stress, ~ 1.0 x 10^{-8} dyn cm^{-3} for the LCD and LPCD wind stresses, and ~ 0.75 x 10^{-8} dyn cm^{-3} for HR wind stress. In this region of positive curls, the HR curls have the smallest magnitudes. It is believed that curl fields in this region are connected to Gulf Stream separation.

The monthly mean climatological wind stresses in January and July show strong seasonal variability. In January strong northeast trades occupy the whole northern WEP, while southeast trades are especially strong in July. This is associated with strong monsoon activity in summer. Over WEP the 1000 mb wind stresses have the largest magnitudes of 2.76 dyn cm^{-2} in January and 2.52 dyn cm^{-2} in July. The 10 m with LPCD wind stress have the smallest magnitudes of 1.64 dyn cm^{-2} in January and 1.25 dyn cm^{-2} in July. In general, over the Northern Hemisphere of NAB, July wind stress fields of all datasets are weaker than those in January, except that the 1000 mb and 10 m with LCD January wind stresses over the Caribbean are 10 percent greater in July. In both January and July the wind stresses over the Caribbean are the largest of the whole NAB. In July the maxima of southeast trades are greater than January by ~ 25 percent for 1000 mb, 100 percent for 10 m with LCD, 50 percent for 10 m with LPCD, 50 percent for direct wind stress, and 100 percent for HR.

The big difference in the curl fields over WEP in January and July is that the zero curl line shifts farther north in July (between 5°S and 12°S) in comparison with January (between 3°S and 13°N). Over NAB the substantial spatial curl differences are found in the Gulf Stream Region, over the Caribbean, off Greenland, and off Gibraltar. In general, both maximum and minimum curl fields in January are 10 to 20 percent greater than those in July, except the minimum of the July direct surface stress is 12 percent greater than January. Over GSSR all wind stress curls of the above datasets show a region of positive curl with stronger magnitudes in January than July. The maximum 1000 mb curl is 3.0 x 10^{-8} dyn cm^{-3} in January and is 1.25 x 10^{-8} dyn cm^{-3} in July. The study also shows that the effect of the drag coefficient on ECMWF wind products is small in comparison with the differences between wind products.

The comparison of monthly global mean wind stress magnitudes for 1985-1989 shows that 1000 mb wind stress magnitudes are the largest of ECMWF wind products. The 10 m with LPCD wind stress has the smallest magnitudes for the above period. There was a strong change in the direct surface stress trend in April 1987. This may be connected with a change in parameterizing boundary layer stratification in the ECMWF model at that time (Trenberth et al., 1989). A major change in the analysis in September 1986 (changing vertical coordinates from standard pressure to sigma levels, Trenberth et al., 1989) did not appear in our results. This indicates that the boundary layer stratification has more effect on surface wind than changing vertical coordinates. The wind stress calibration values of 1000 mb, 10 m with LCD, and a normalized 1000 mb with the linear $C_D = 1.06 \times 10^{-3}$ show that ECMWF wind stress magnitudes differ only by a constant multiple.

The NRL global non-eddy resolving model was run to study the sensitivity of the model to ECMWF operational wind forcing. The study shows that the model transports through the Yucatan Straits and between the Pacific and Indian Oceans are not sensitive to small differences in 1000 mb normalized and 10 m wind stresses.

References

Amorocho, J., and J. J. DeVries (1981). Reply *J. Geophys. Rev.*, 86, 4308.

Böning, C.W., R. Doscher, and H. Isemer (1991). Monthly mean wind stress and Sverdrup transports in the North Atlantic: A comparison of the Hellerman-Rosenstein and Isemer-Hasse climatologies. *J. Phys. Oceanogr., 21*, 221-235.

Bunker, A.F. (1976). Computations of surface energy flux and annual air-sea interaction cycles of the North Atlantic Ocean. *Mon. Wea. Rev., 104*, 1127-1140.

Donelan, M.A. (1982). The dependence of aerodynamic drag coefficient on wave parameters. In *Proceedings of the First International Conference on Meteorology and Coastal Zone*, Boston, MA, Amer. Meteorol. Soc., 381-387.

Garratt, J.R. (1977). Review of drag coefficients over oceans and continents. *Mon. Wea. Rev., 105*, 915-929.

Geernaert, G.L., Katsaros, K., and K. Richer (1986). Variation of the drag coefficient and its dependence on sea state. *J. Geophys. Res.*, *91*, 7667-7679.

Geernaert, G.L. (1987). On the importance of the drag coefficient in air-sea interaction. *Dyn. Atmos. Oceans*, *11*, 19-38.

Harrison, D.E. (1989). On climatological monthly mean wind stress and wind stress curl fields over the World Ocean. *J. of Climate*, *2*, 57-70.

Hellerman, S. (1967). An updated estimate of the wind stress in the World Ocean. *Mon. Wea. Rev.*, *95*, 607-611.

Hellerman, S., and M. Rosenstein (1983). Normal monthly wind stress over the World Ocean with error estimates. *J. Phys. Oceanogr.*, *13*, 1093-1104.

Hsu, S.A. (1986). A mechanism for the increase of wind stress (drag) coefficient with wind speed over water surface: A parametric mode. *J. Phys. Oceanogr.*, *16*, 144-150.

Isemer, H.J., and L. Hasse (1987). The Bunker climate atlas of the North Atlantic Ocean. *Air-Sea Interactions*, Vol 2, Springer-Verlag, 256 pp.

Kondo, J. (1975). Air-sea bulk transfer coefficients in diabatic conditions. *Boundary-Layer Meteorol.*, *9*, 91-112.

Large, W.G., and S. Pond (1982). Sensible and latent heat flux measurements over the oceans. *J. Phys. Oceanogr.*, *12*, 464-482.

Large, W.G., and S. Pond (1981). Open ocean momentum flux measurements in moderate to strong winds. *J. Phys. Oceanogr.*, *11*, 324-336.

Levitus, S. (1982). Climatological atlas of the world ocean. National Oceanic and Atmospheric Administration. Professional Paper No. 13, U.S. Government Printing Office, Washington, D.C.

Ly, N.L. (1990). Numerical Studies of the Surface-Wave Effects on the Upper Turbulent Layer in the Ocean. *Tellus, 42A*, 557-567.

Ly, N.L. (1992). On the effect of the angle between wind stress and wind velocity vectors on the aerodynamic drag coefficient at the air-sea interface. *J. Phys. Oceanogr.* (in press).

Schott, F.A., T.N. Lee, and R. Zantop (1988). Variability of structure and transport of Florida current in the period range of days to seasonal. *J. Phys. Oceanogr., 18*, 1209-1230.

Scoggins, R.J., and C.N.K. Mooers (1988). Atmospheric forcing of ocean circulation. Report of a Workshop. Institute for Naval Oceanography, New Orleans, LA, 389 pp.

Trenberth, K.E., and J.G. Olson (1988a). Evaluation of NMC global analyses: 1979-1987. NCAR Tech. Note NCAR/TN-299+STR, 82 pp.

Trenberth, K.E., and J.G. Olson (1988b). ECMWF global analyses 1979-1986: Circulation statistics and data evaluation. NCAR Tech. Note NCAR/TN-300+STR, 94 pp plus fiche.

Trenberth, K.E., and J.G. Olson (1988c). Intercomparison of NMC and ECMWF global analyses: 1980-1986. NCAR Tech. Note NCAR/TN-301+STR, 81 pp.

Trenberth, K.E., J.G. Olson, and W.G. Large (1989). A global ocean wind stress climatology based on ECMWF analyses. NCAR Technical Note, Boulder, CO, 93 pp.

The WAMDI Group (1988). The WAM model - A third generation ocean wave prediction model. *J. Phys. Oceanogr., 18*, 1775-1810.

White, D.W. (1988). *In Situ* observational networks: present and future. In *Atmospheric Forcing of Ocean Circulation, Report of a Workshop.* Institute for Naval Oceanography, New Orleans, 389 pp.

Wu, J. (1982). Wind-stress coefficients over sea surface from breeze to hurricane. *J. Geophys. Res., 87*, 9704-9706.

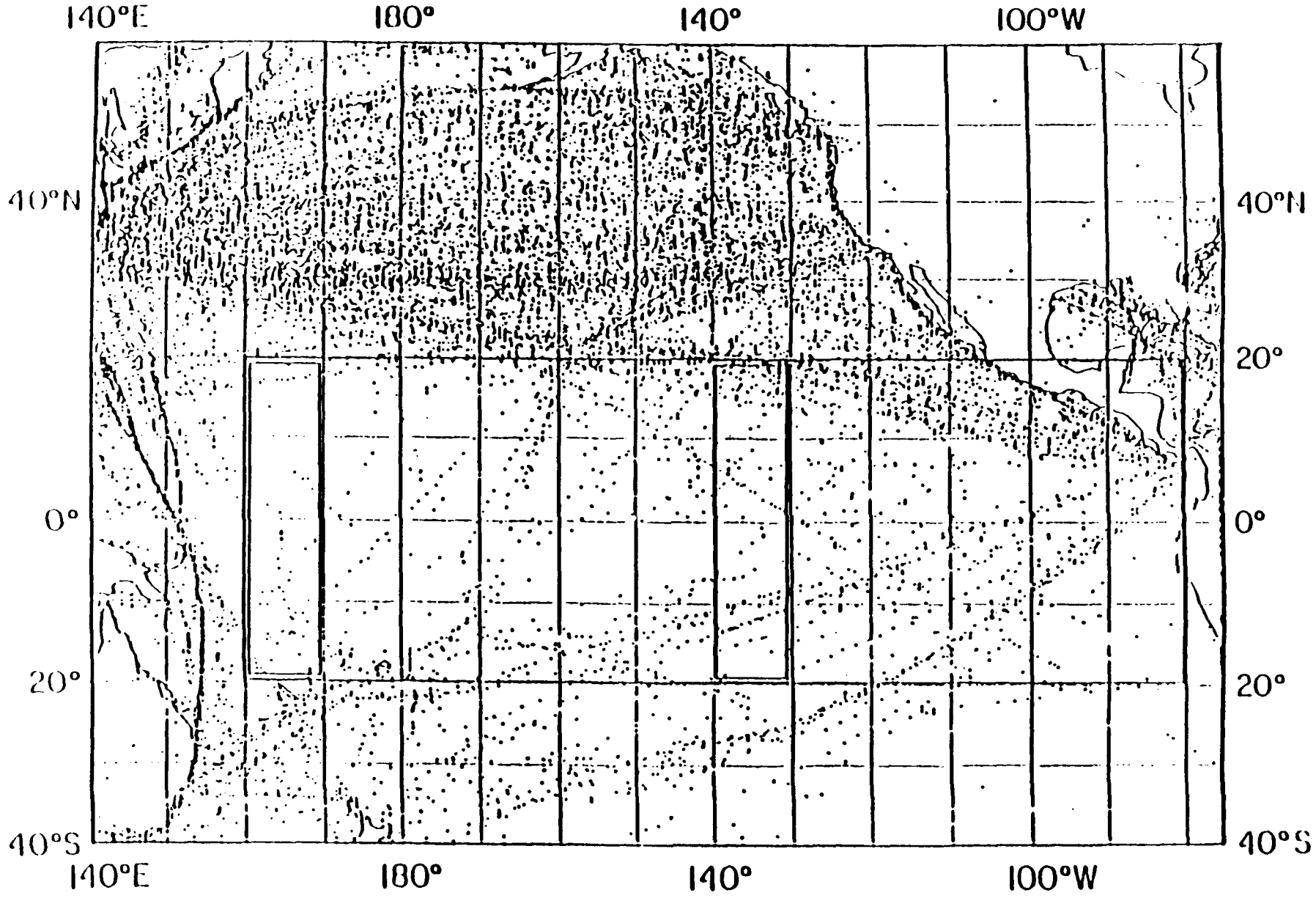

Fig. 1 Distribution of ships' observations reported by radio during January, 1977. (After White, 1988).

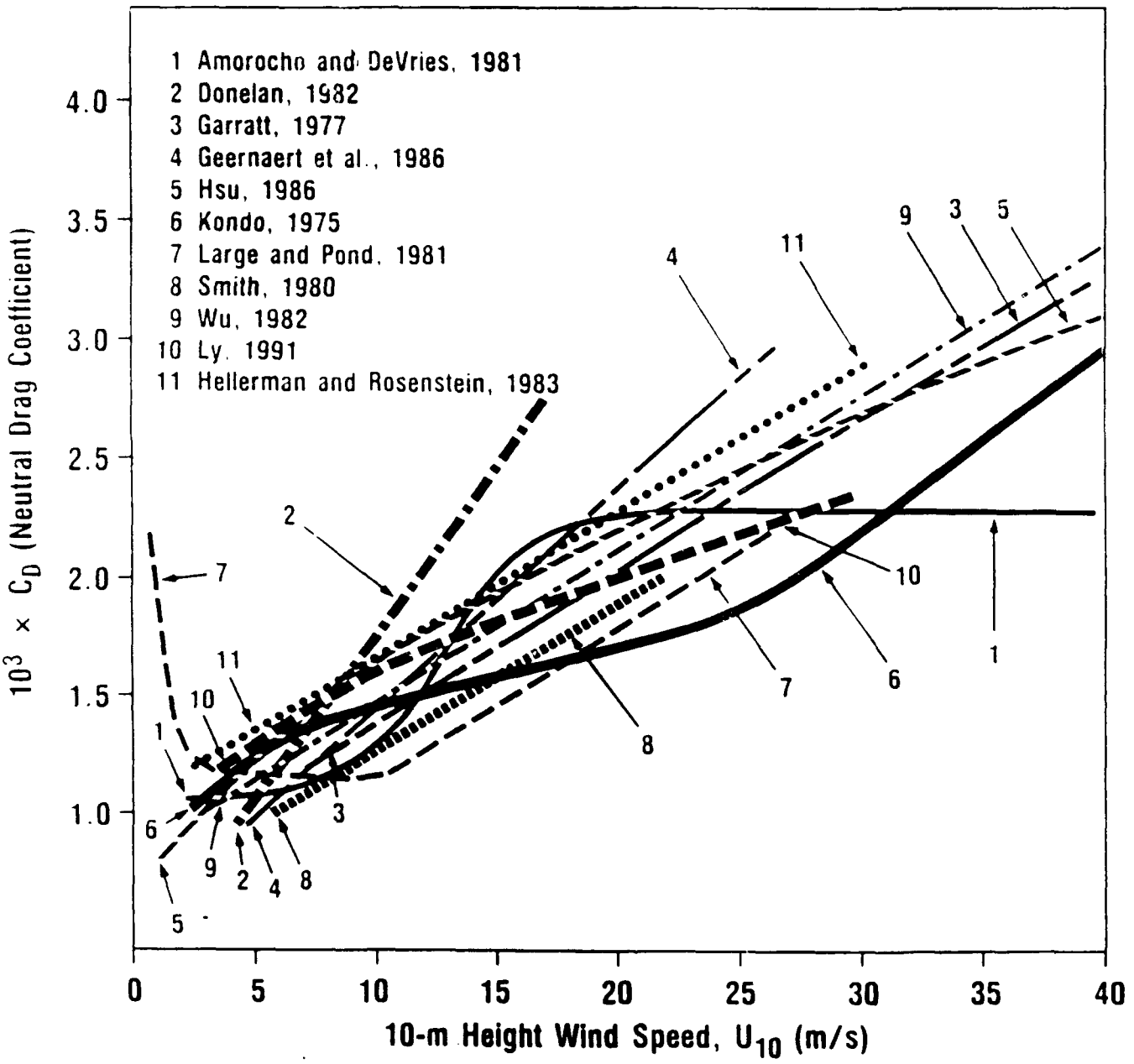

Fig. 2 The published neutral drag coefficient as a function of wind speed at 10 m height, U_{10}.

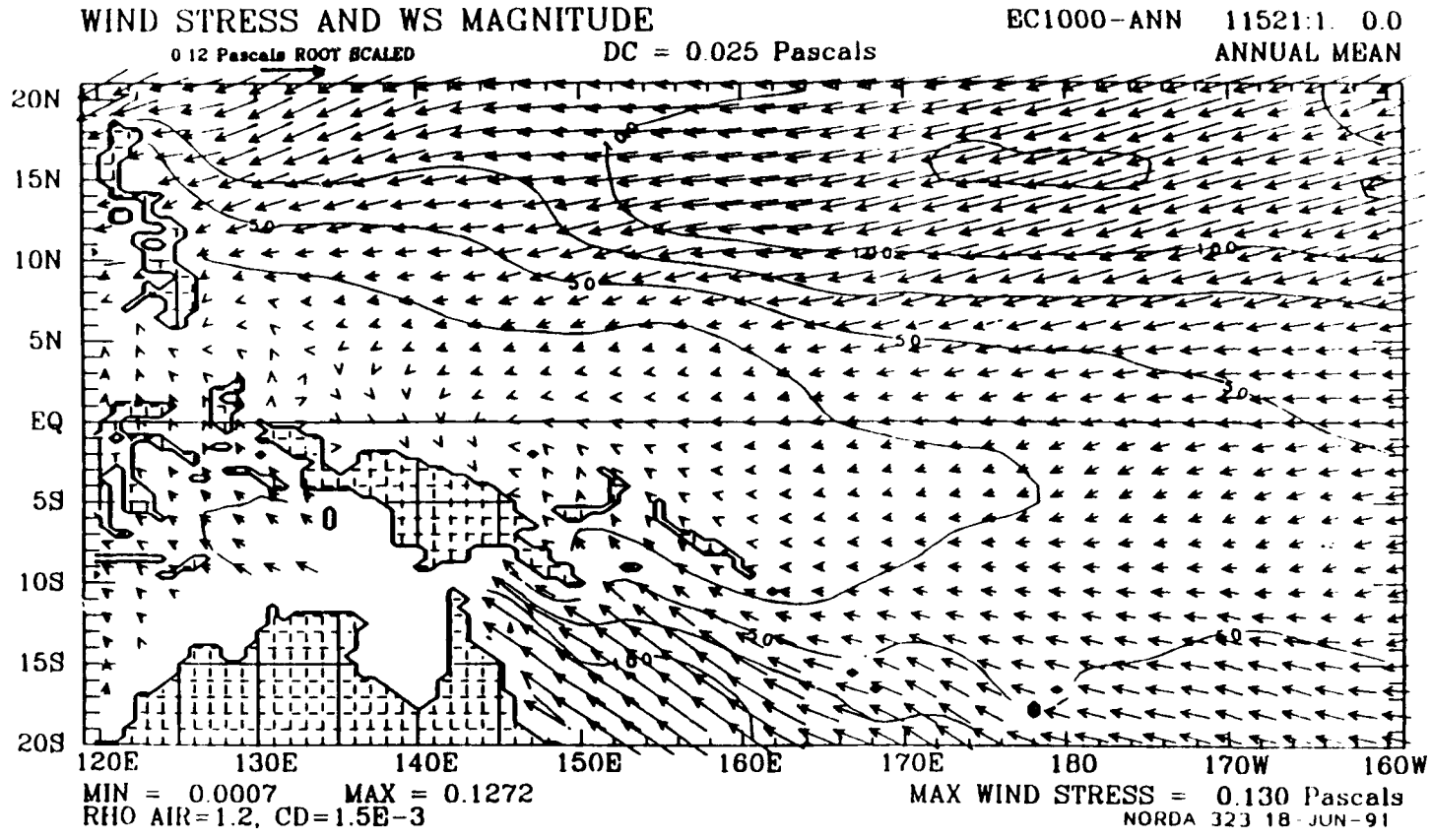

Fig. 3a Annual mean 1000 *mb* wind stress vectors and magnitudes over the Western Equatorial Pacific (WEP). The contour interval is 0.25 $dyn\ cm^{-2}$ (1 Pa = 10 $dyn\ cm^{-2}$). The arrow at top left corresponds to 1.25 $dyn\ cm^{-2}$. The linear drag coefficient is used.

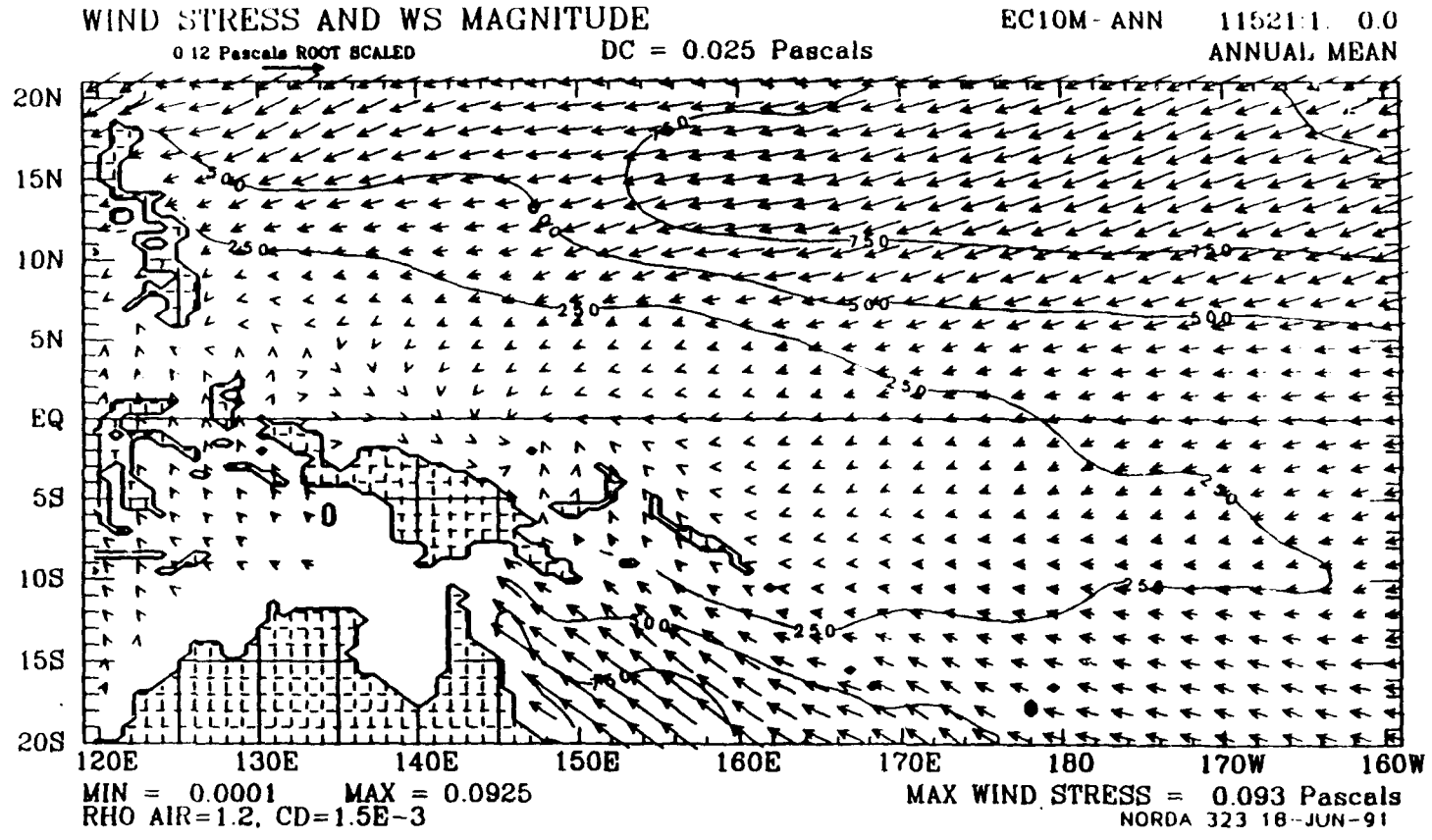

Fig. 3b Same as Fig. 3a but for 10 m height winds.

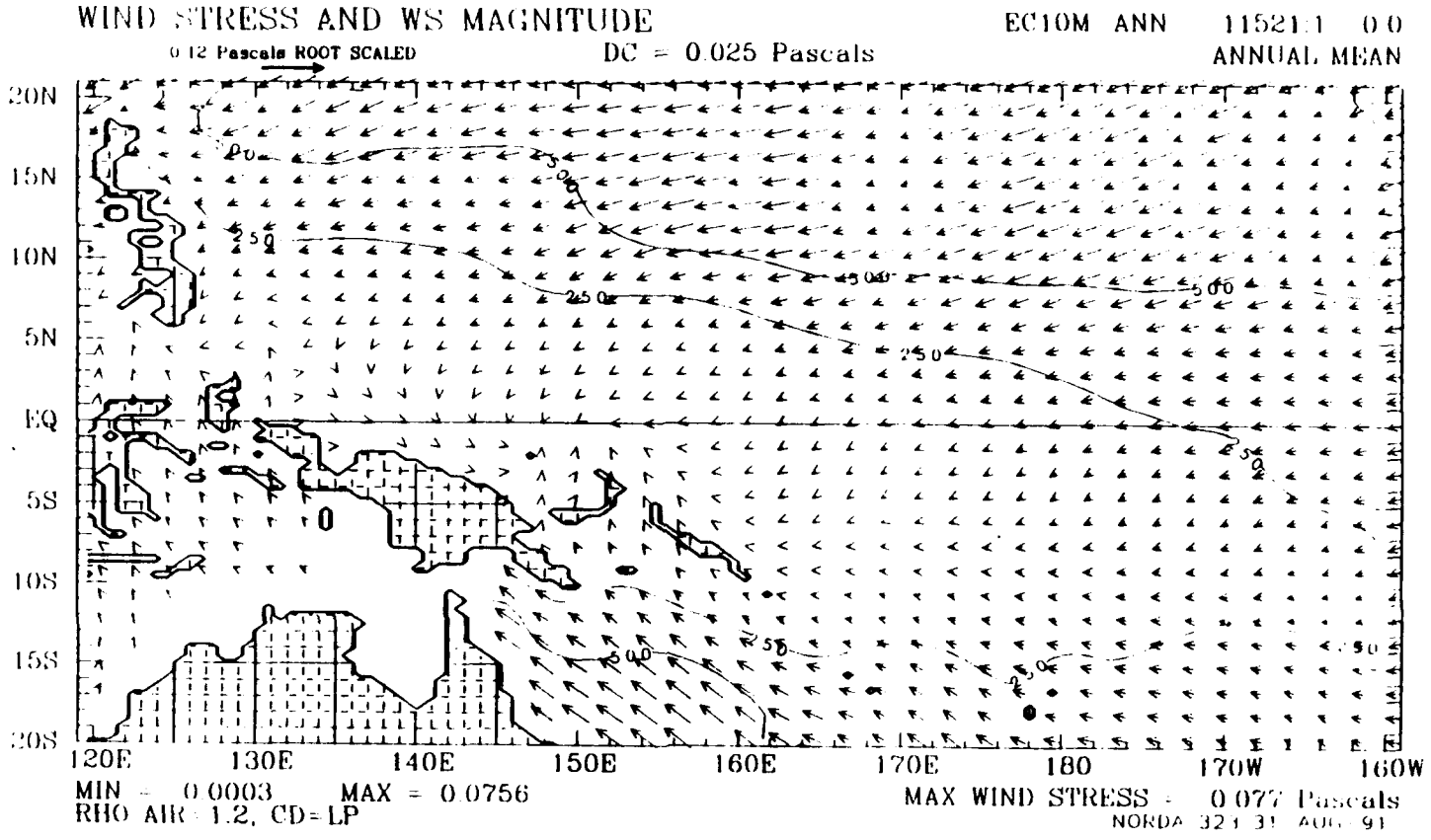

Fig. 3c Same as Fig. 3a but for 10 m height winds and nonlinear drag coefficient.

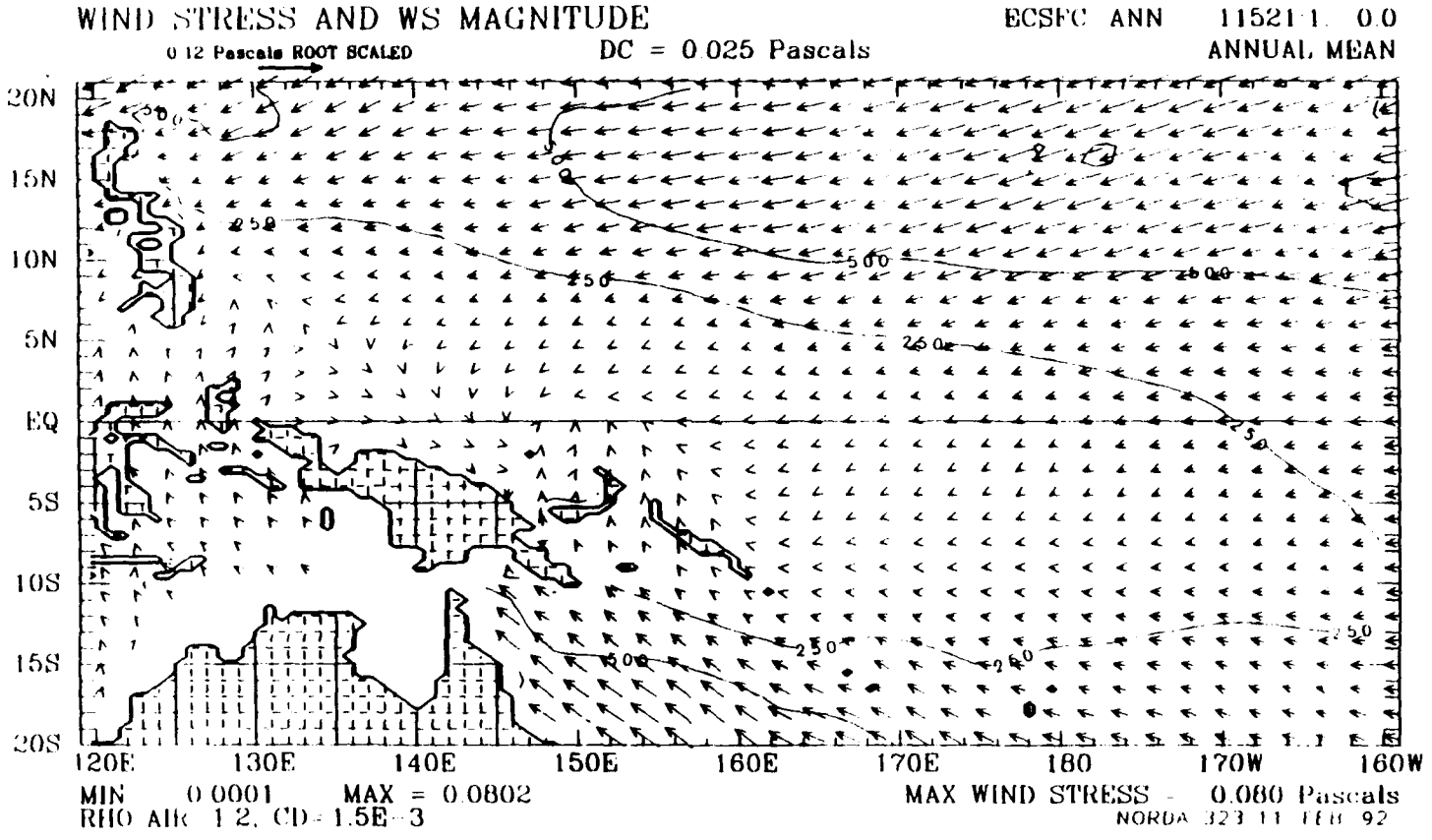

Fig. 3d Same as Fig. 3a but for direct surface wind stress.

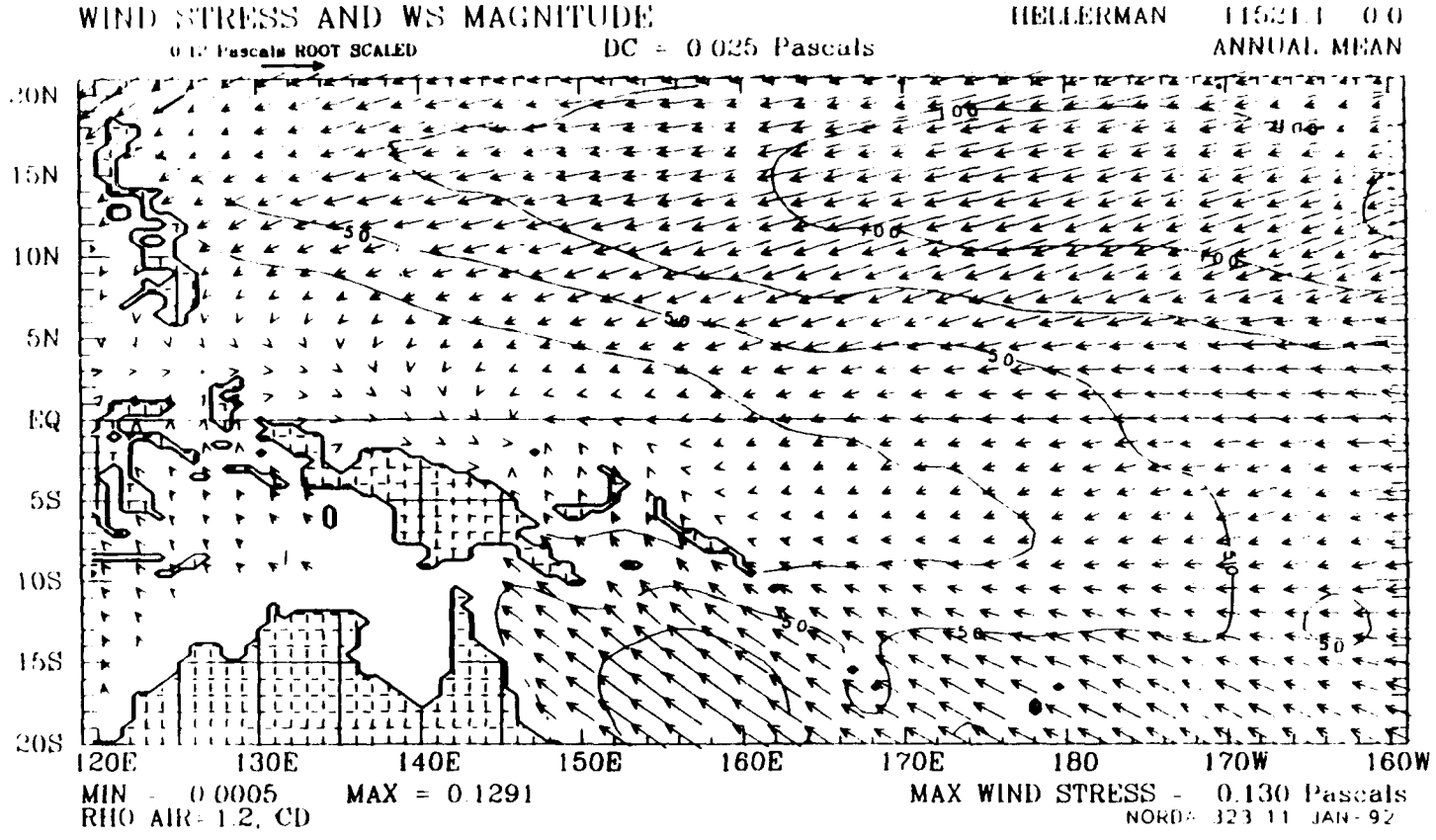

Fig. 3e Same as Fig. 3a but for Hellerman and Rosenstein (HR) wind stress.

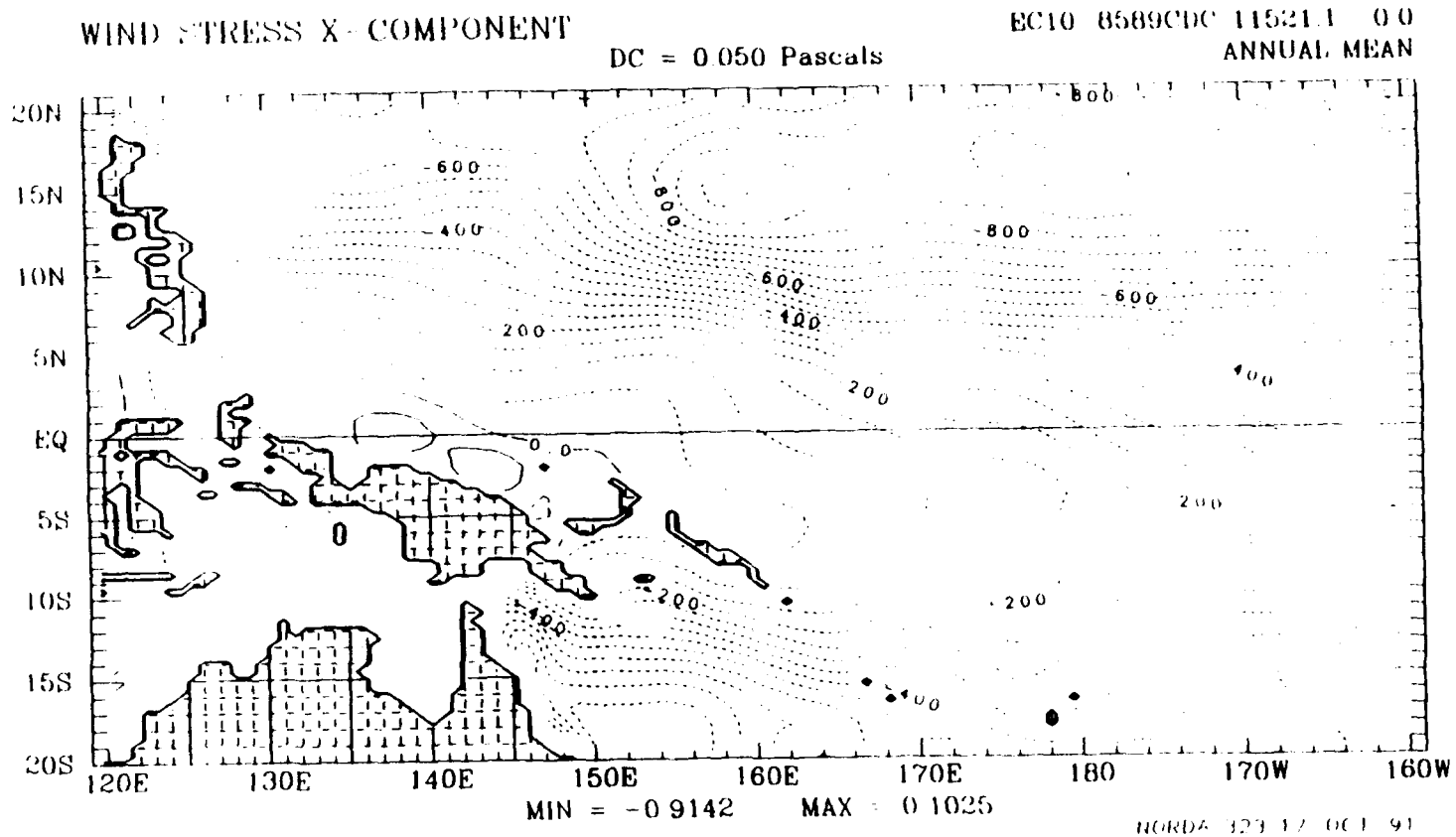

Fig. 4a Zonal mean annual component of 10 m height wind stress over WEP. The linear drag coefficient (LCD) is used. The contour interval is 0.5 $dyn\ cm^{-2}$. The negative values are dashed.

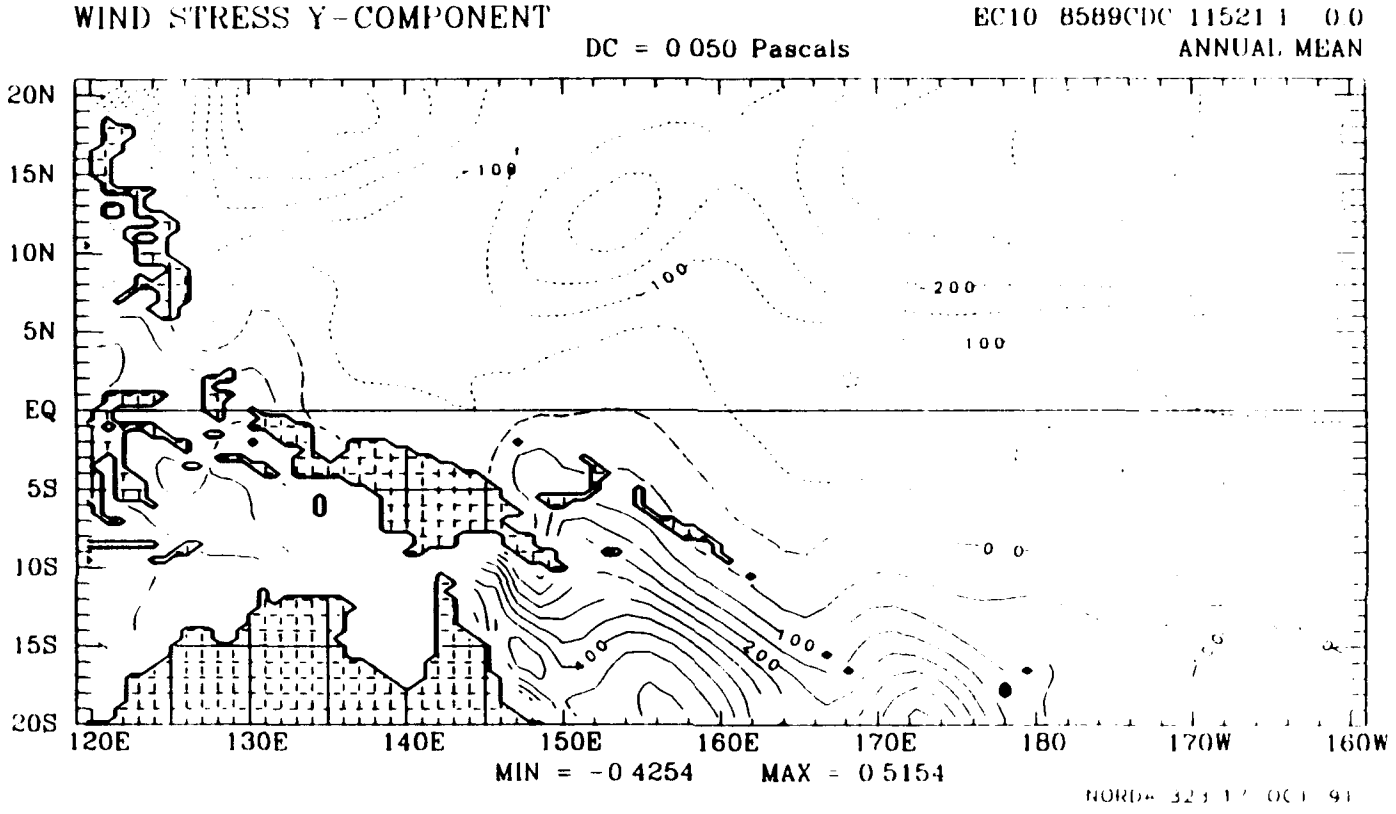

Fig. 4b Same as Fig. 4a but for meridional component. The positive (northward) values are solid.

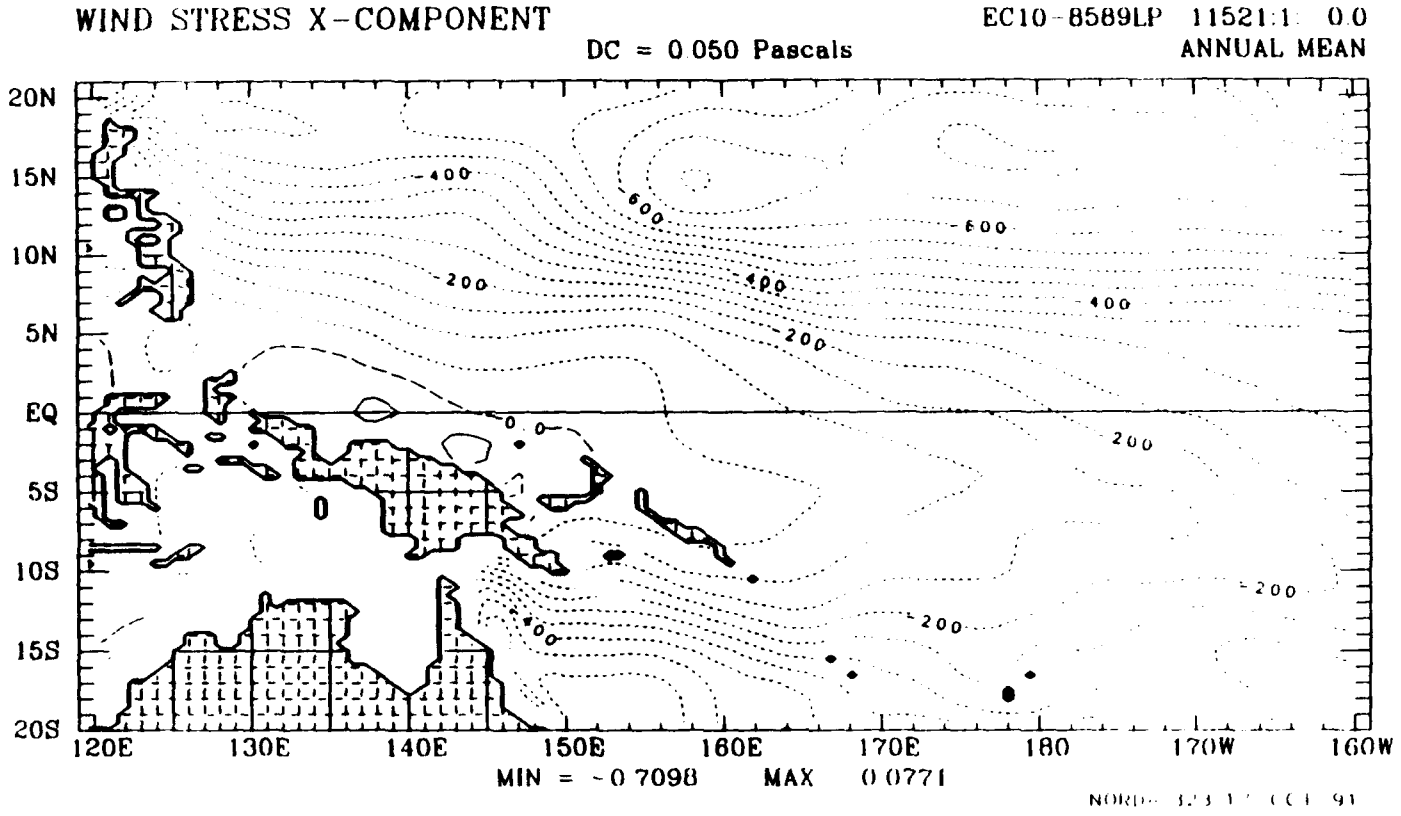

Fig. 4c Same as Fig. 4a but LPCD is used.

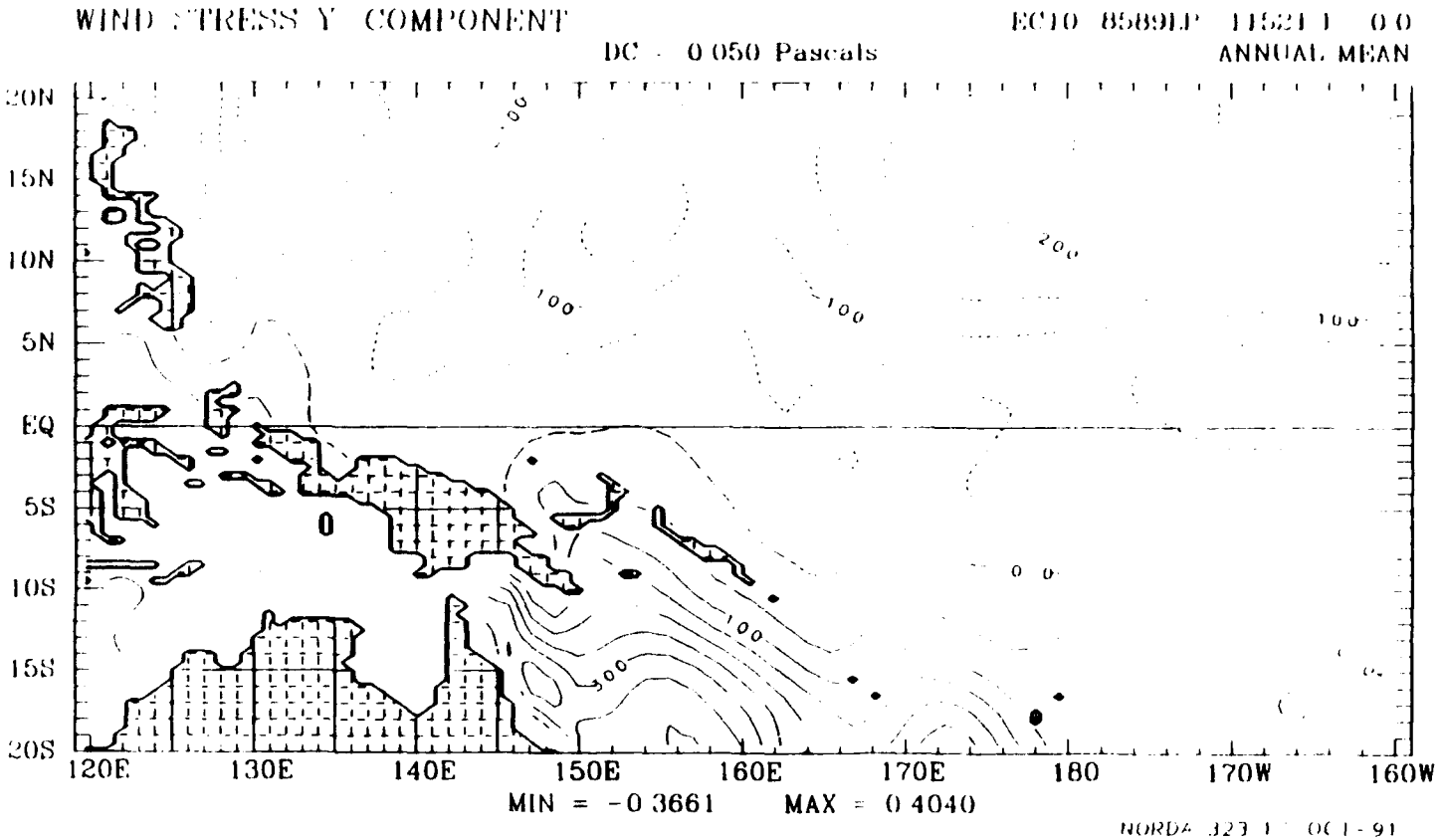

Fig. 4d Same as Fig. 4b but LPCD is used.

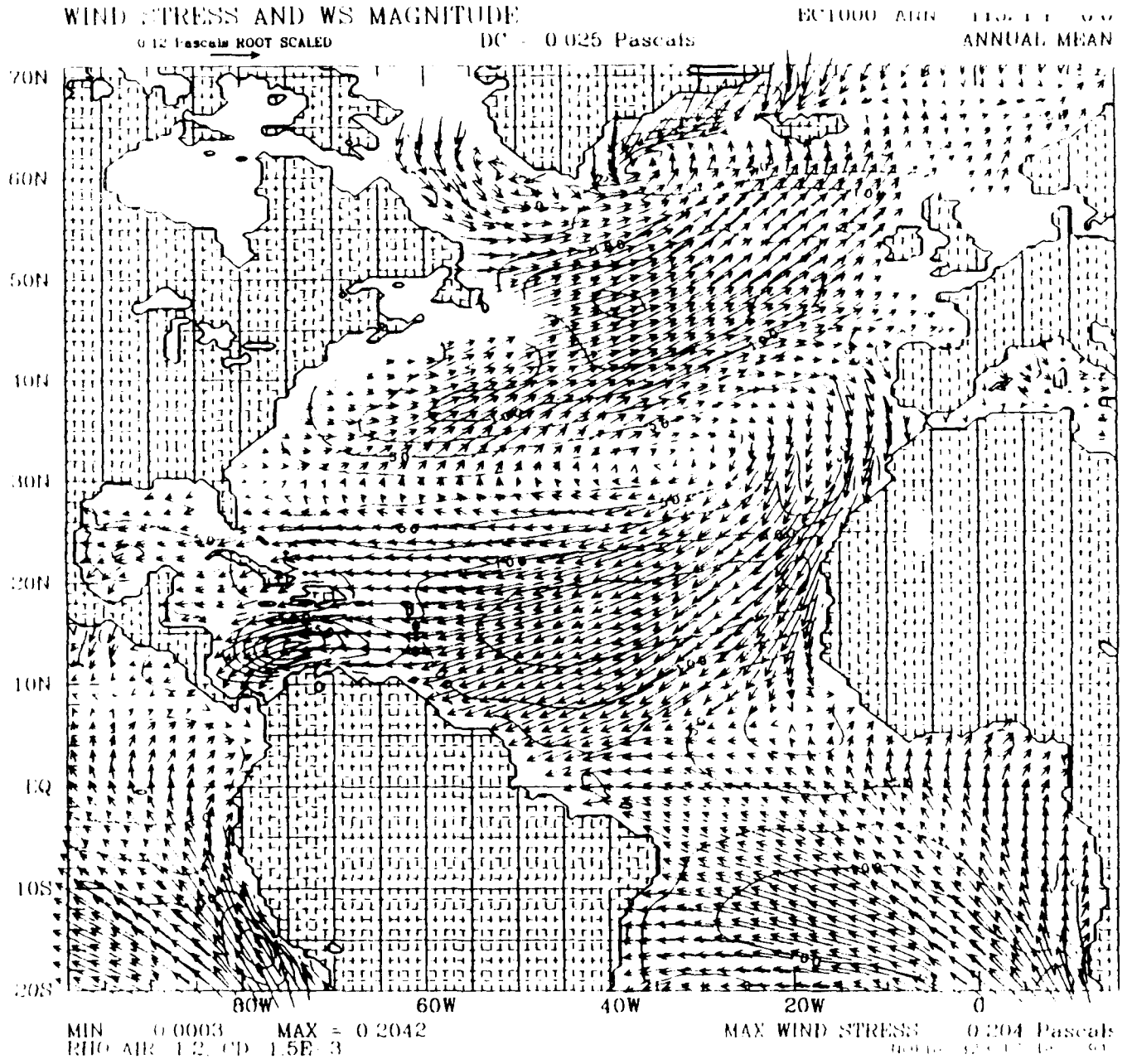

Fig. 5a Annual mean 1000 *mb* wind stress vectors and magnitudes over the North Atlantic Basin (NAB) from 20°*S* to 70°*N* and 100°*W* to 15°*E*. The LCD is used. The contour interval is 0.25 *dyn cm*$^{-2}$. The arrow at top left corresponds to 1.25 *dyn cm*$^{-2}$.

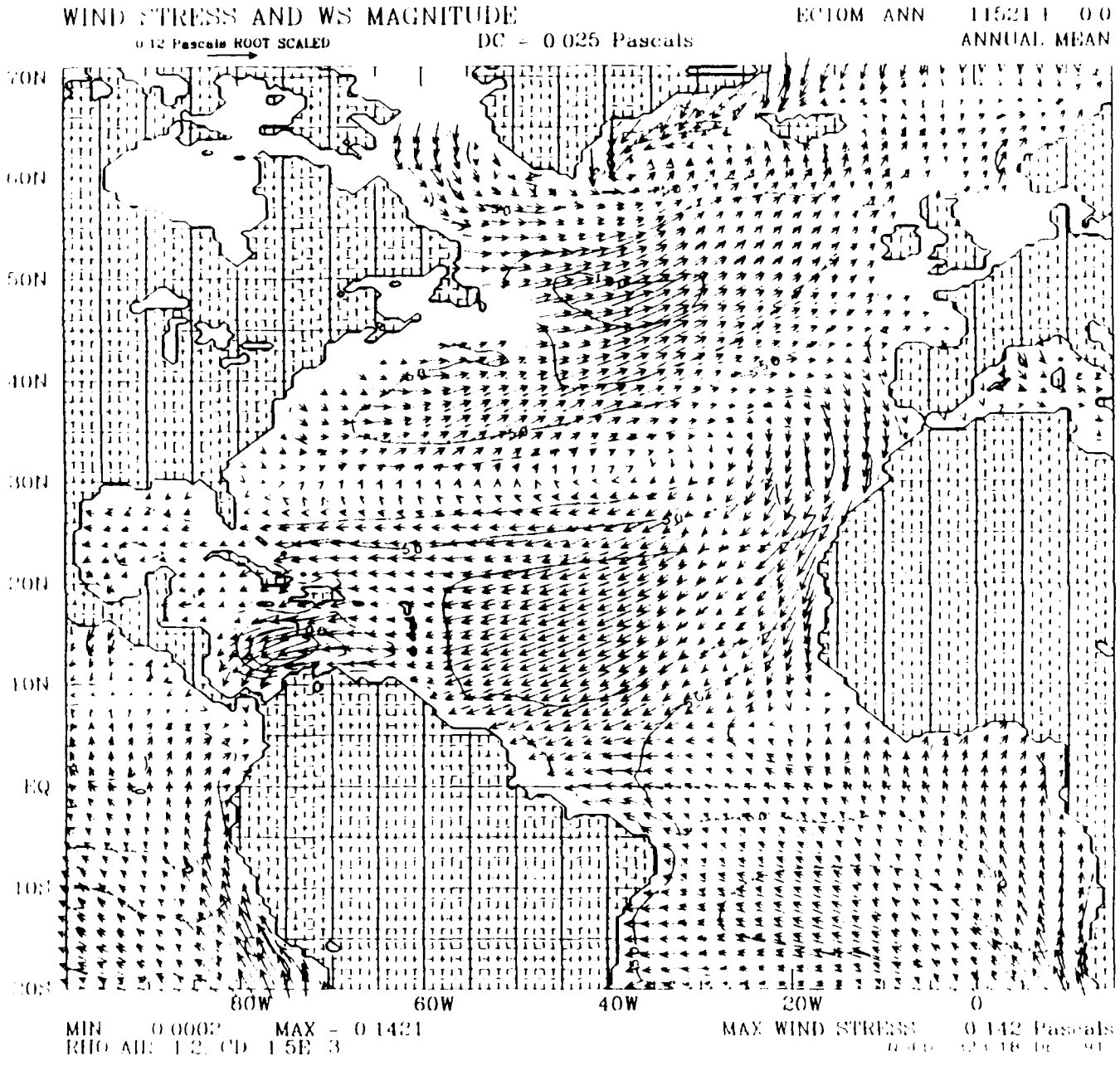

Fig. 5b Same as Fig. 5a but for 10 *m* height winds.

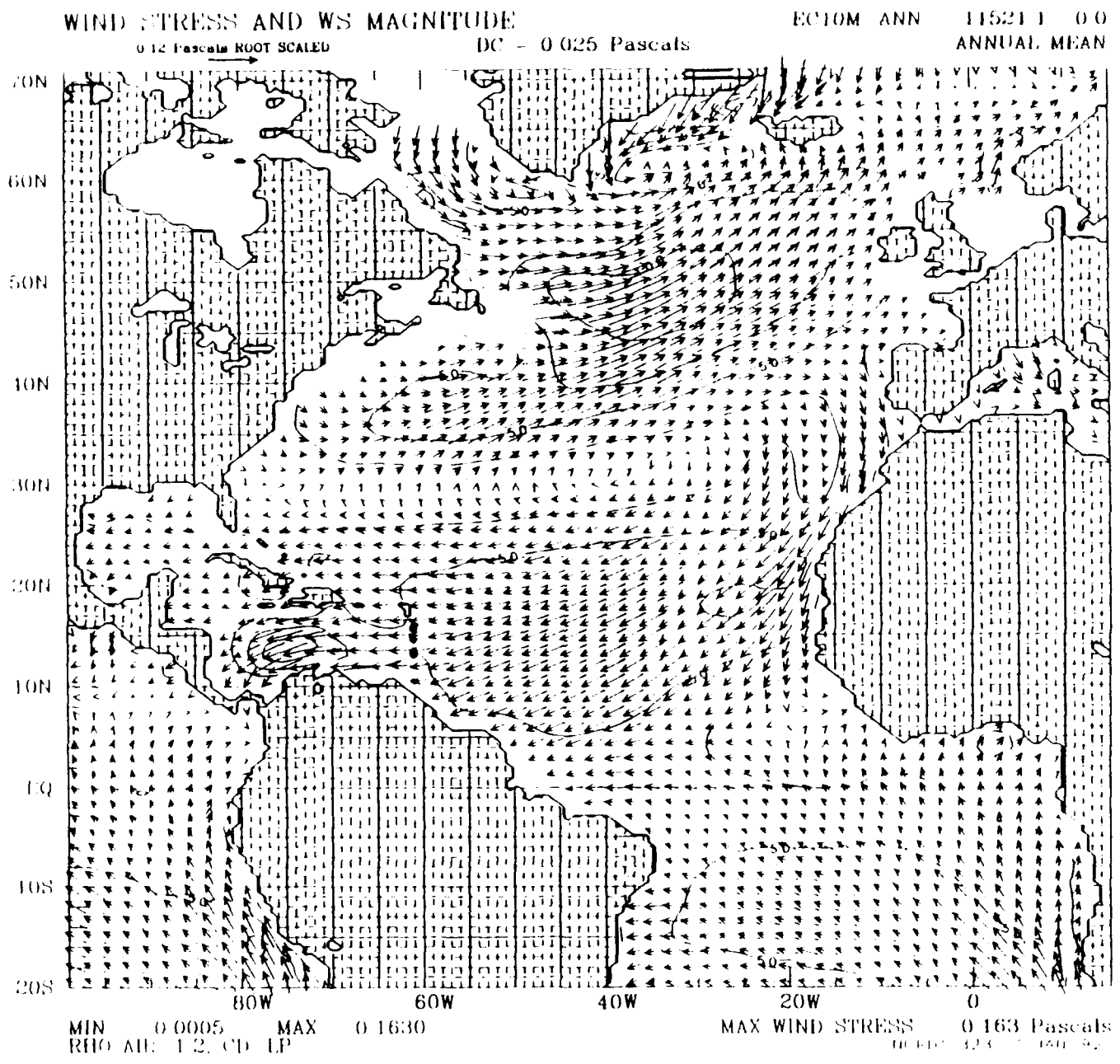

Fig. 5c Same as Fig. 5a but for 10 *m* height winds and the LCD.

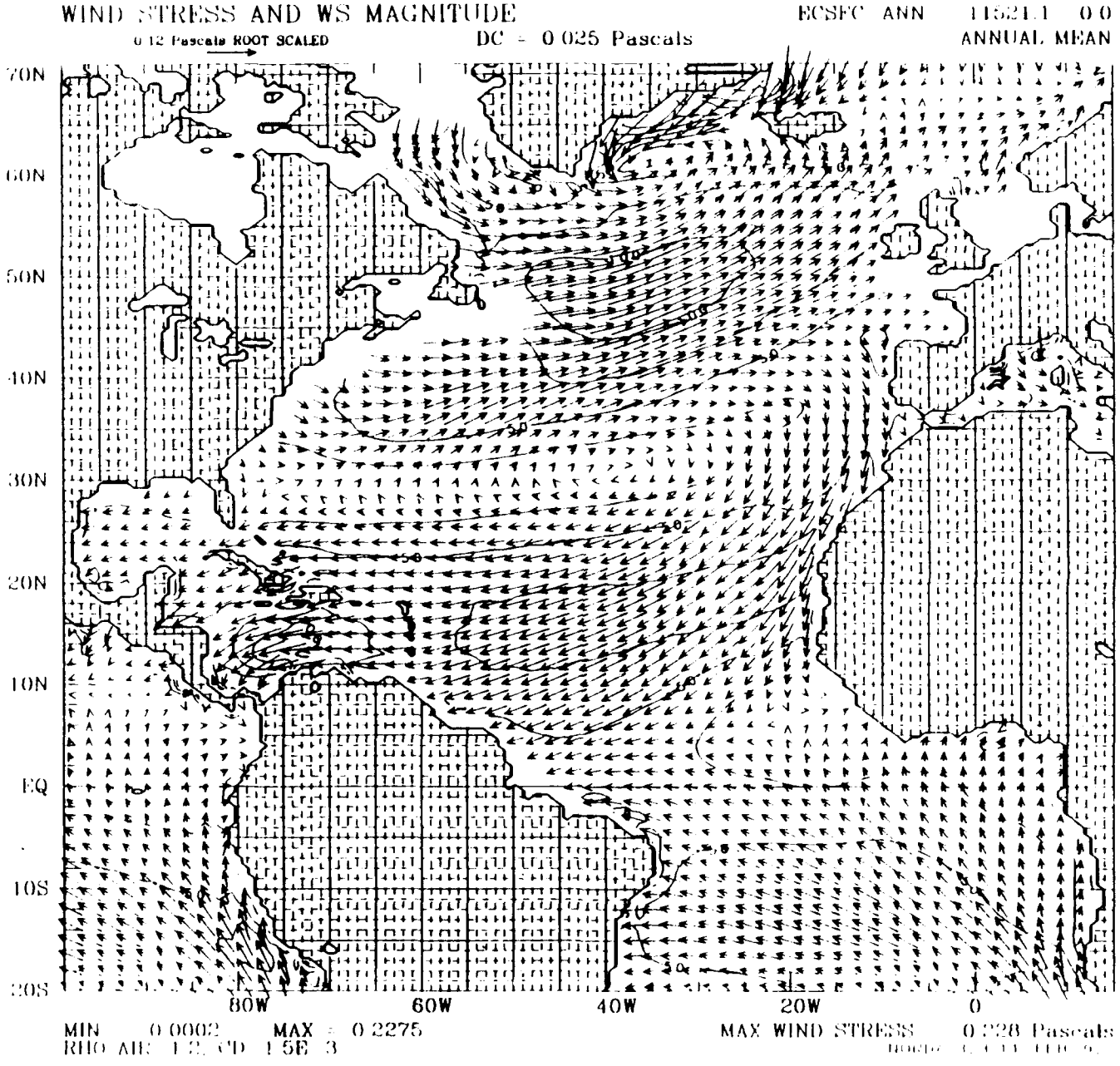

Fig. 5d Same as Fig. 5a but for the surface wind stress.

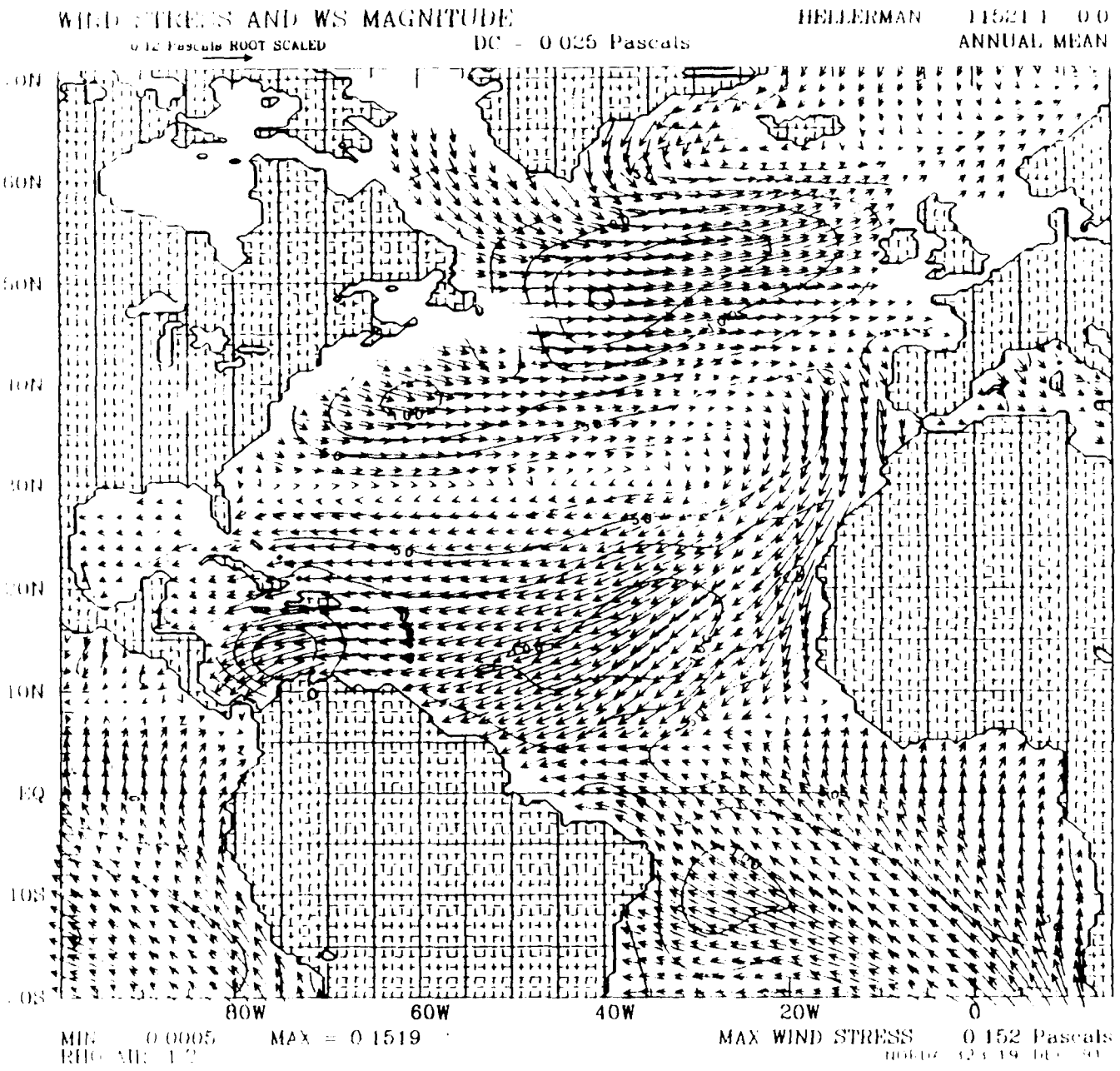

Fig. 5c Same as Fig. 5a but for HR wind stress.

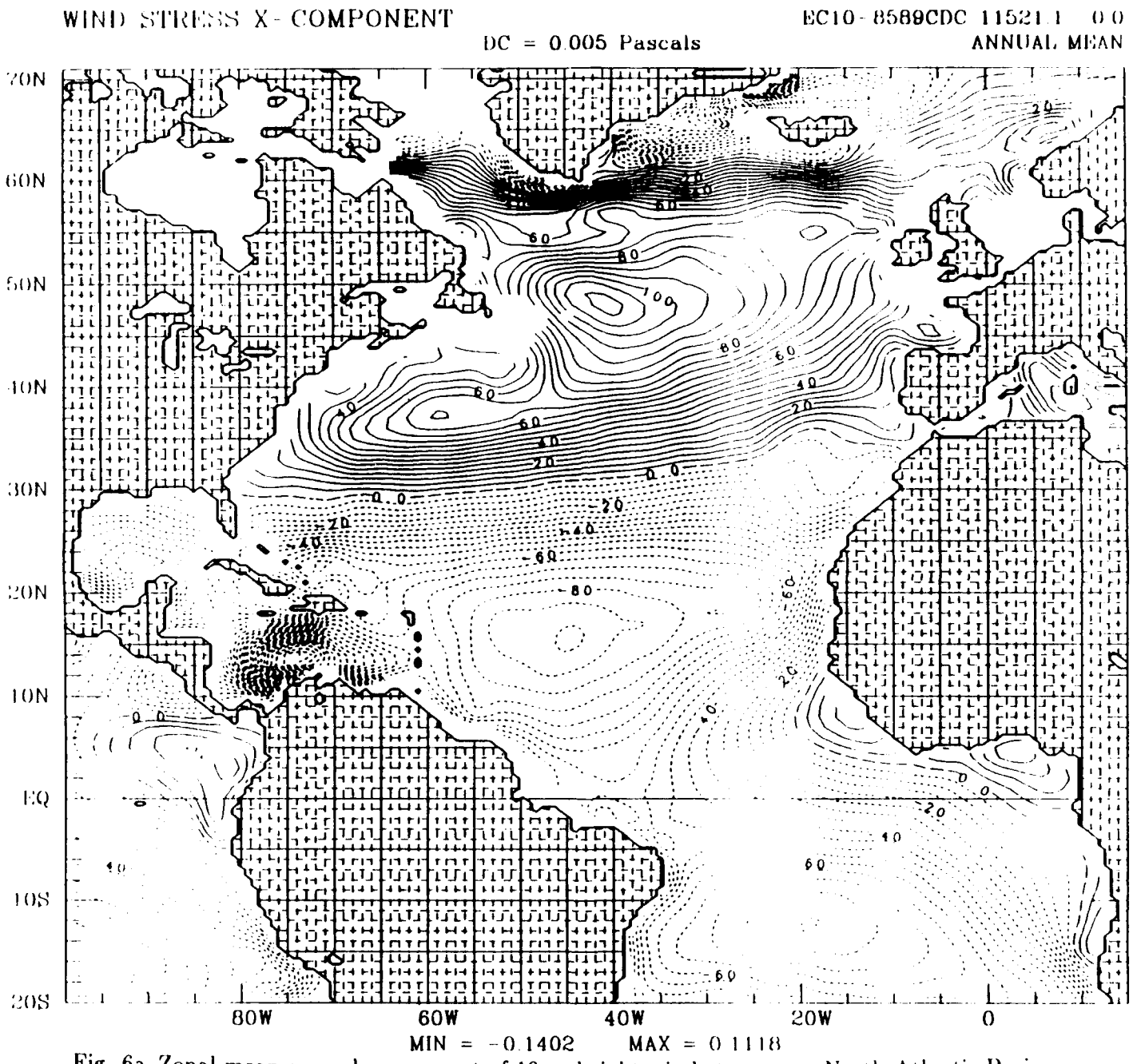

Fig. 6a Zonal mean annual component of 10 m height wind stress over North Atlantic Basin. The LCD is used. The contour interval is 0.05 $dyn\ cm^{-2}$. The positive (eastward) values are solid and the negative are dashed.

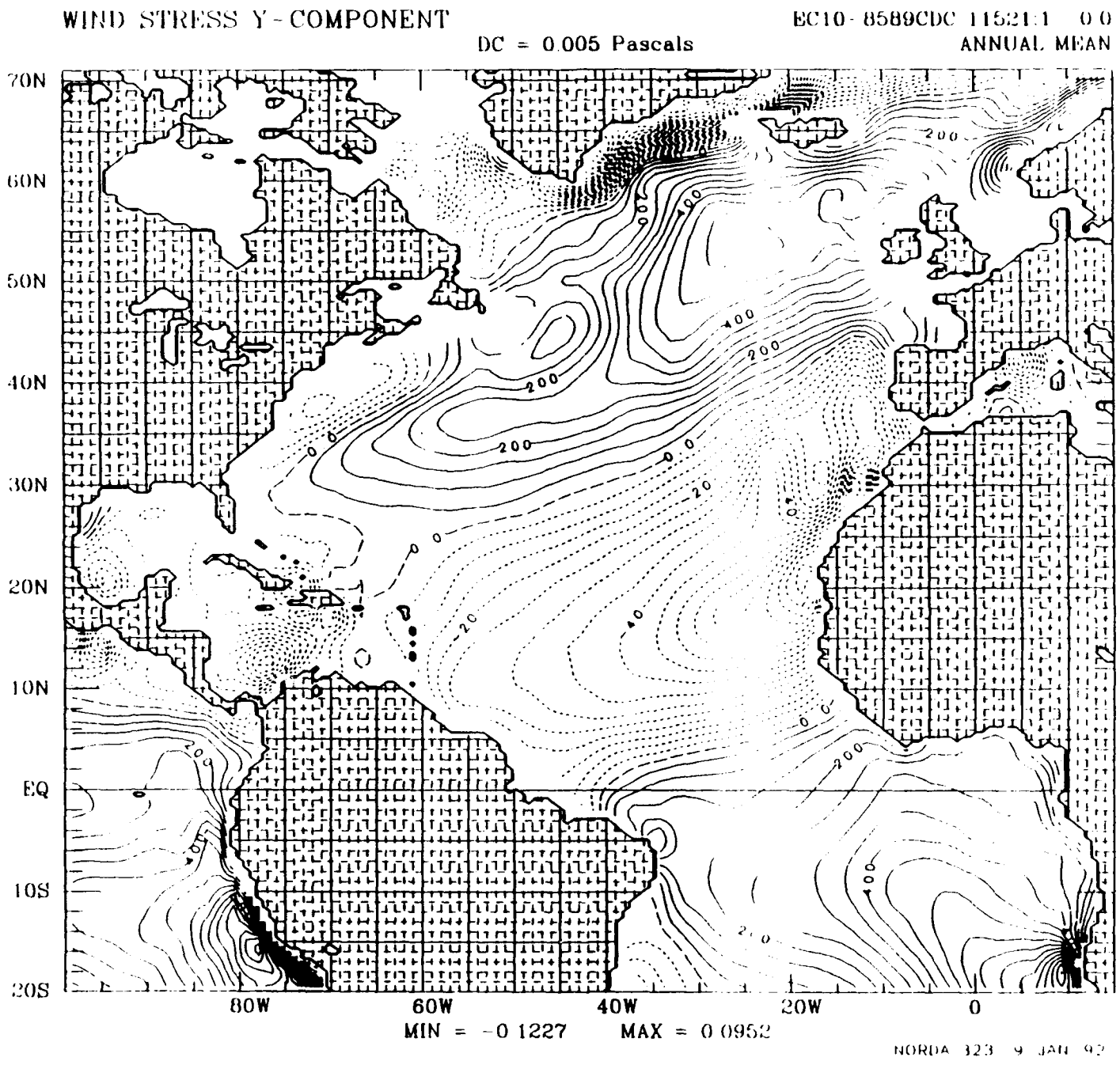

Fig. 6b Same as Fig. 6a but for meridional component.

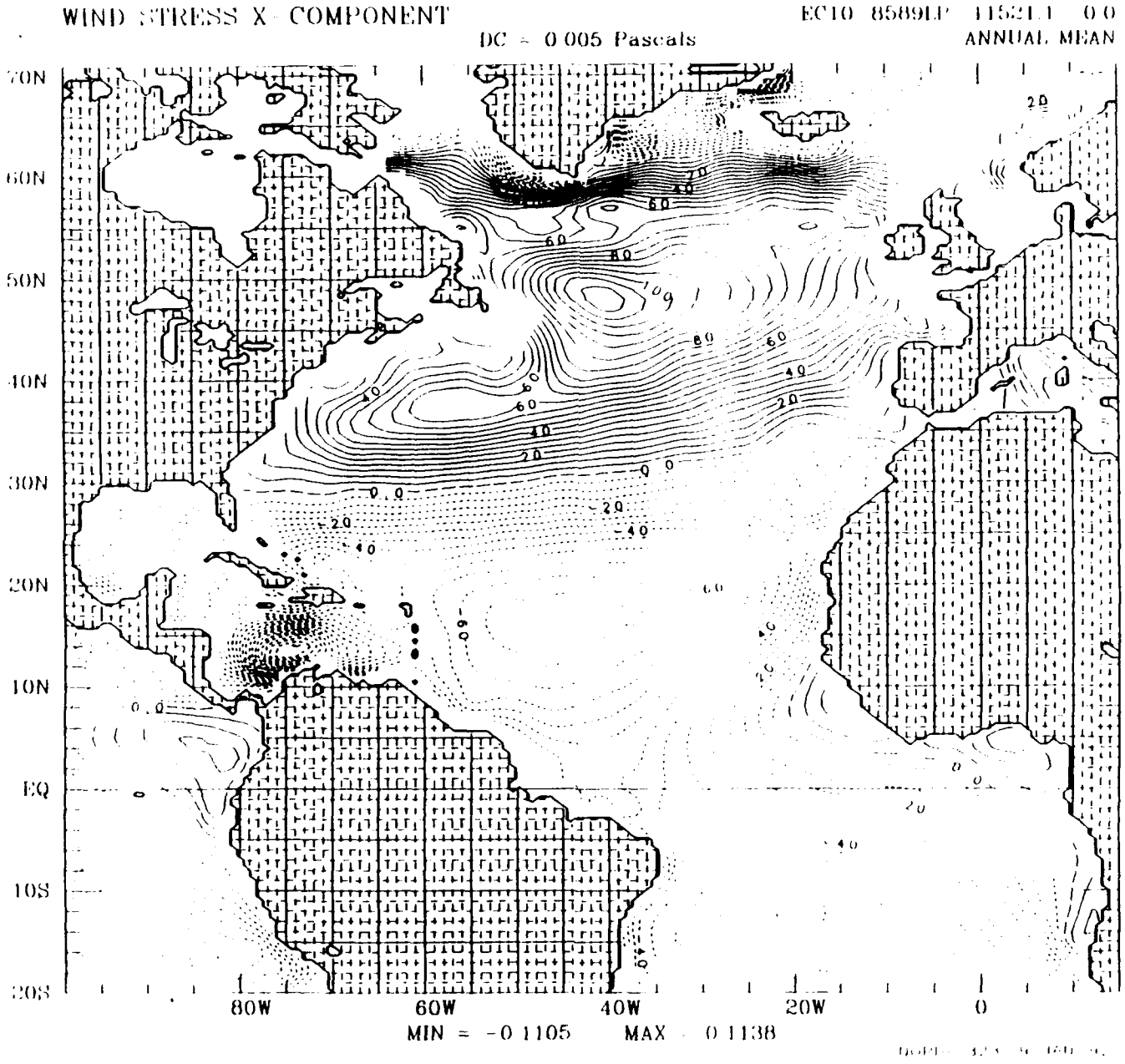

Fig. 6c Same as Fig. 6a but LPCD is used.

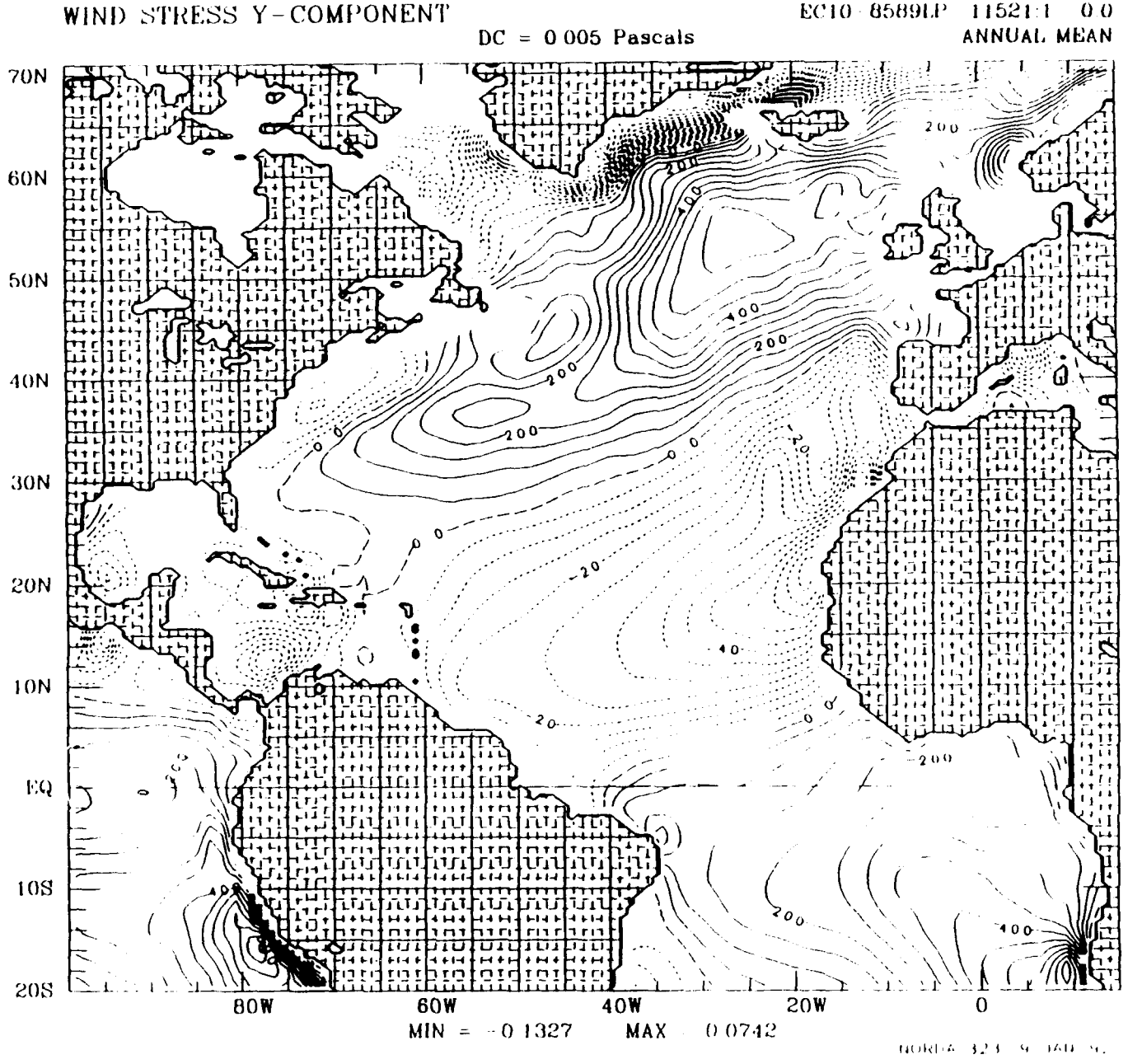

Fig. 6d Same as Fig. 6b but LPCD is used.

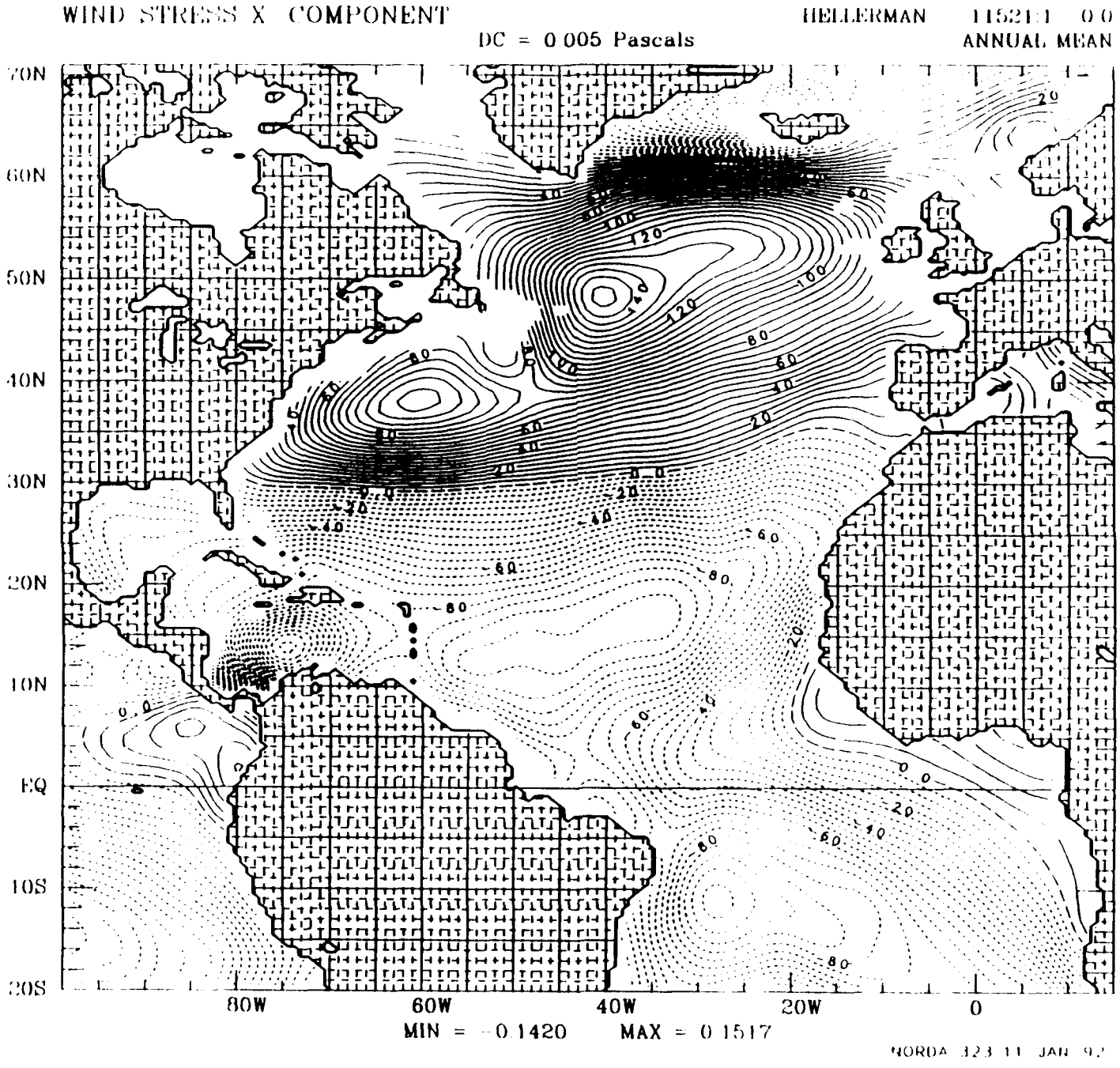

Fig. 6c Same as Fig. 6a but for HR wind stress.

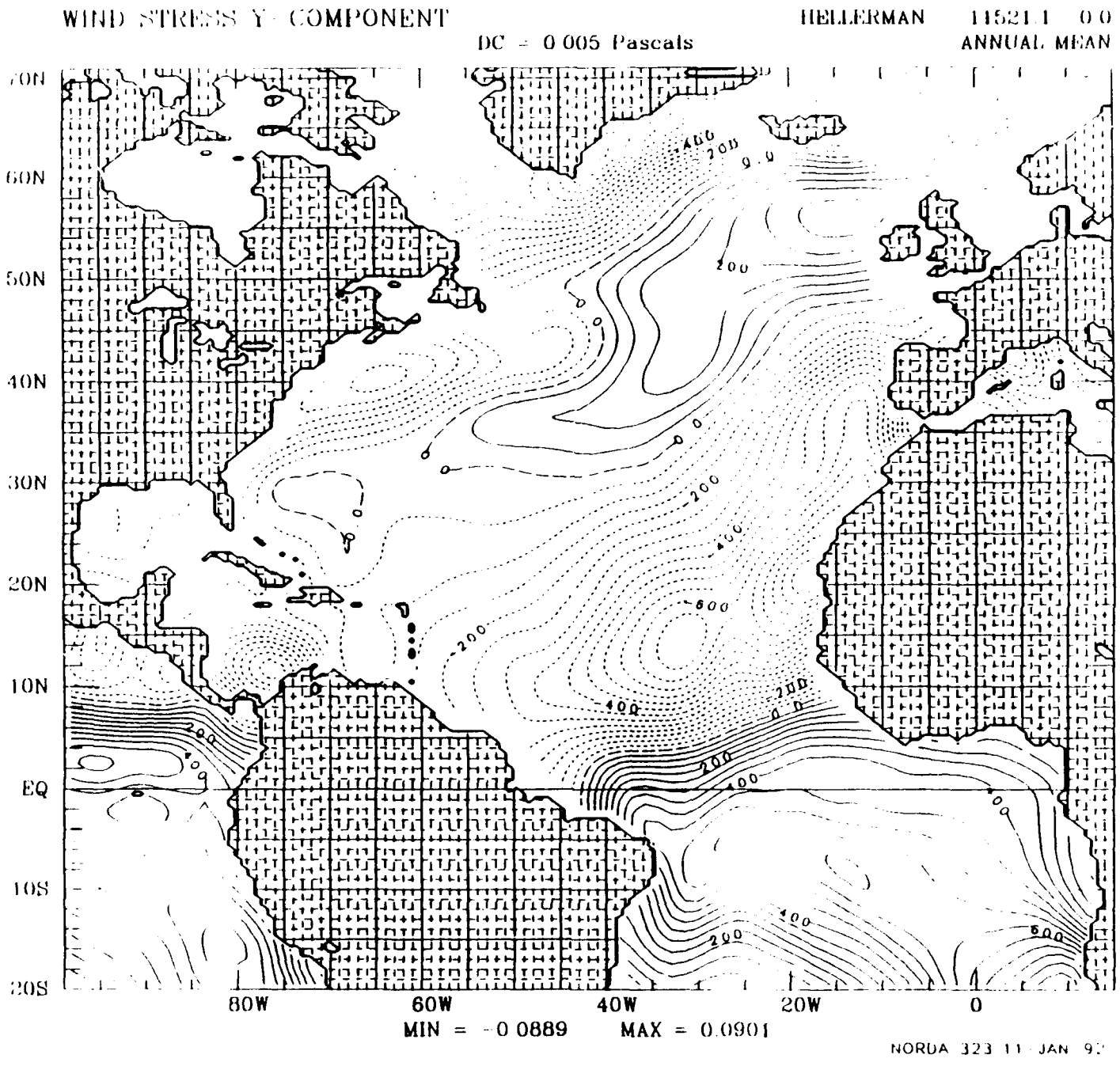

Fig. 6f Same as Fig. 6b but for HR wind stress.

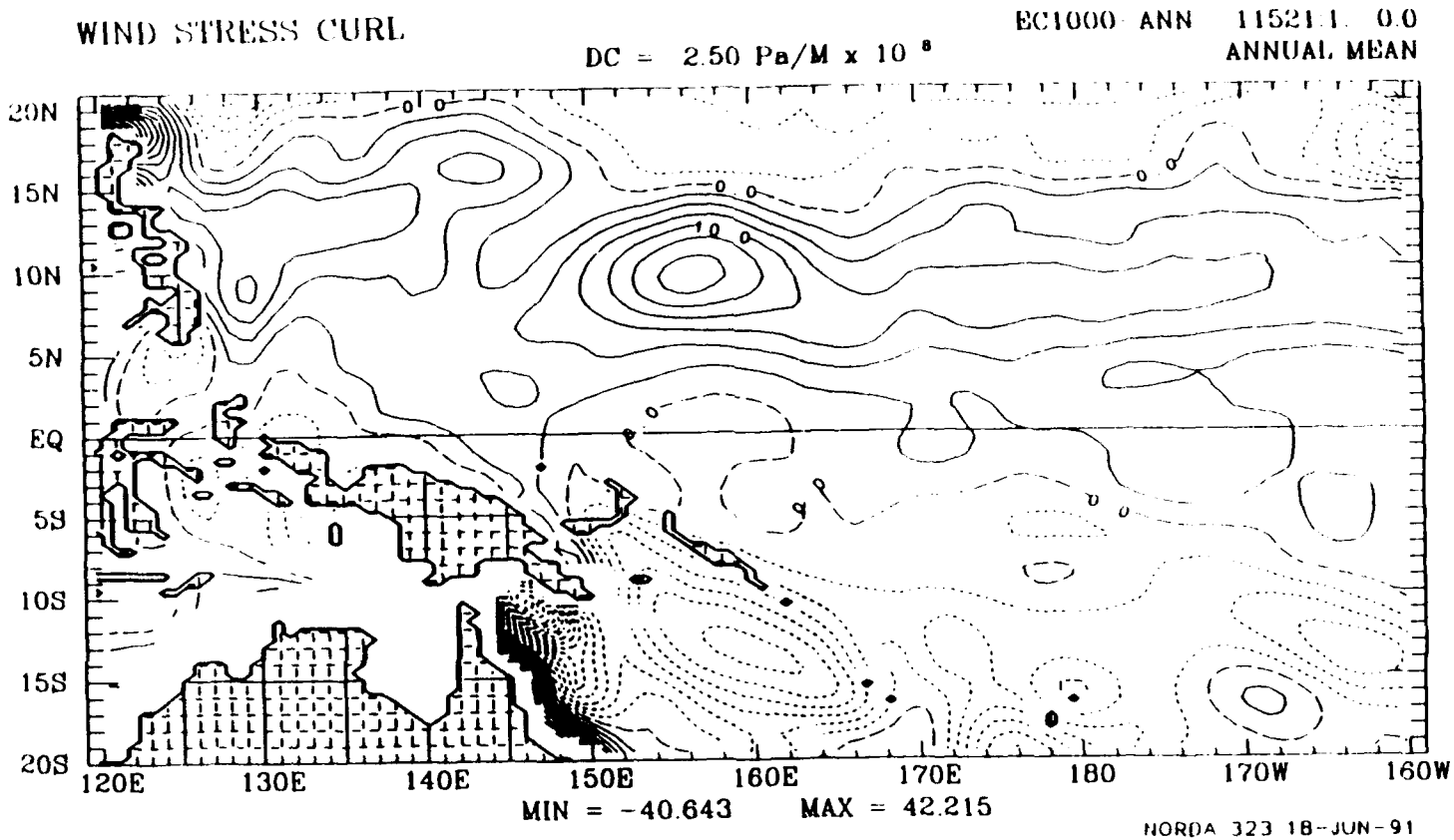

Fig. 7a Annual mean curl of the 1000 *mb* wind stress over WEP. The LCD is used. The contour interval is 25 $\times 10^{-8} dyn\ cm^{-3}$ ($1\ Pa\ m^{-1} = 10^{-7} dyn\ cm^{-3}$). The positive (negative) values are solid (dashed).

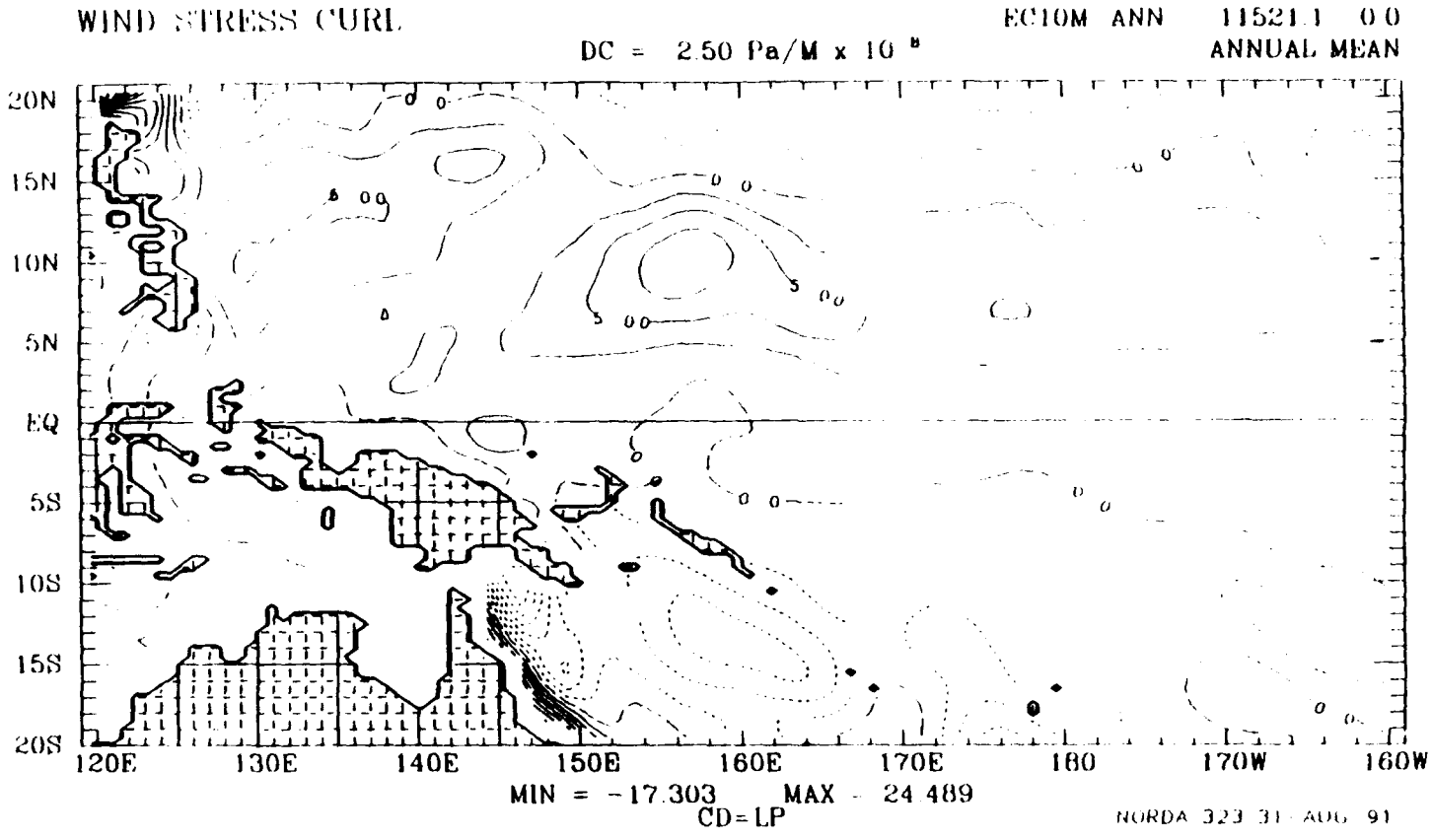

Fig. 7b Same as Fig. 7a but for 10 m height wind stress curls.

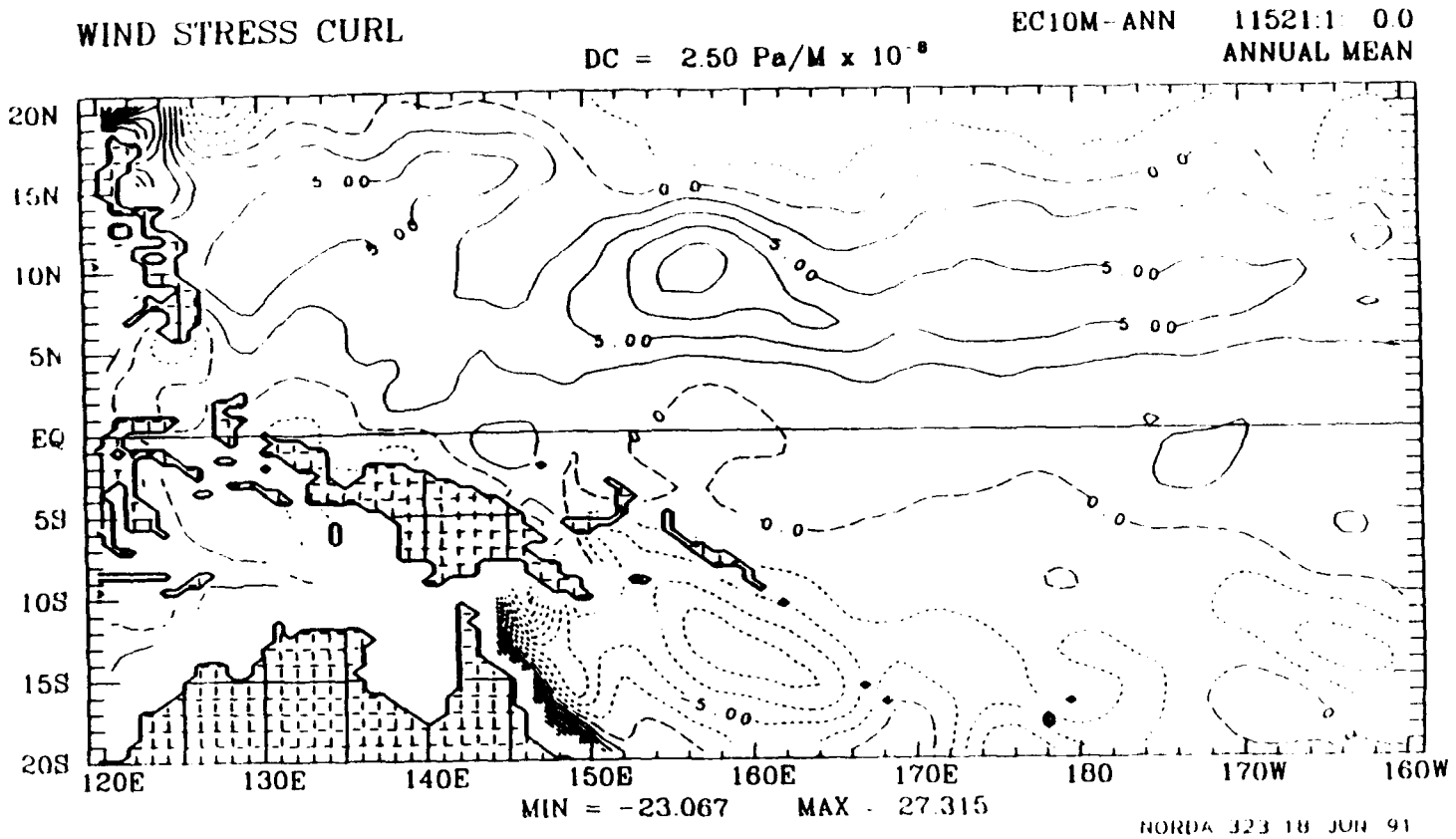

Fig. 7c Same as Fig. 7b but the LPCD is used.

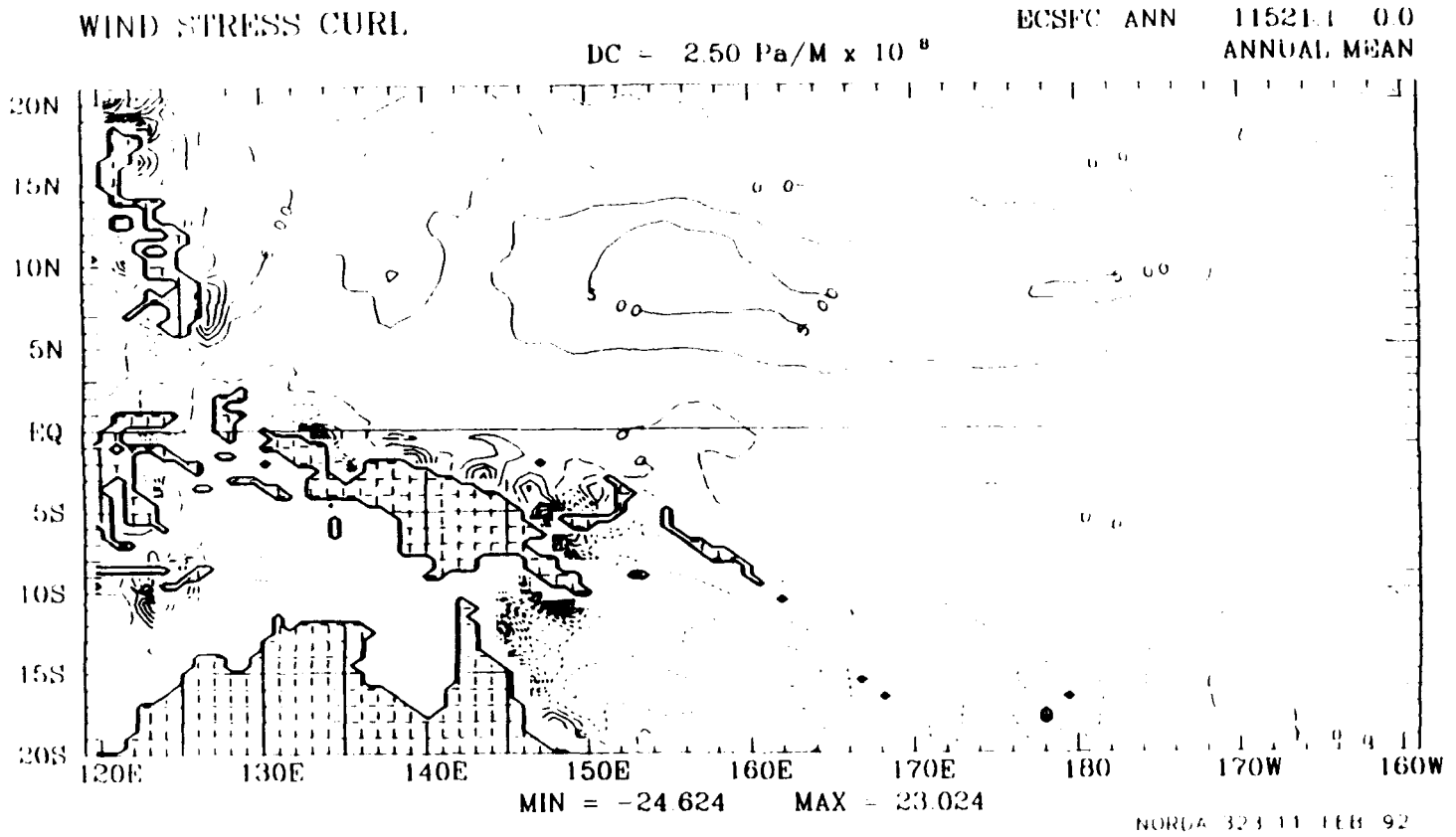

Fig. 7d Same as Fig. 7a but for the surface wind stress curls.

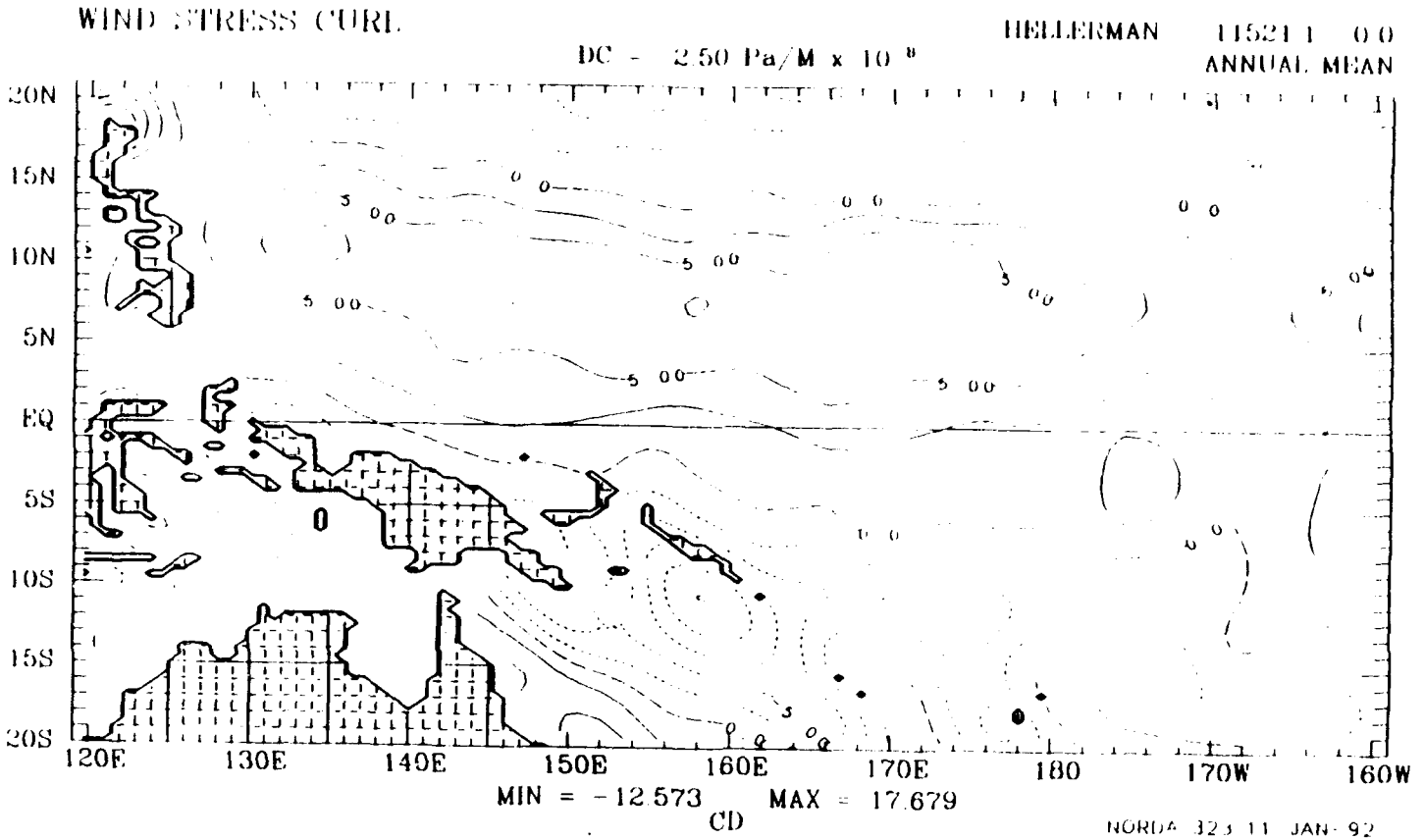

Fig. 7e Same as Fig. 7a but for HR wind stress curls.

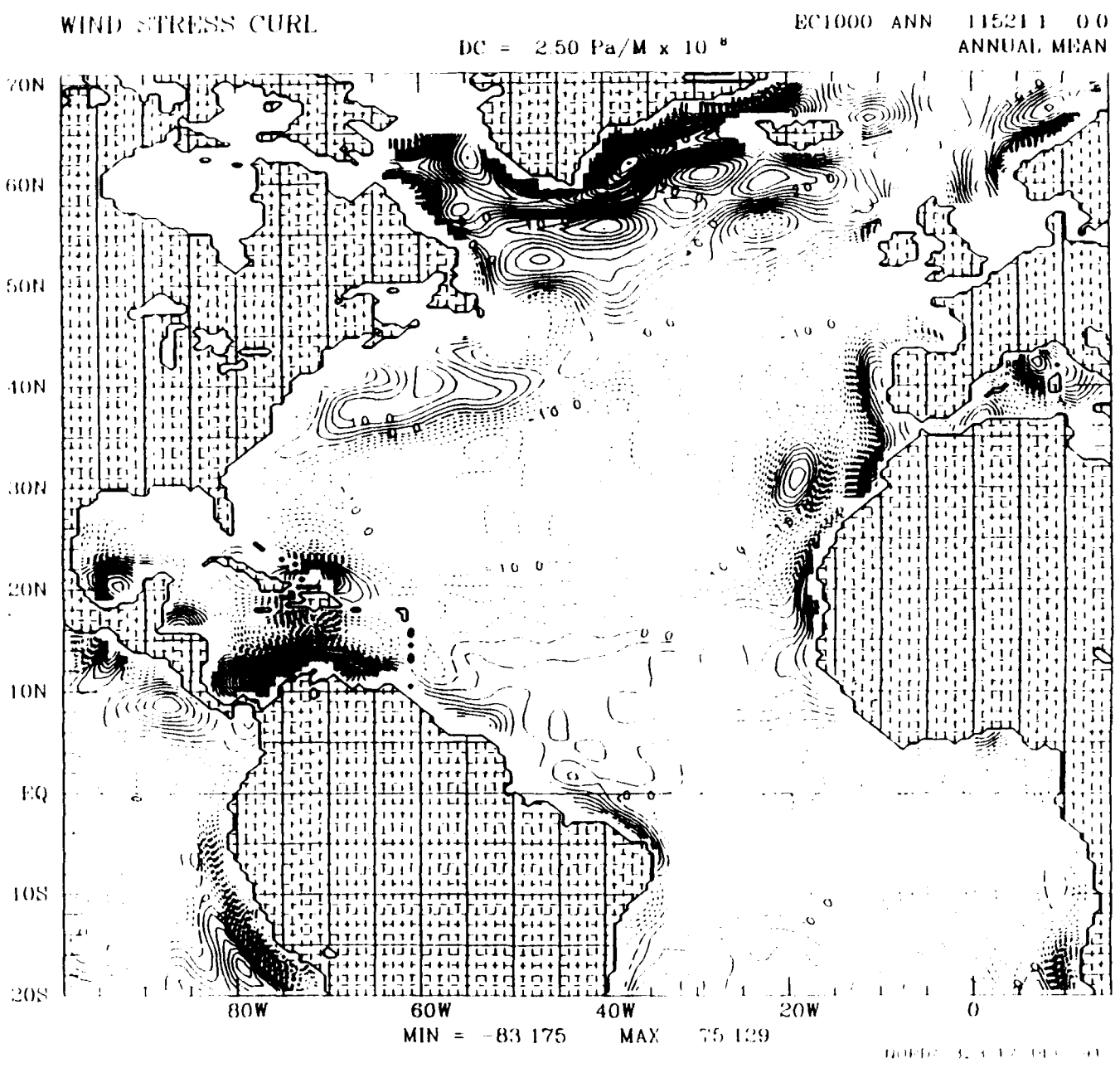

Fig. 8a Annual mean curl of the 1000 *mb* wind stress over NAB. The LCD is used. The contour interval is 25 $\times 10^{-8} dyn\ cm^{-3}$. The positive (negative) values are solid (dashed).

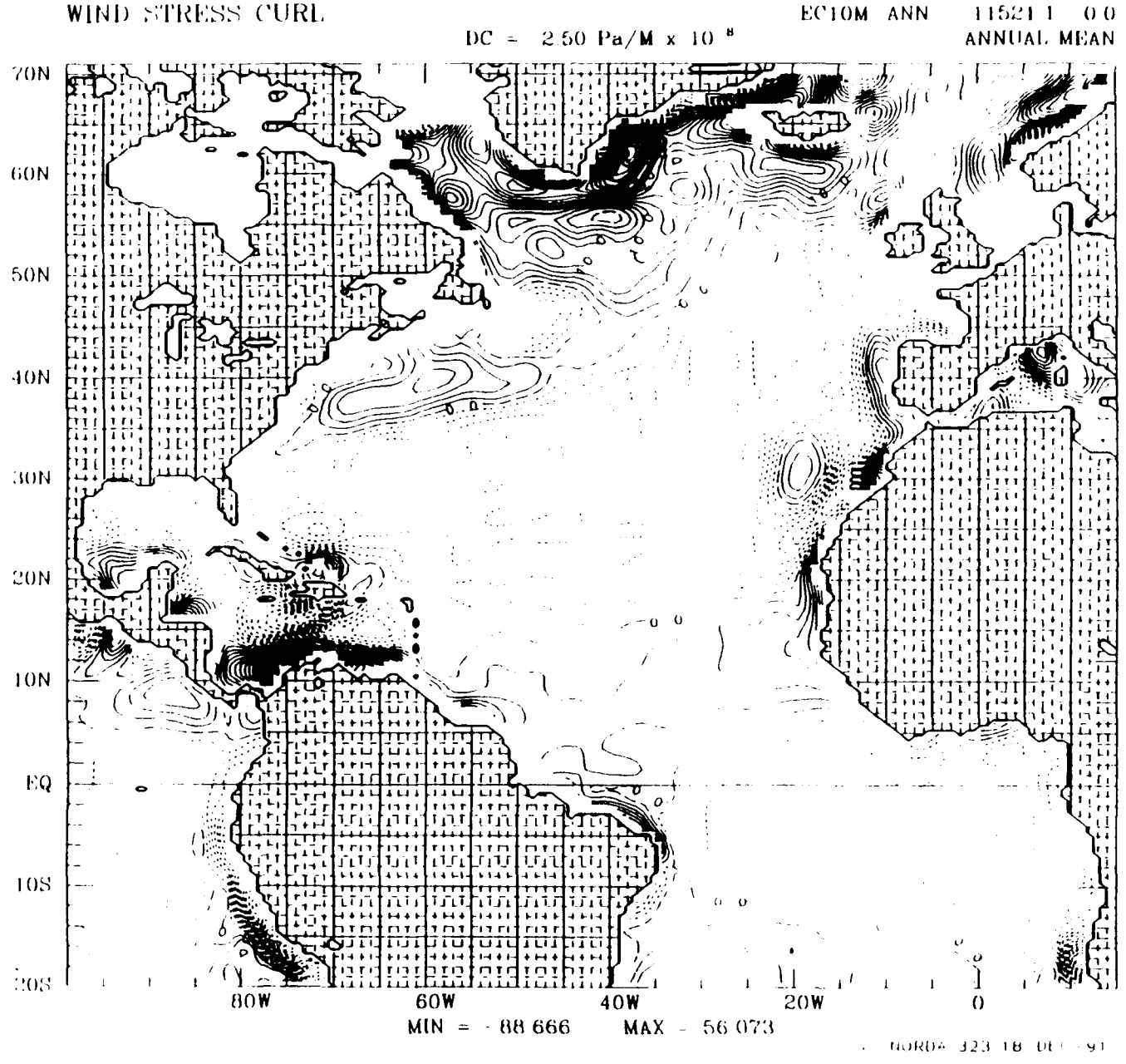

Fig. 8b Same as Fig. 8a but for 10 *m* height wind stress curls.

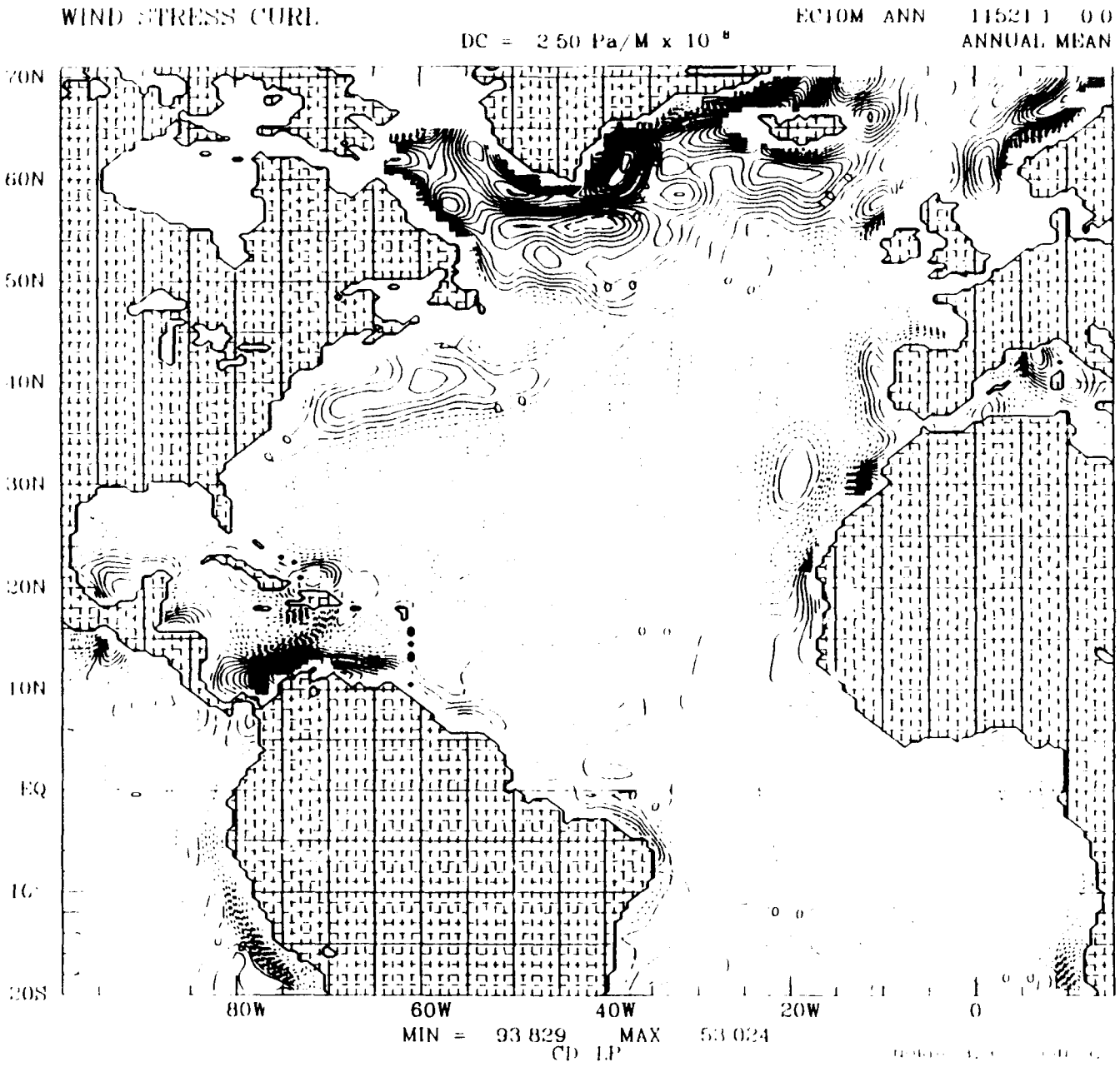

Fig. 8c Same as Fig. 8b but the LPCD is used.

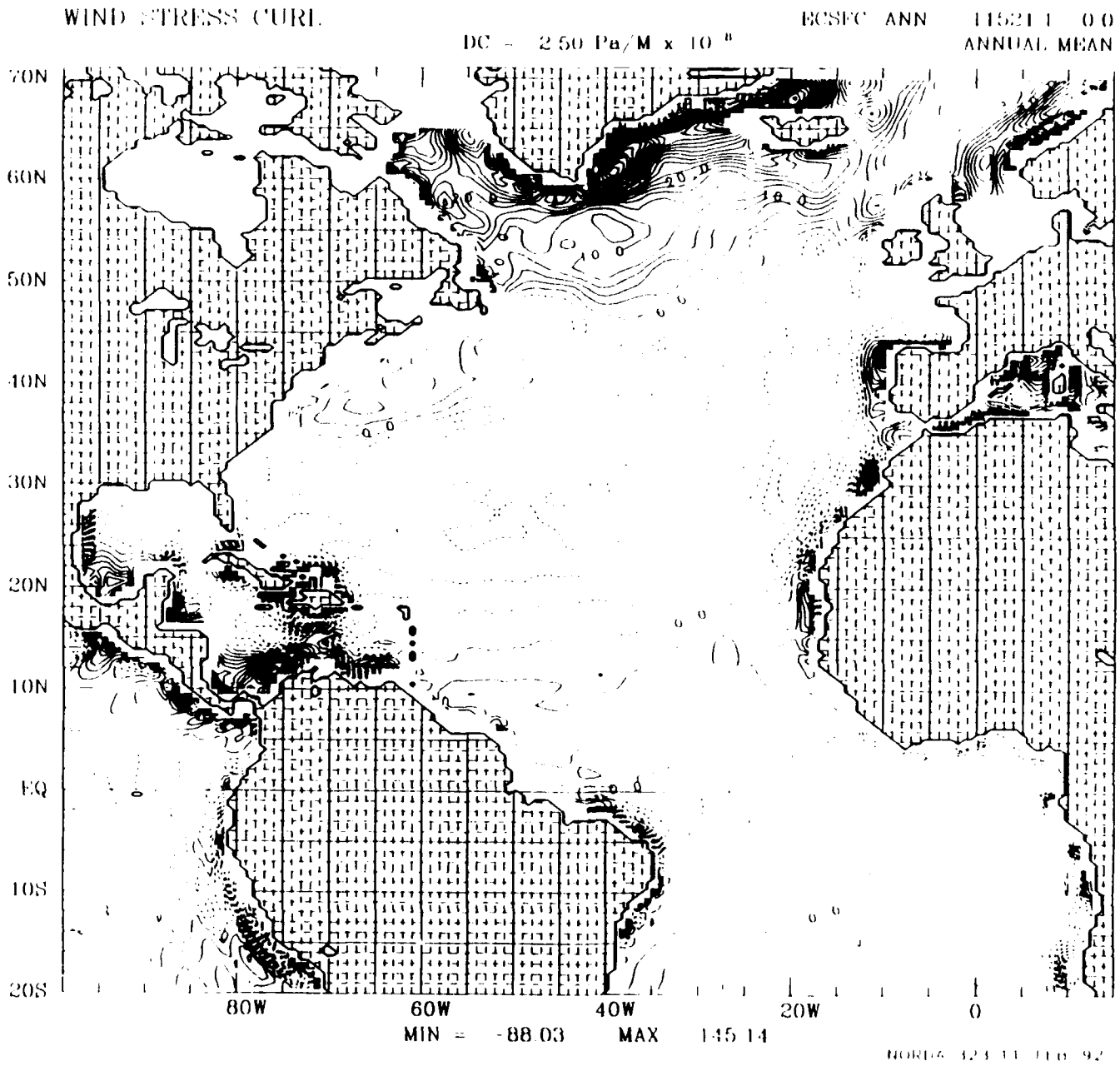

Fig. 8d Same as Fig. 8a but for the surface wind stress curls.

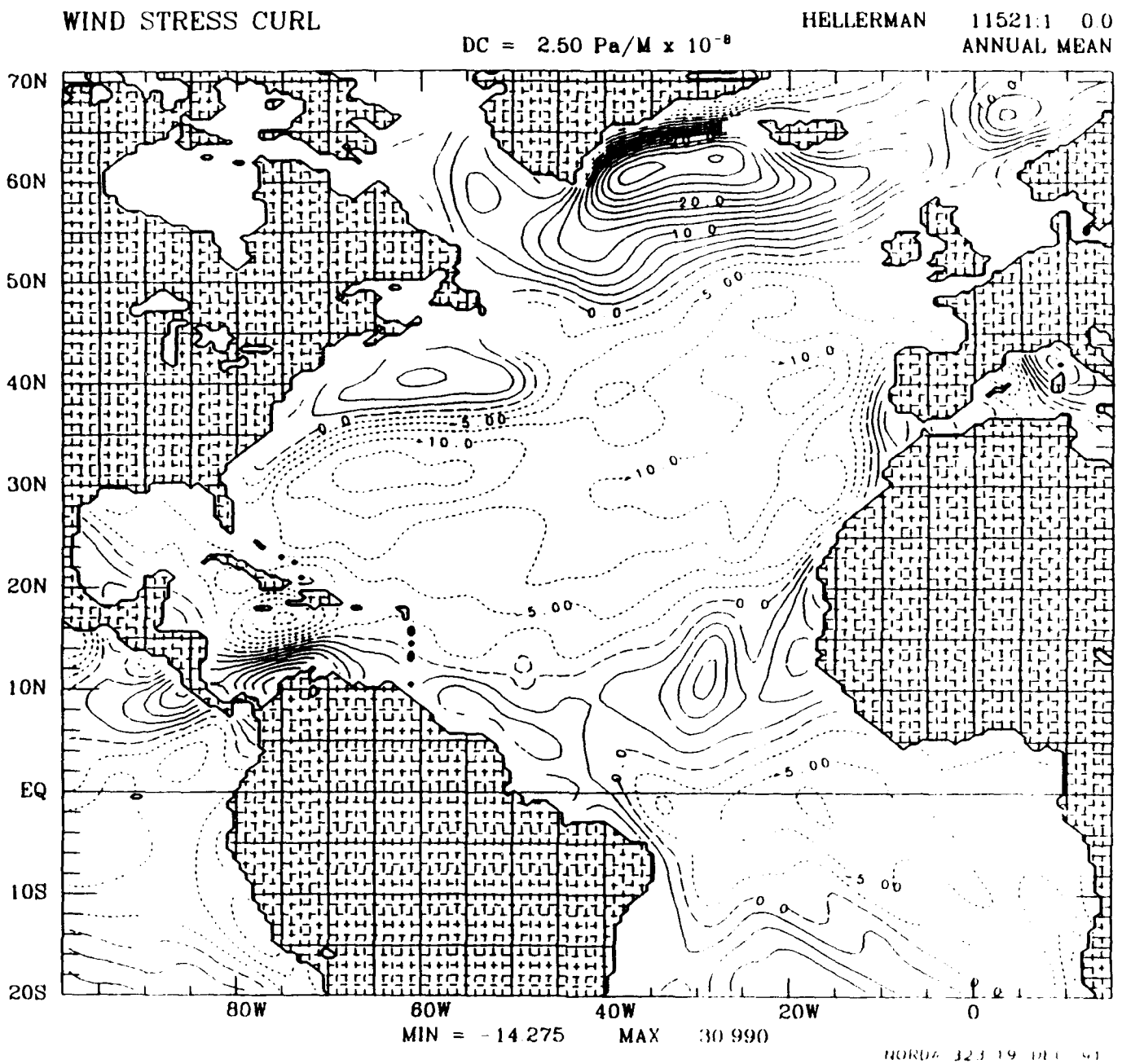

Fig. 8e Same as Fig. 8a but for HR wind stress curls.

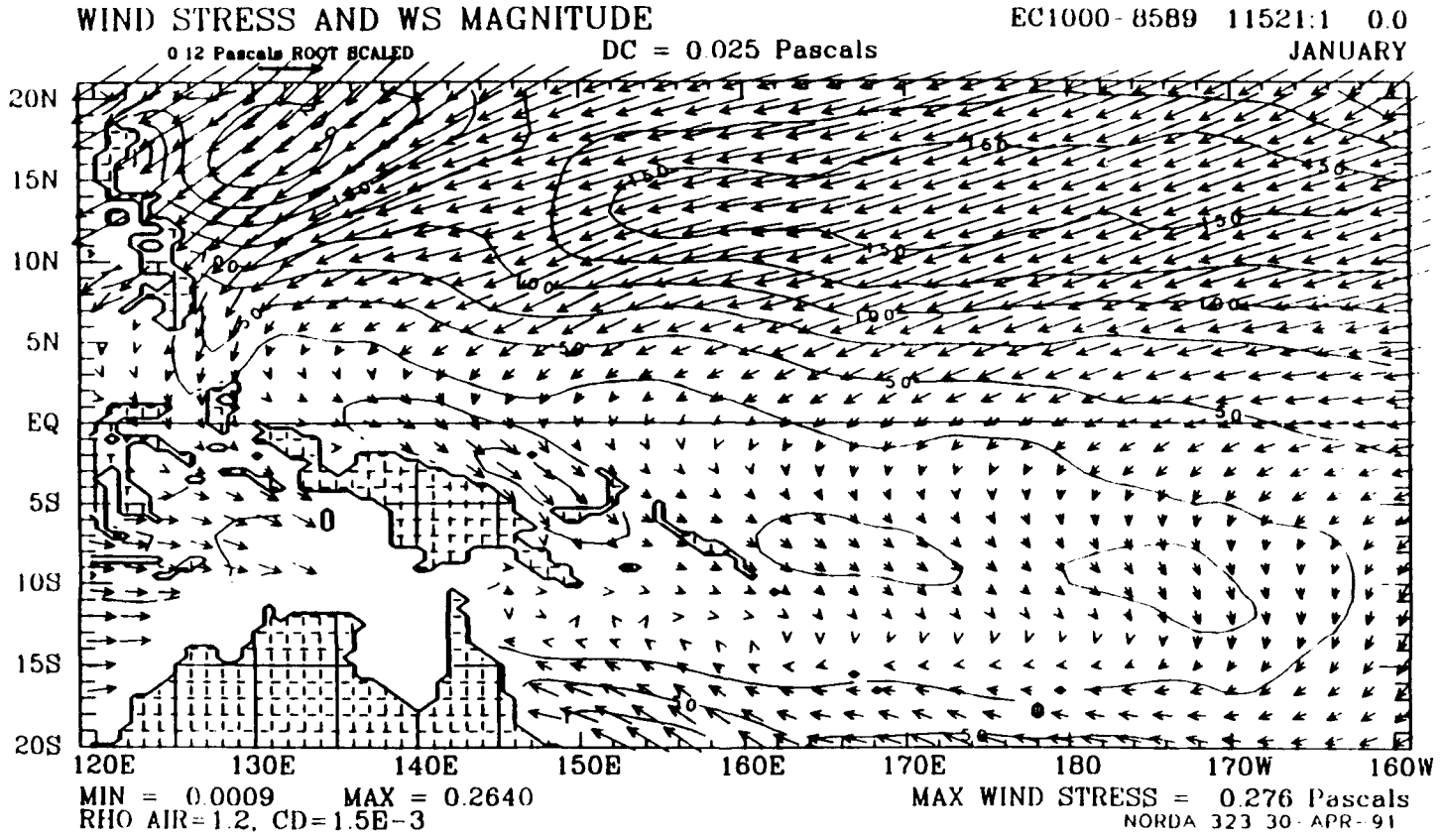

Fig. 9a January 1000 *mb* mean wind stress vectors and magnitudes over WEP. The LCD is used. The contour interval is 0.25 *dyn cm*$^{-2}$. The arrow at top left corresponds to 1.25 *dyn cm*$^{-2}$.

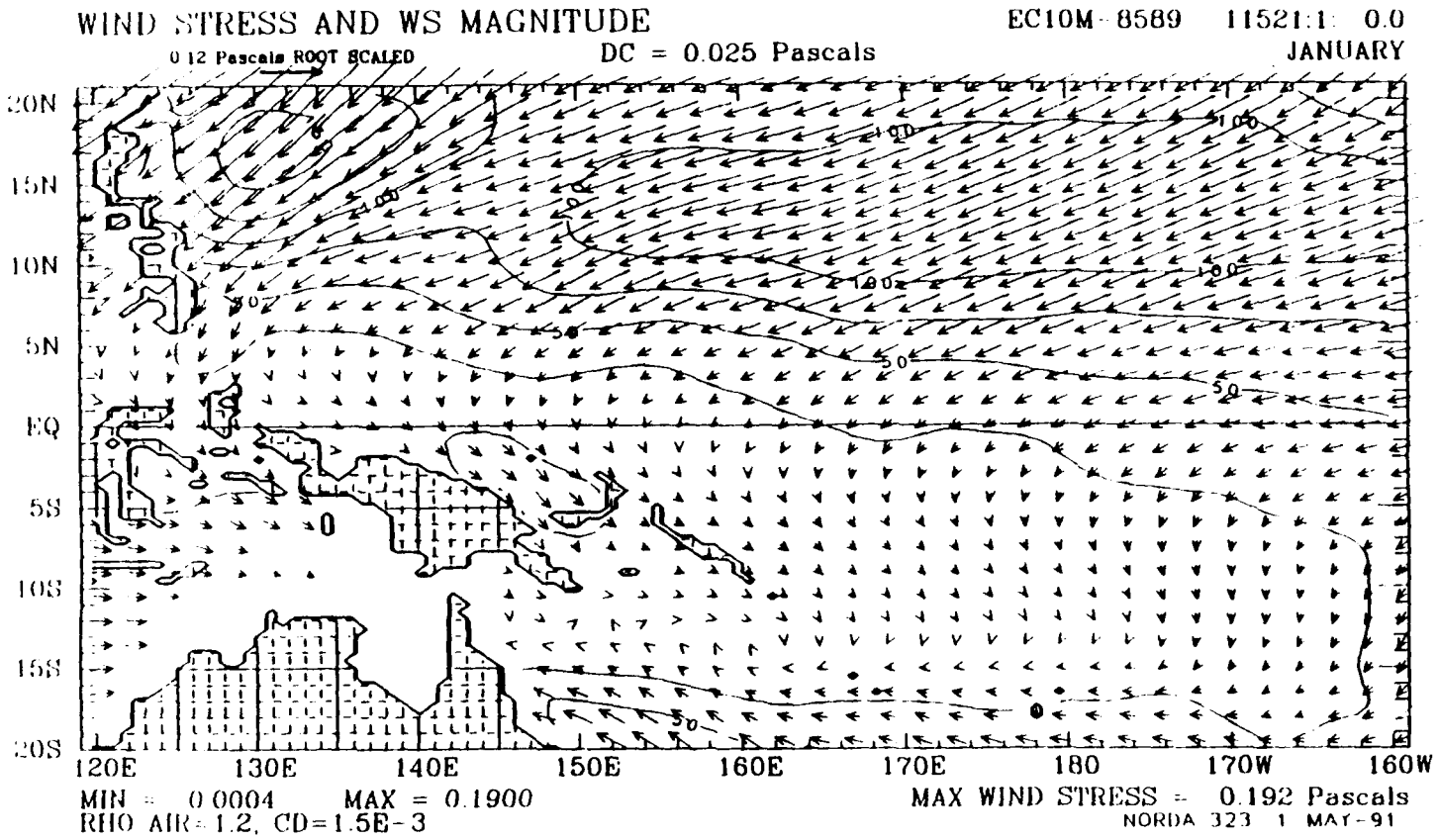

Fig. 9b Same as Fig. 9a but for 10 m height wind stress.

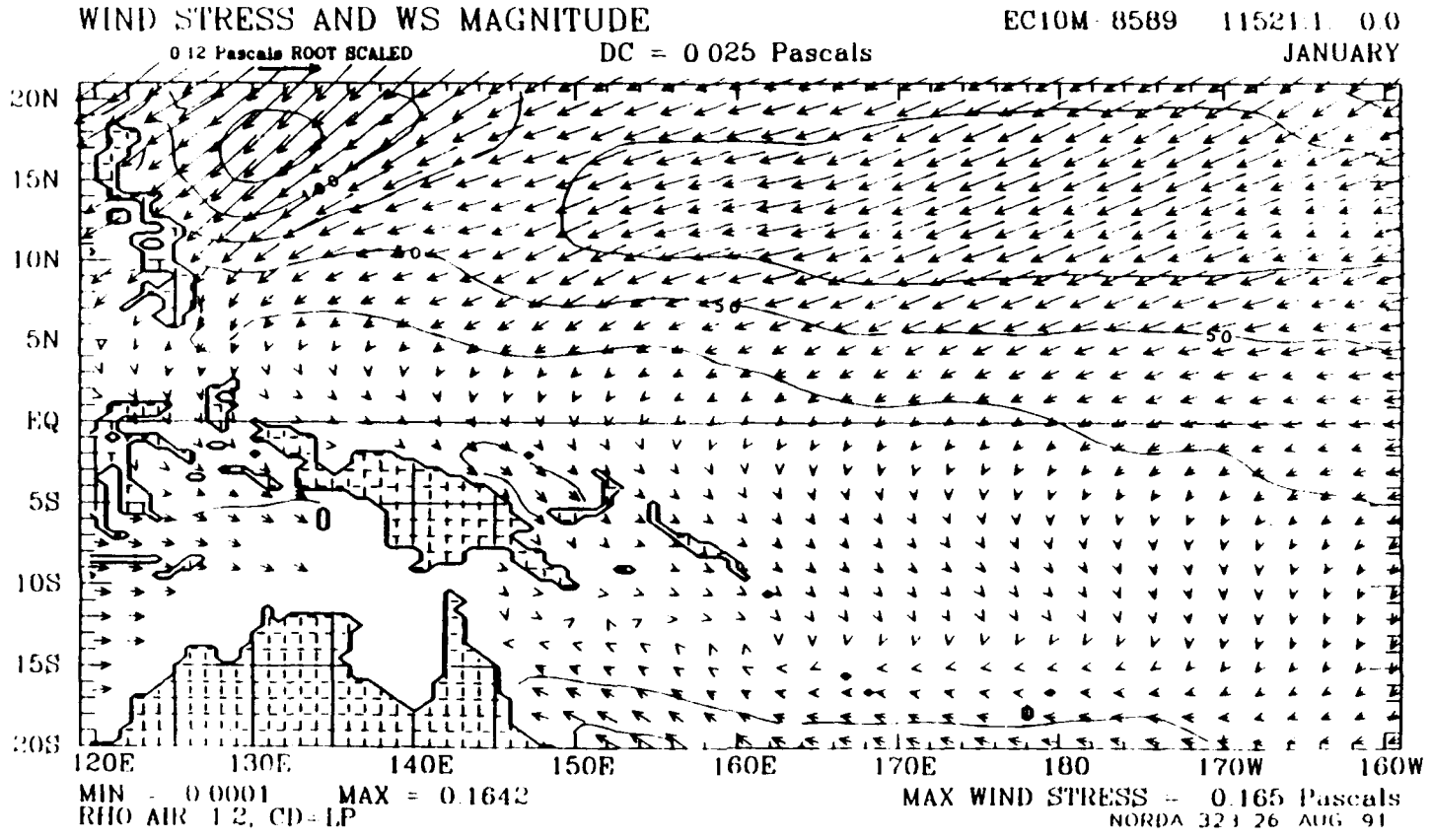

Fig. 9c Same as Fig. 9b but LPCD is used.

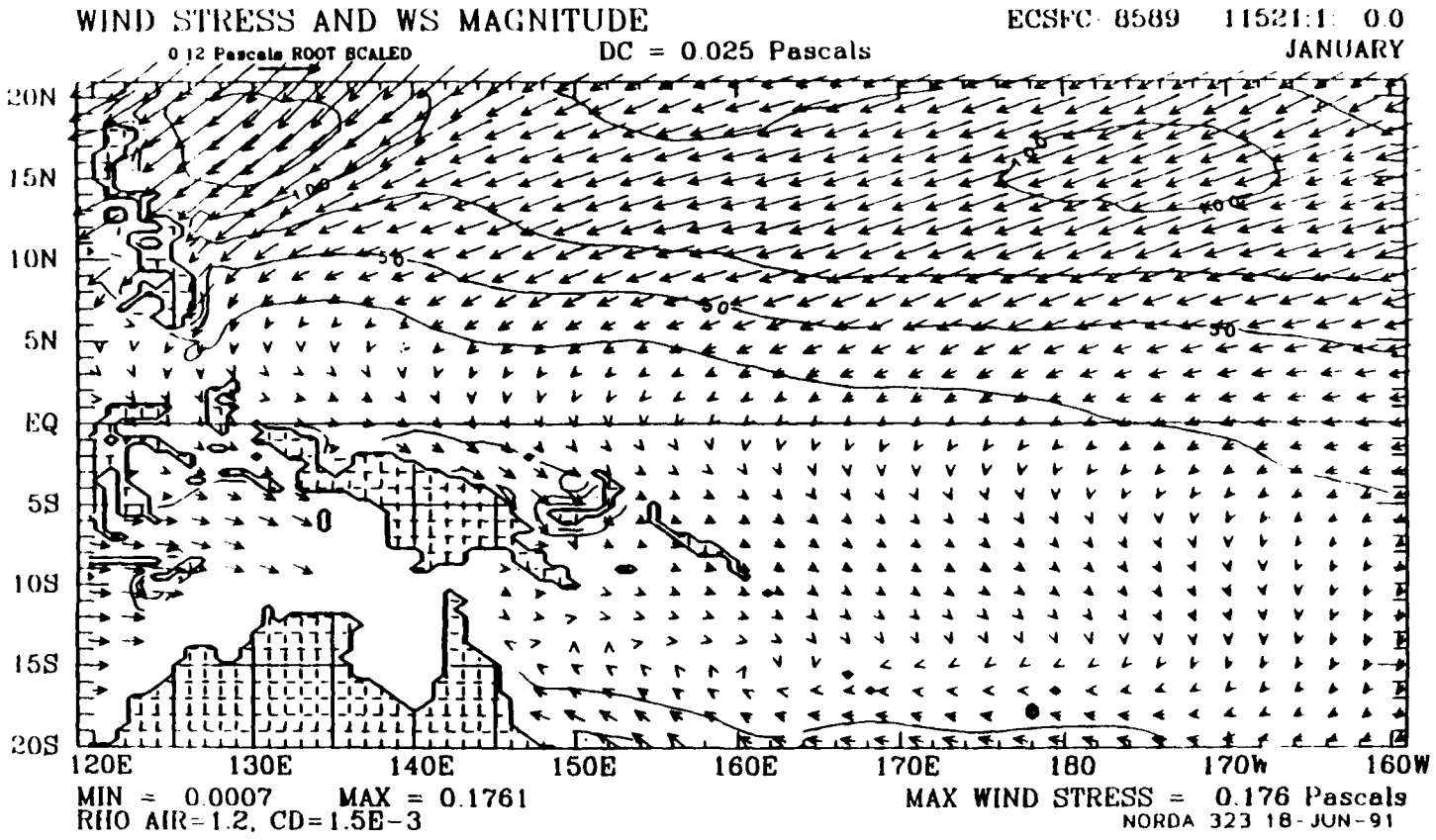

Fig. 9d Same as Fig. 9a but for the direct surface stress.

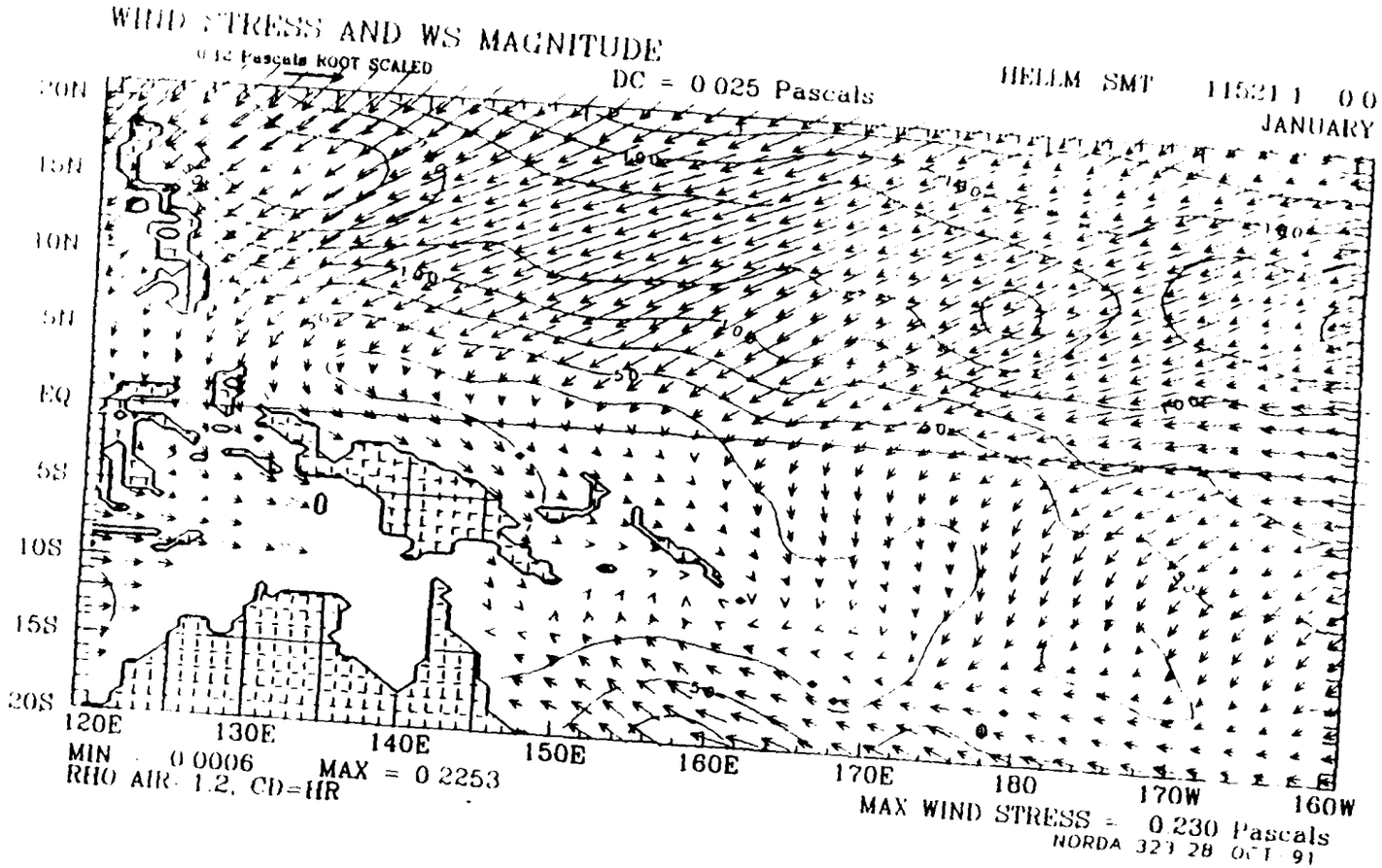

Fig. 9e Same as Fig. 9a but for HR wind stress.

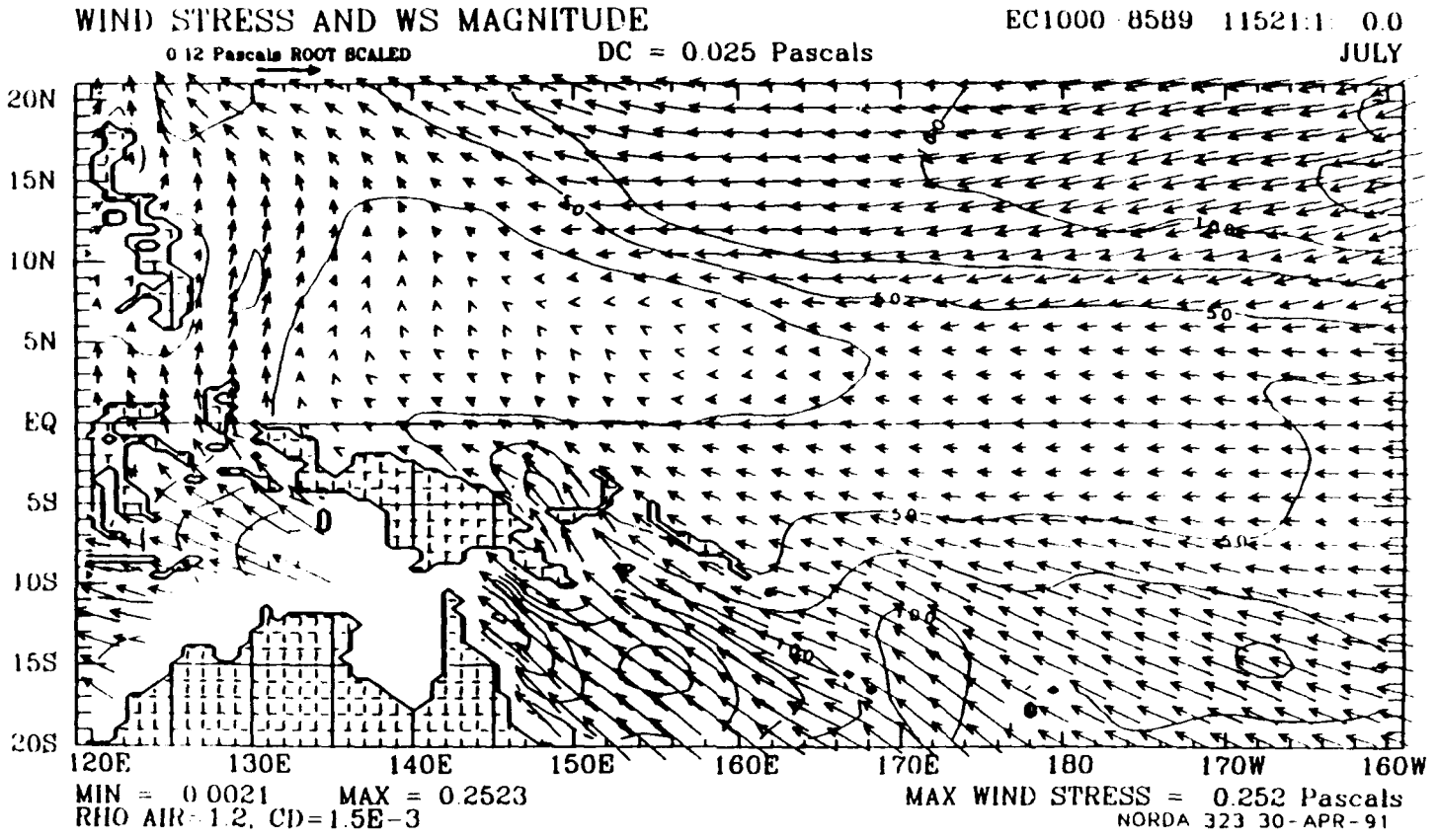

Fig. 10a Same as Fig. 9a but for July 1000 *mb* mean wind stress vectors and magnitudes.

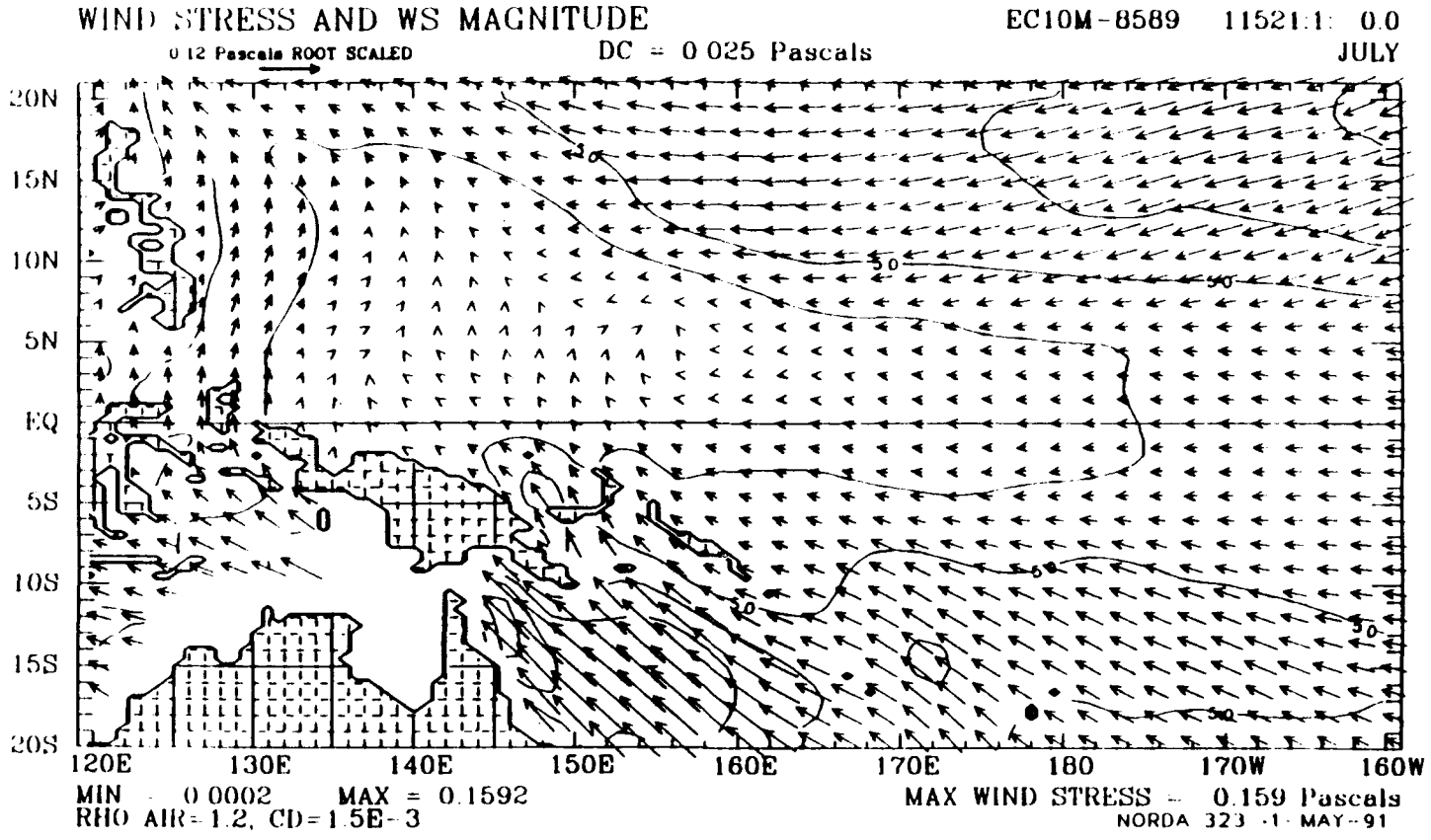

Fig. 10b Same as Fig. 10a but for 10 m height wind stress.

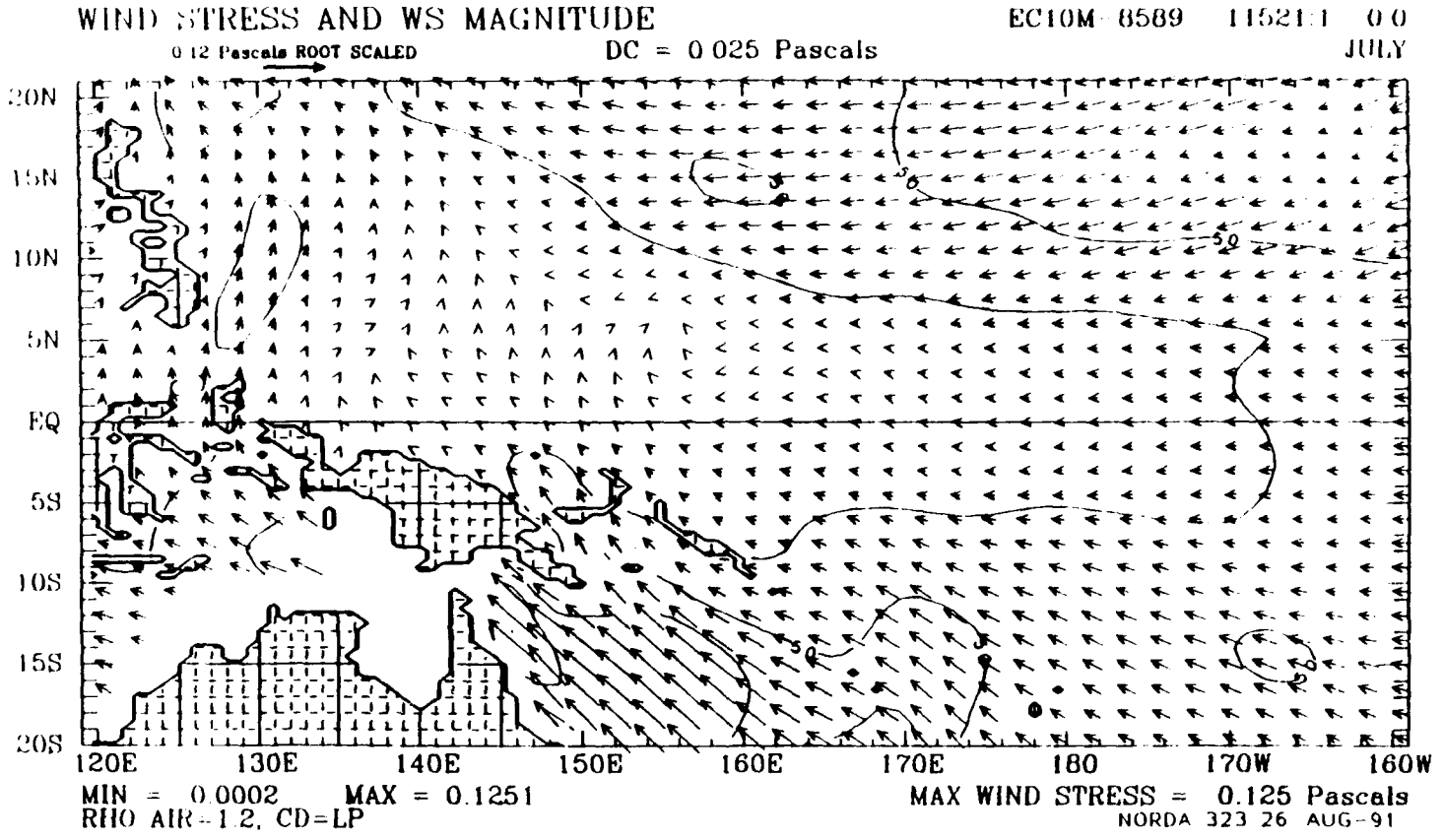

Fig. 10c Same as Fig. 10b but LPCD is used.

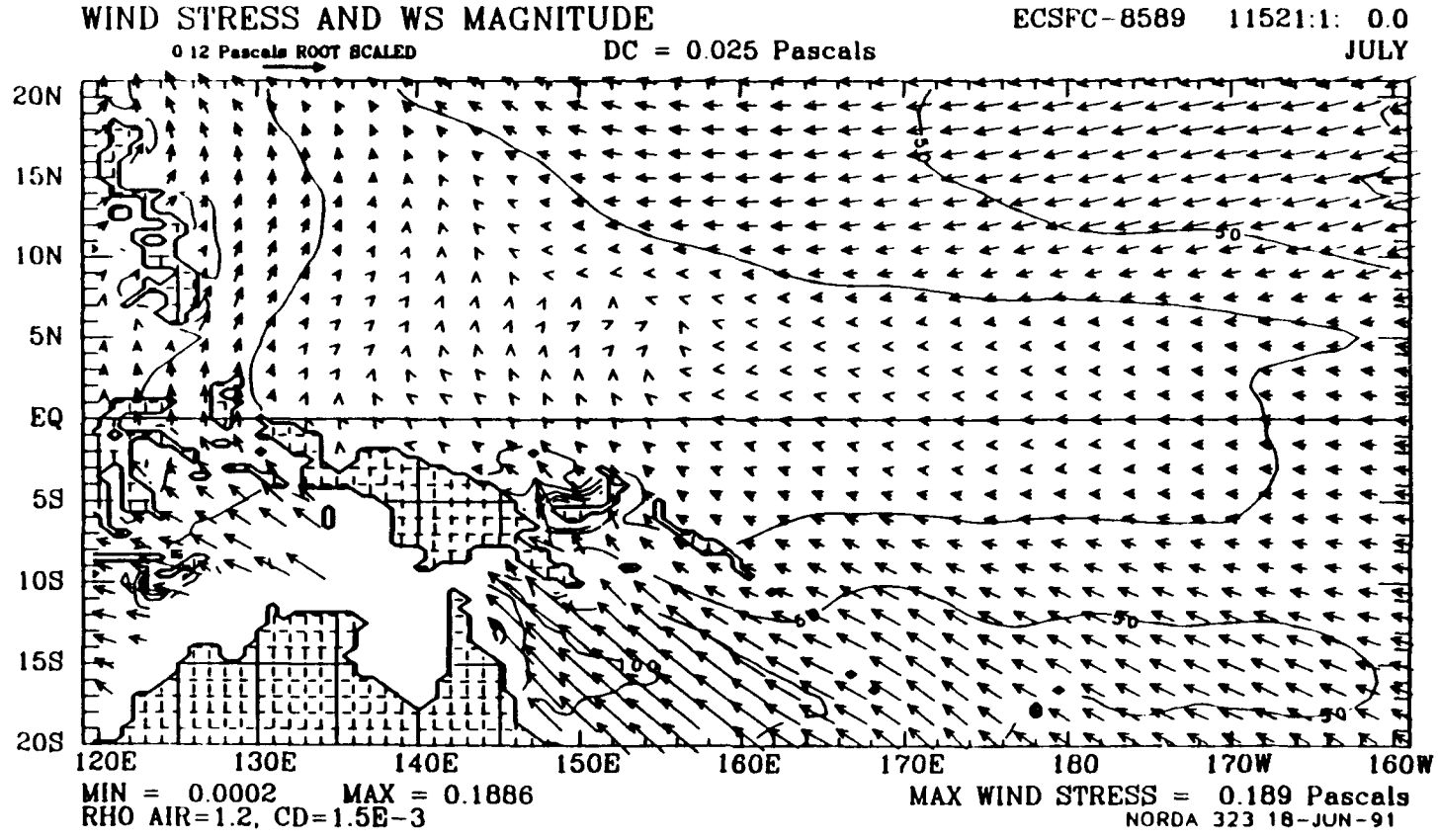

Fig. 10d Same as Fig. 10a but for the direct surface wind stress.

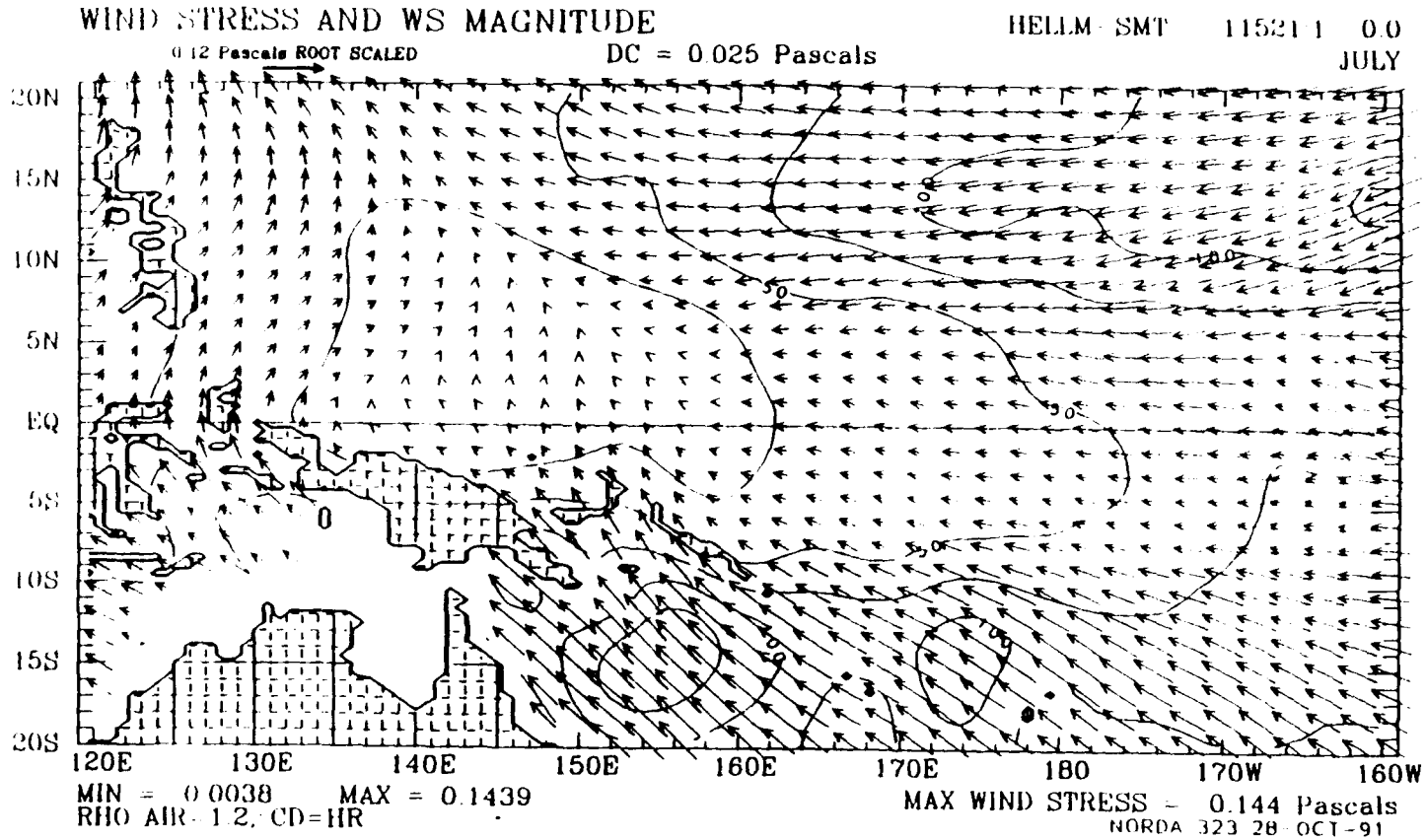

Fig. 10e Same as Fig. 10a but for HR wind stress.

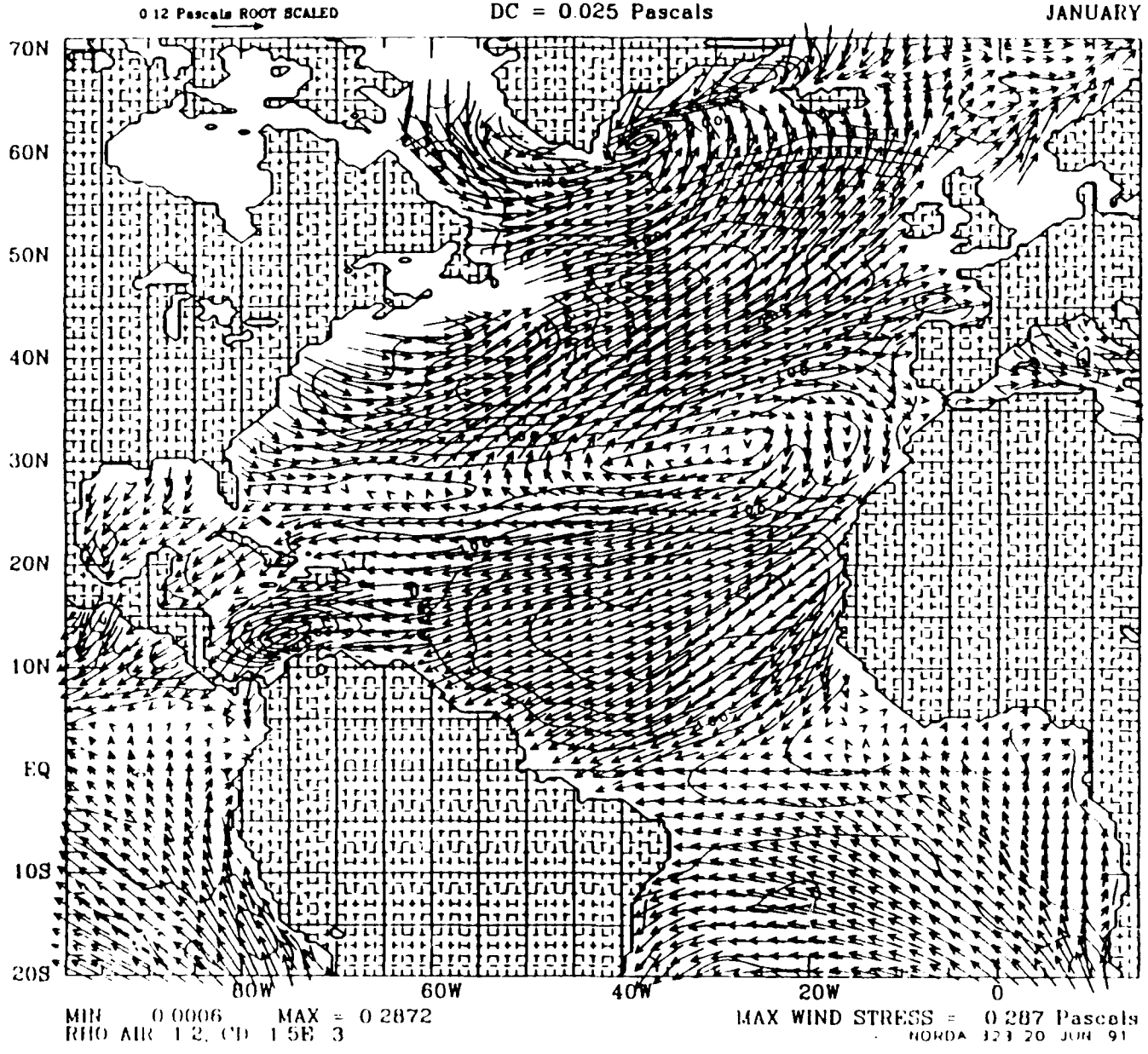

Fig. 11a Five year January 1000 *mb* mean wind stress vectors and magnitudes over NAB. The contour interval is 0.25 *dyn cm* $^{-2}$. The LCD is used. The arrow at top left corresponds to 1.25 *dyn cm* $^{-2}$.

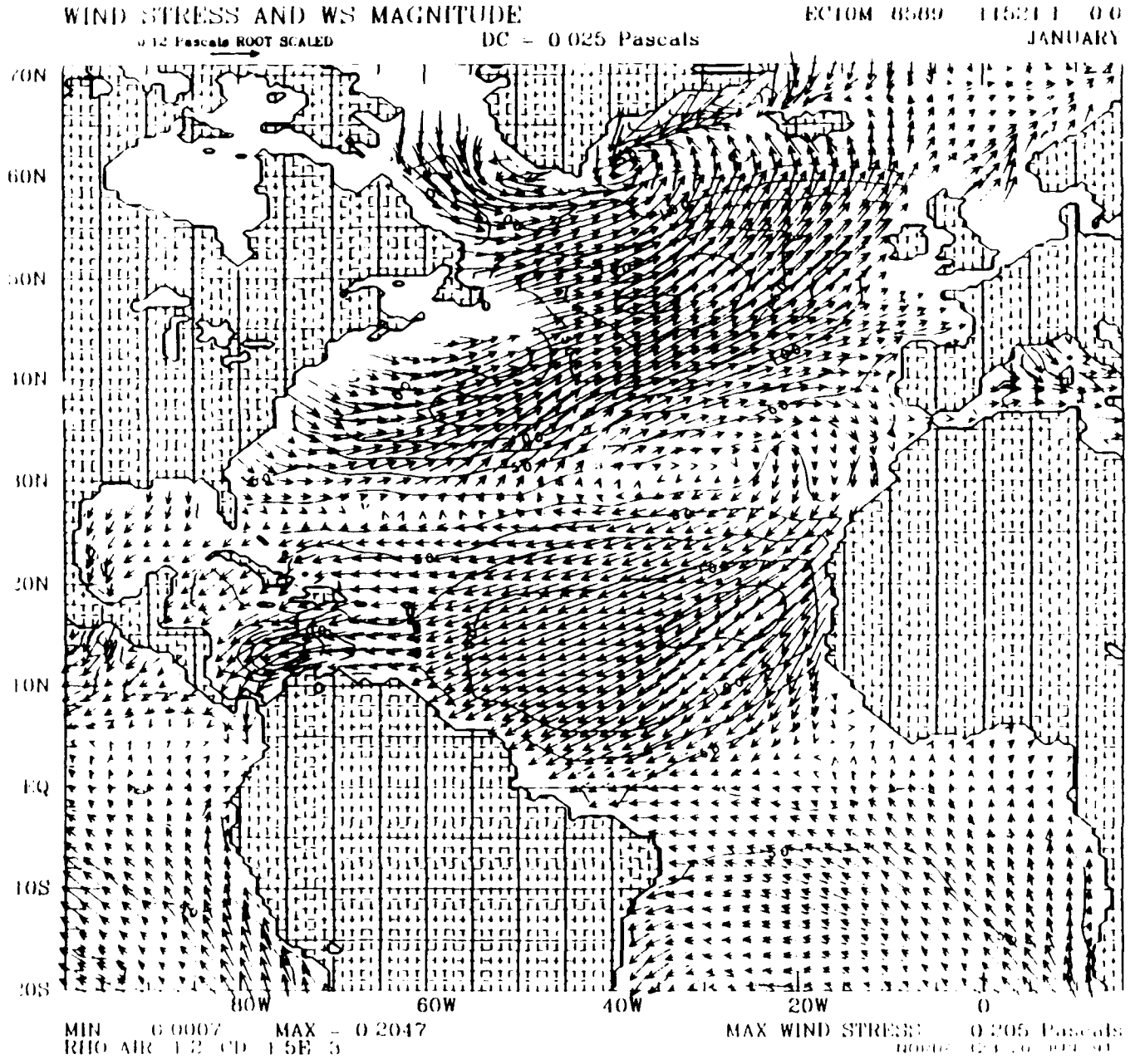

Fig. 11b Same as Fig. 11a but for the January 10 *m* height wind stress.

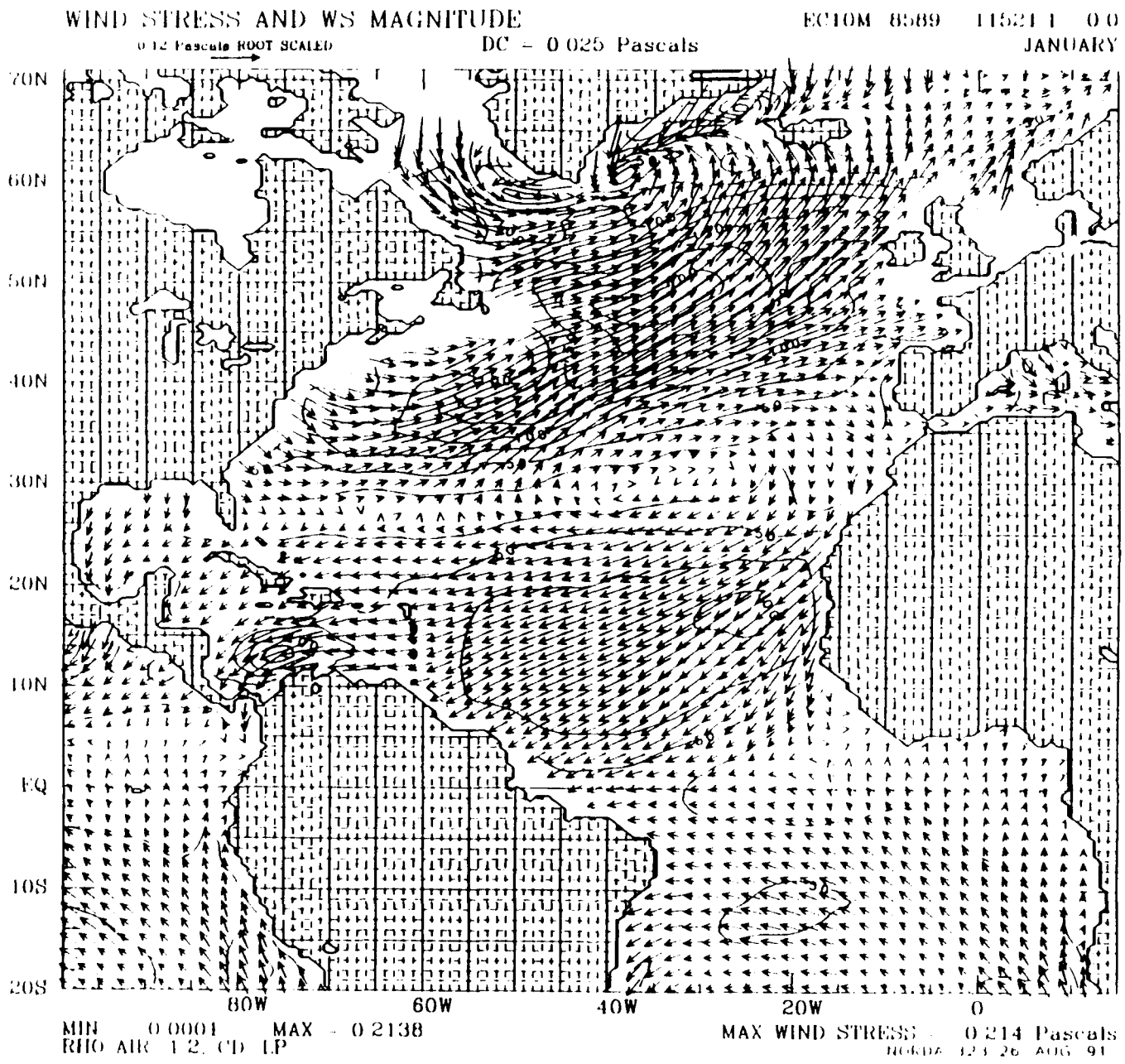

Fig. 11c Same as Fig. 11b but LPCD is used.

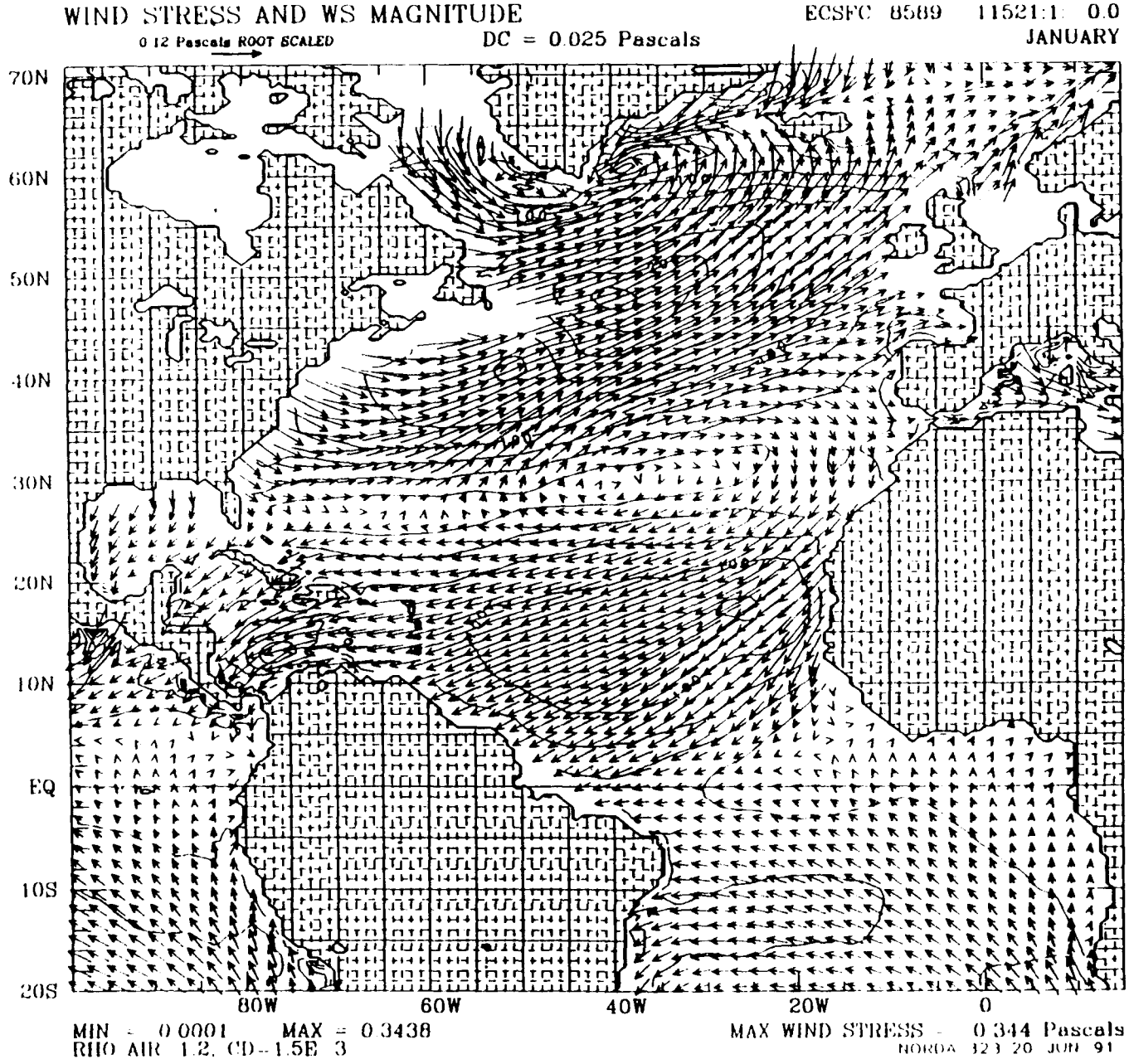

Fig. 11d Same as Fig. 11a but for the direct surface wind stress.

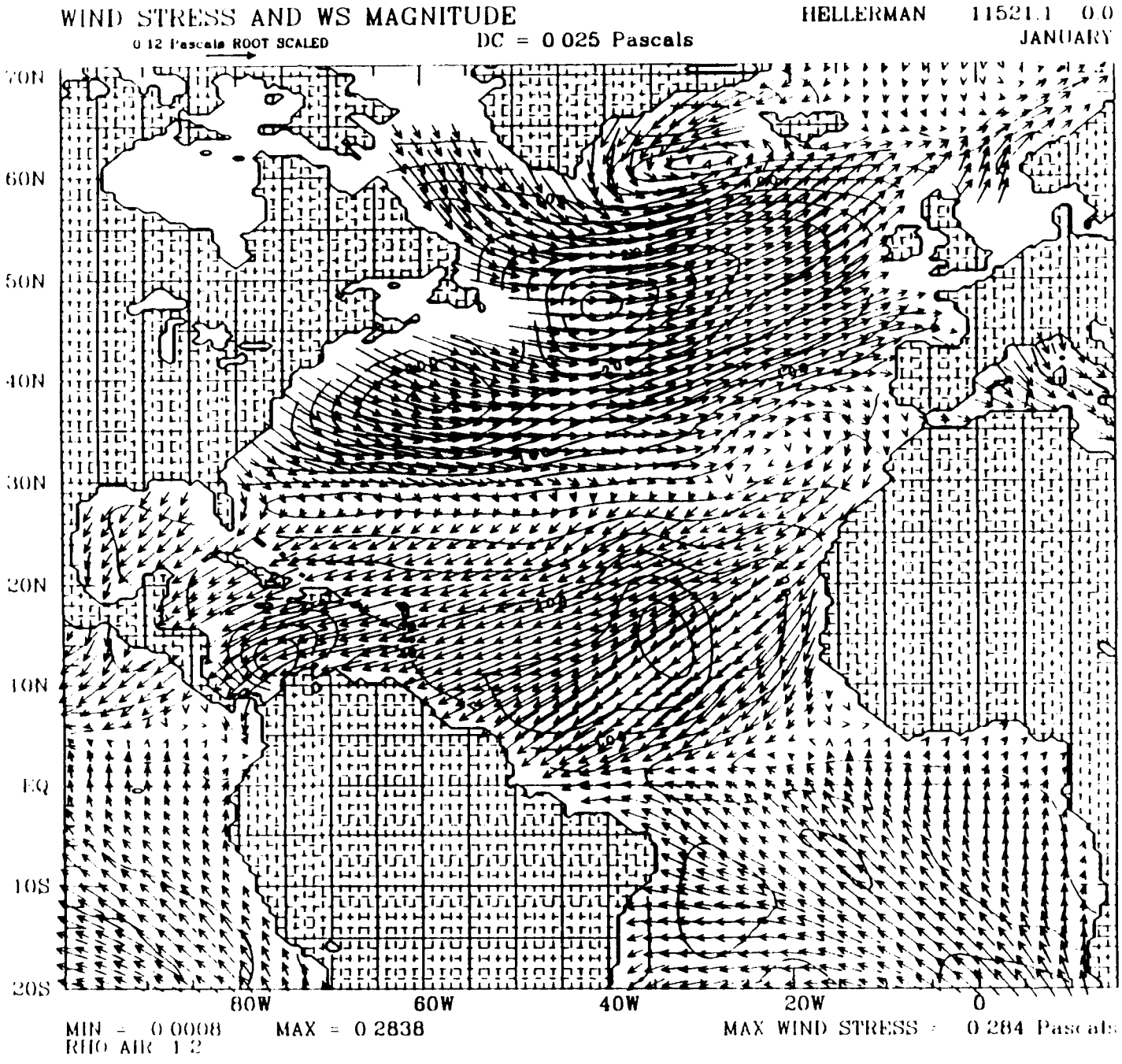

Fig. 11c Same as Fig. 11a but for HR wind stress.

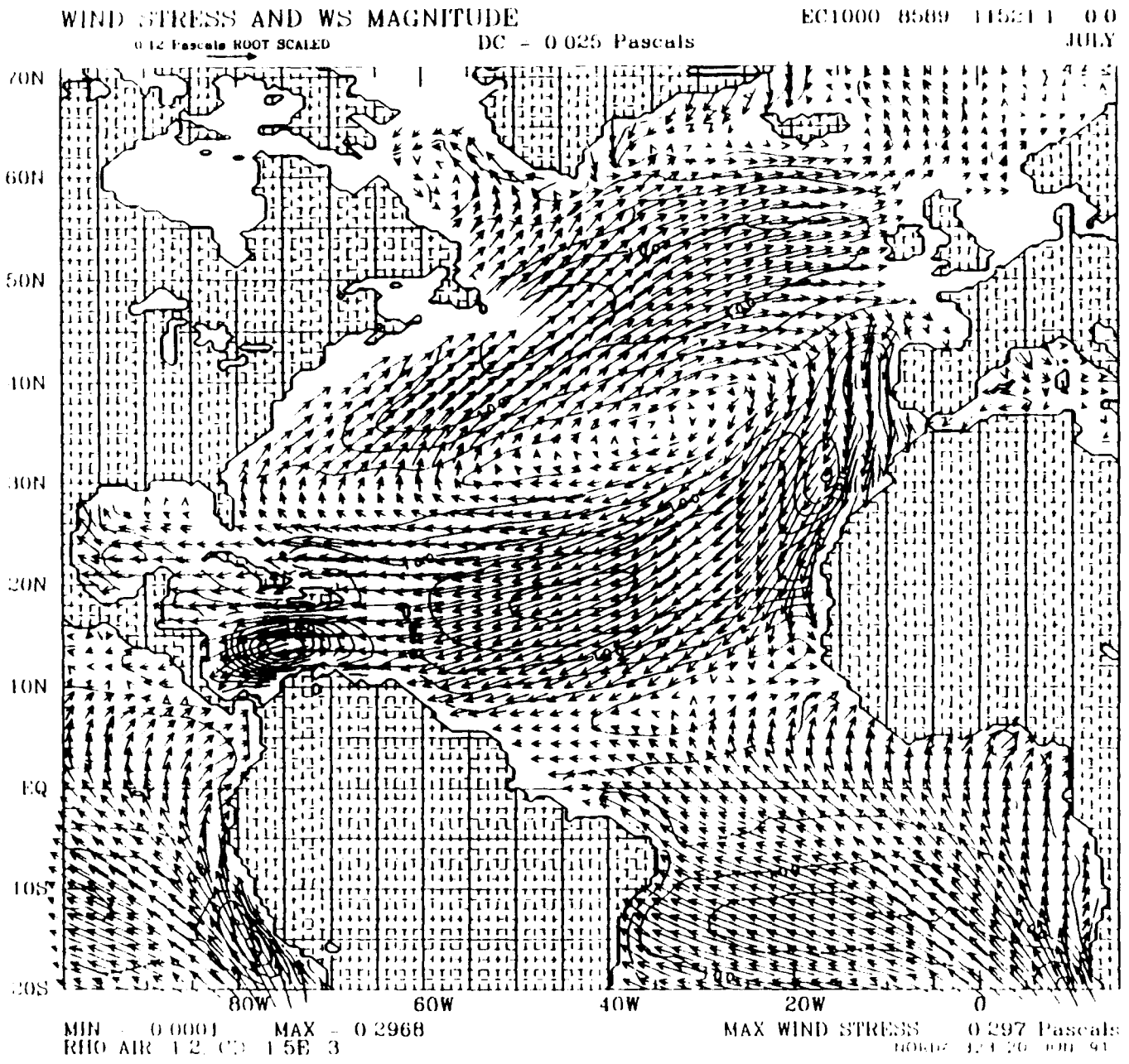

Fig. 12a Same as Fig. 11a but for July 1000 *mb* mean wind stress vectors and magnitudes over NAB.

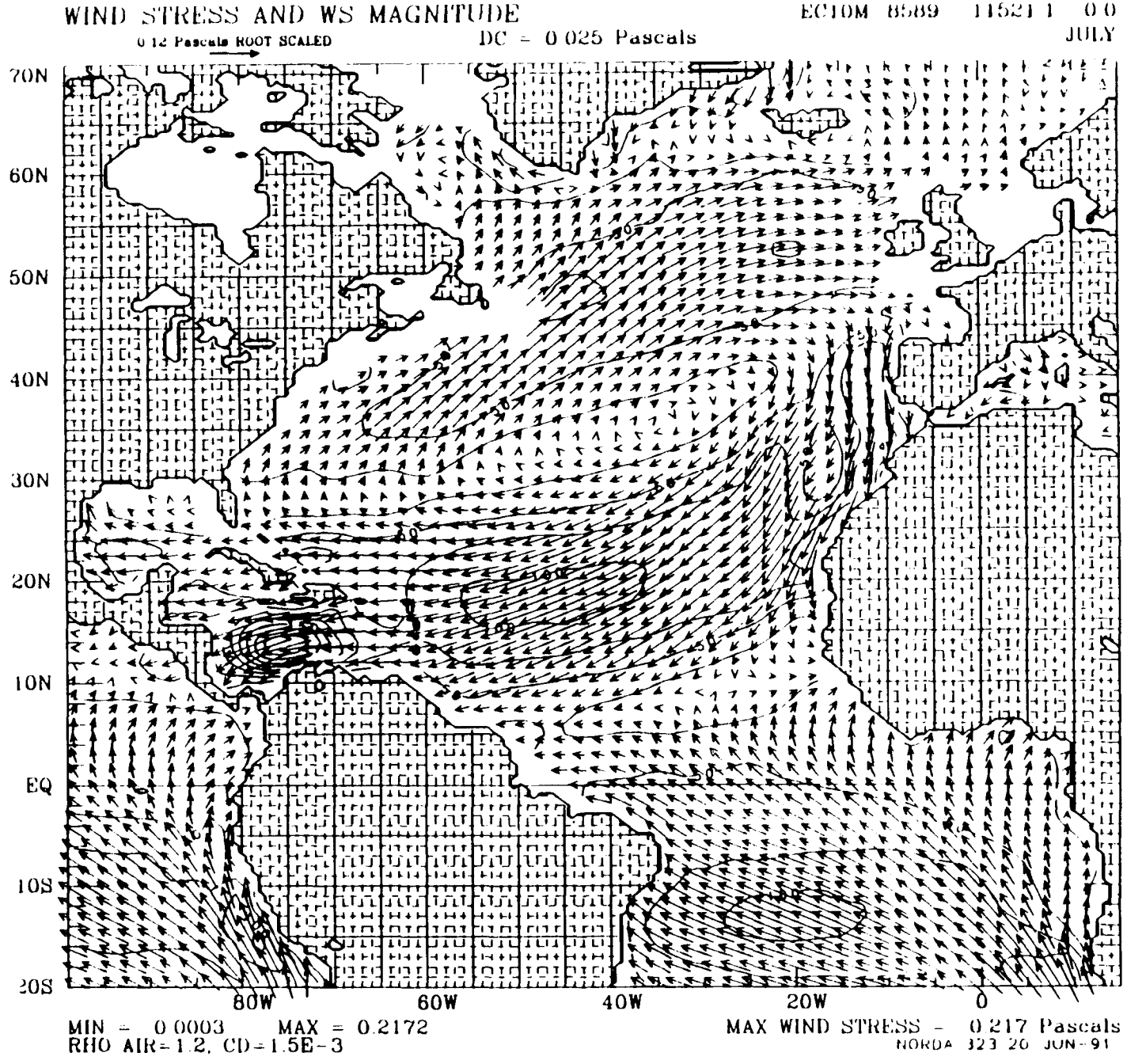

Fig. 12b Same as Fig. 12a but for July 10 *m* height wind stress.

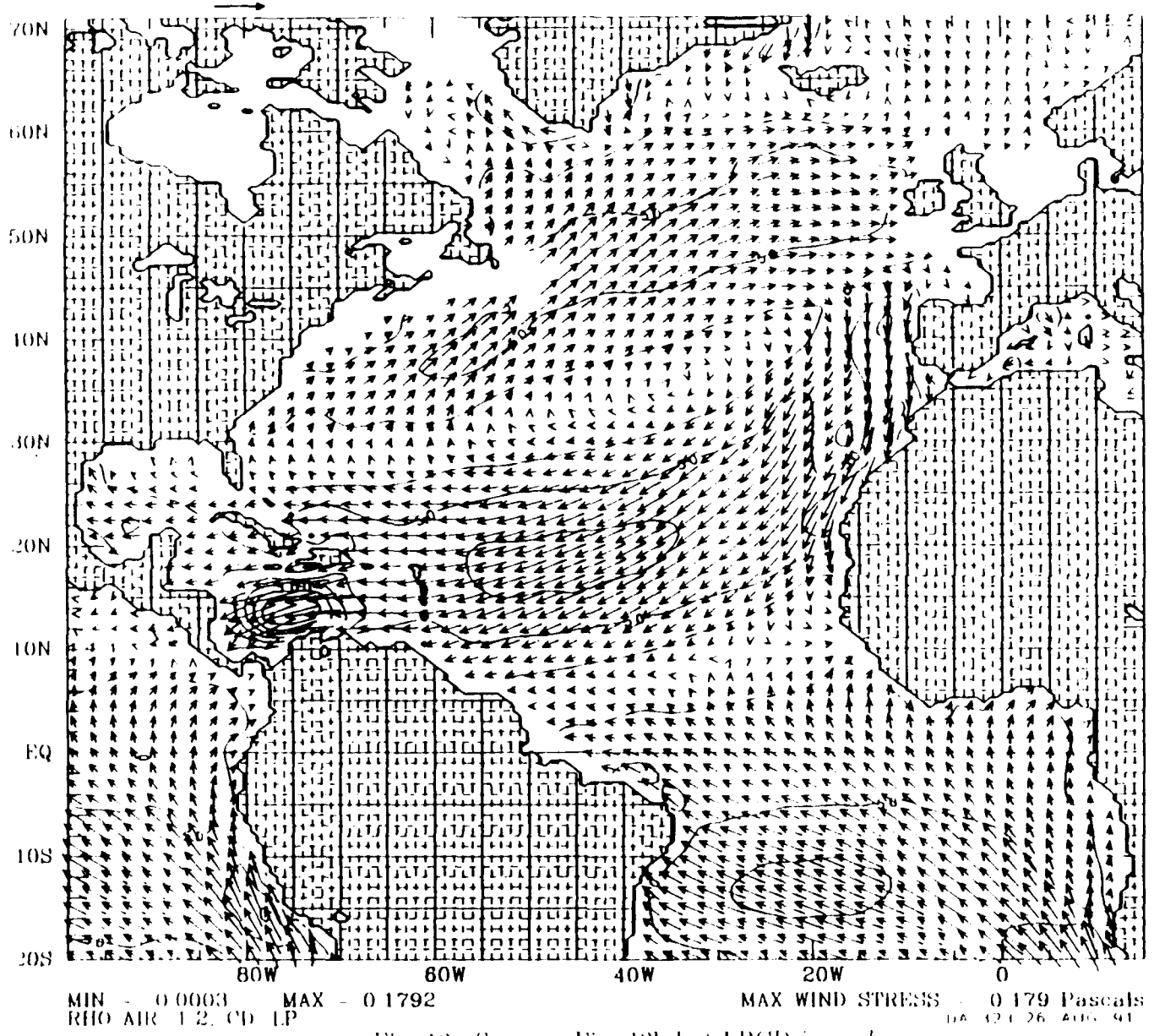

Fig. 12c Same as Fig. 12b but LPCD is used.

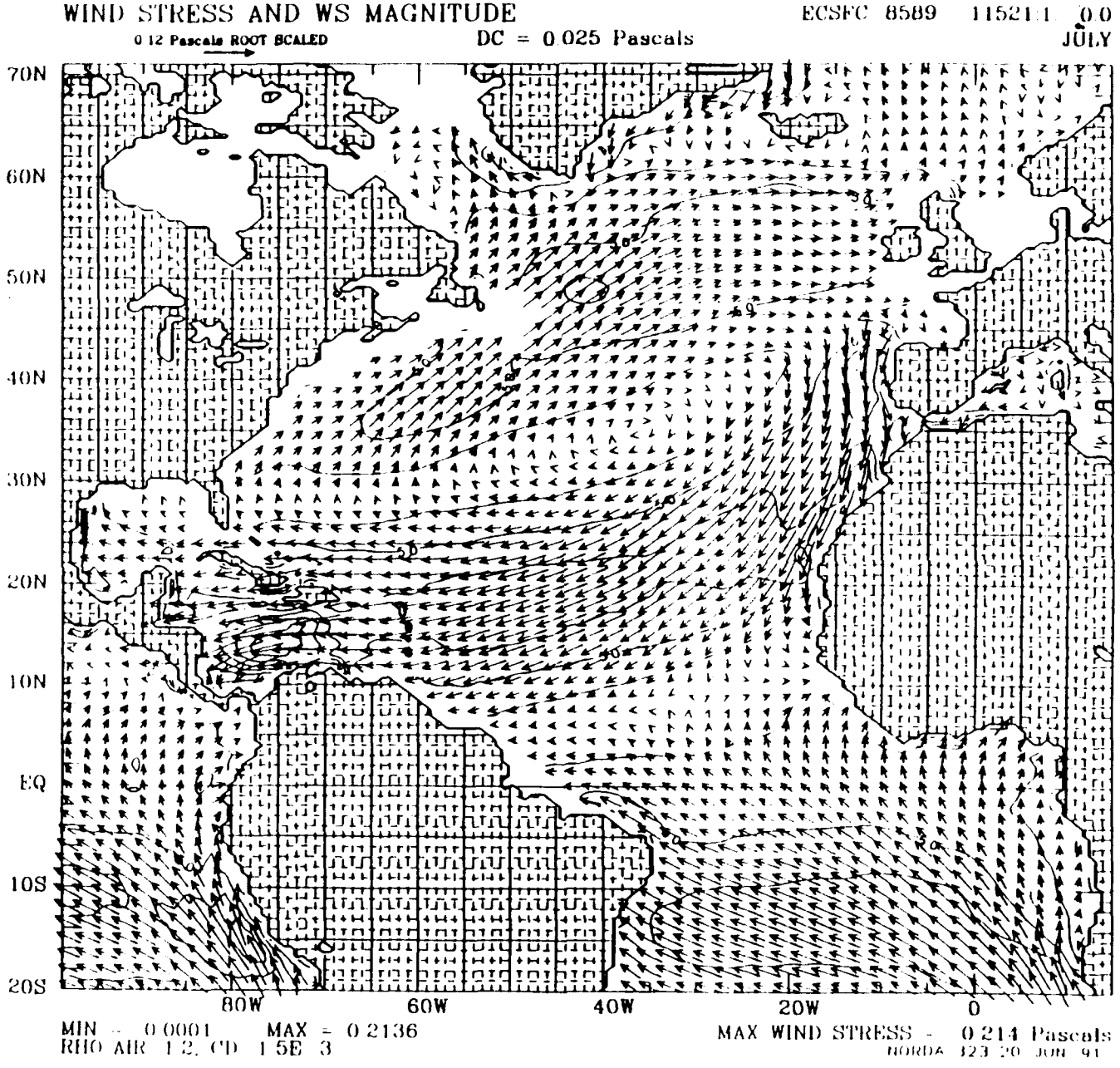

Fig. 12d Same as Fig. 12a but for the direct surface stress.

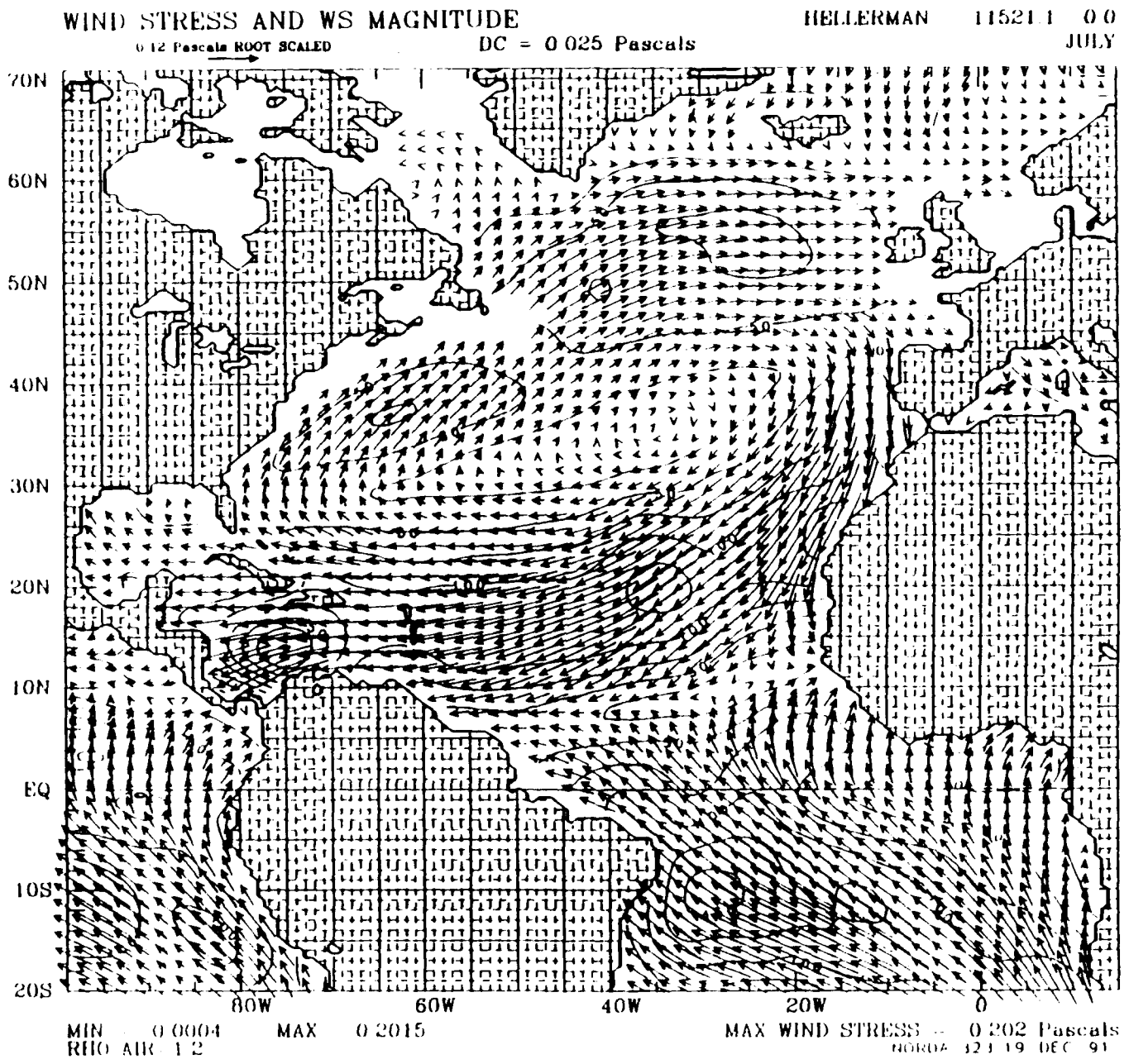

Fig. 12c Same as Fig. 12a but for the July HR wind stress.

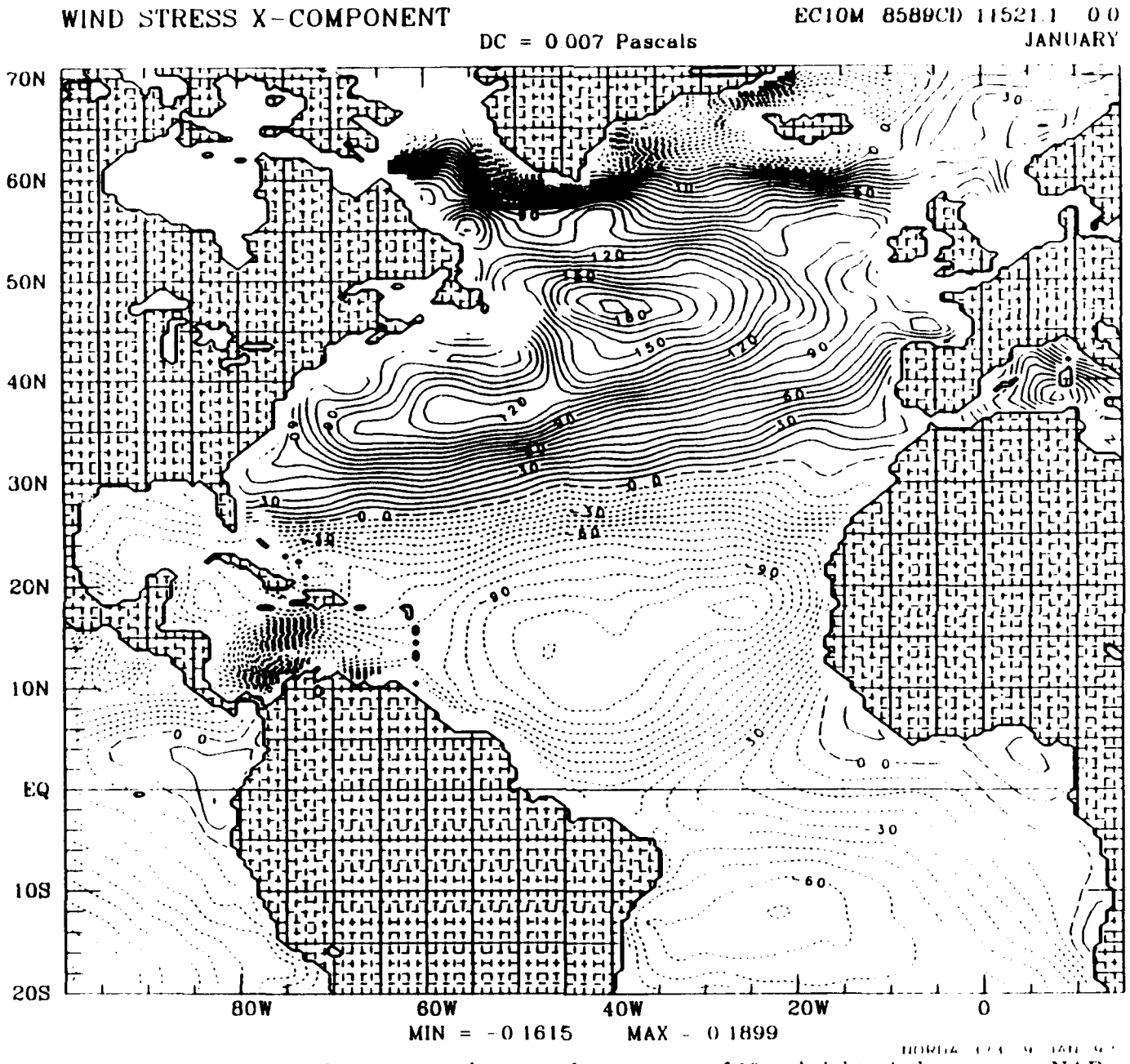

Fig. 13a January zonal mean annual eastward component of 10 m height wind stress over NAB. The LCD is used. The contour interval is 0.075 $dyn\ cm^{-2}$. The positive (negative) values are solid (dashed).

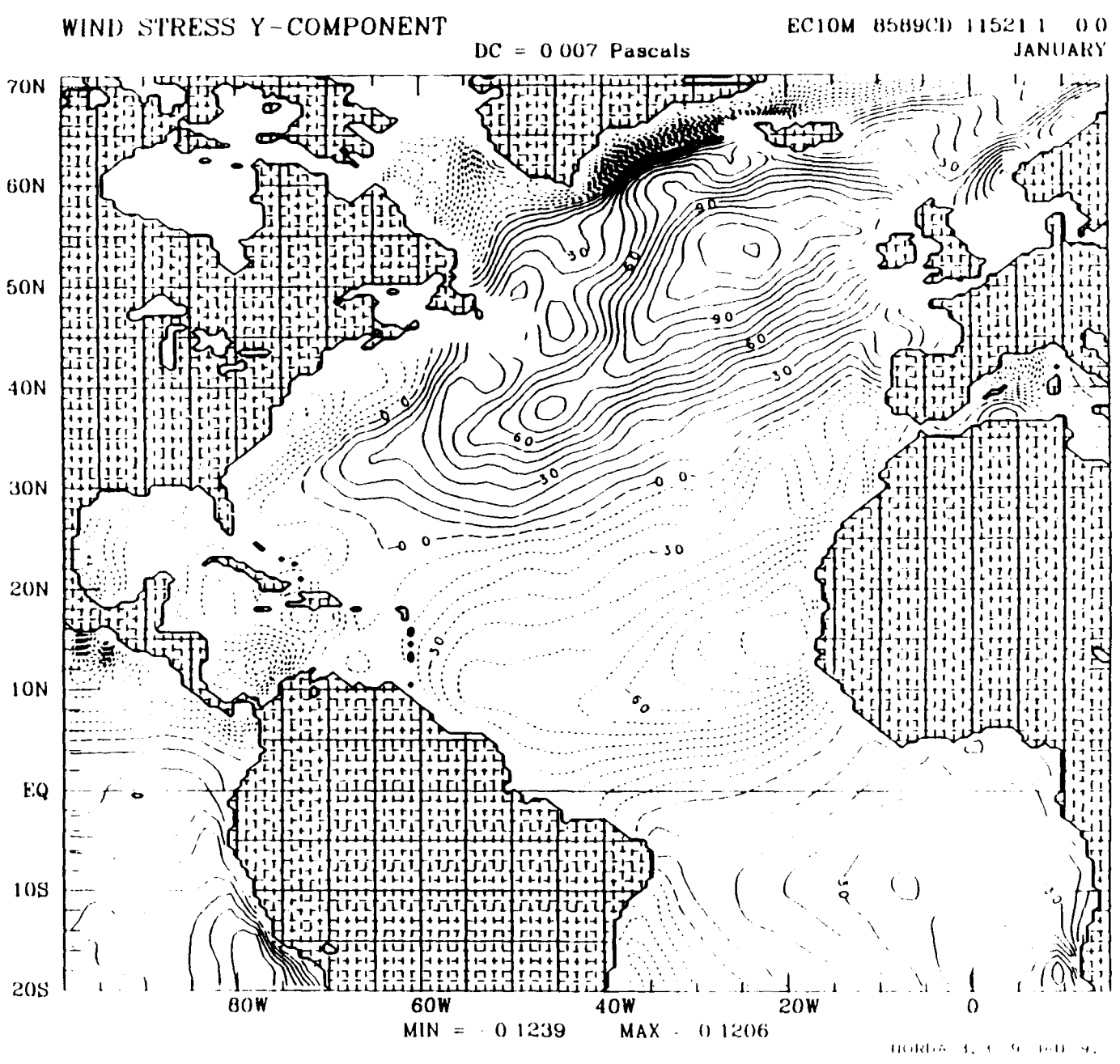

Fig. 13b Same as Fig. 13a but for meridional component.

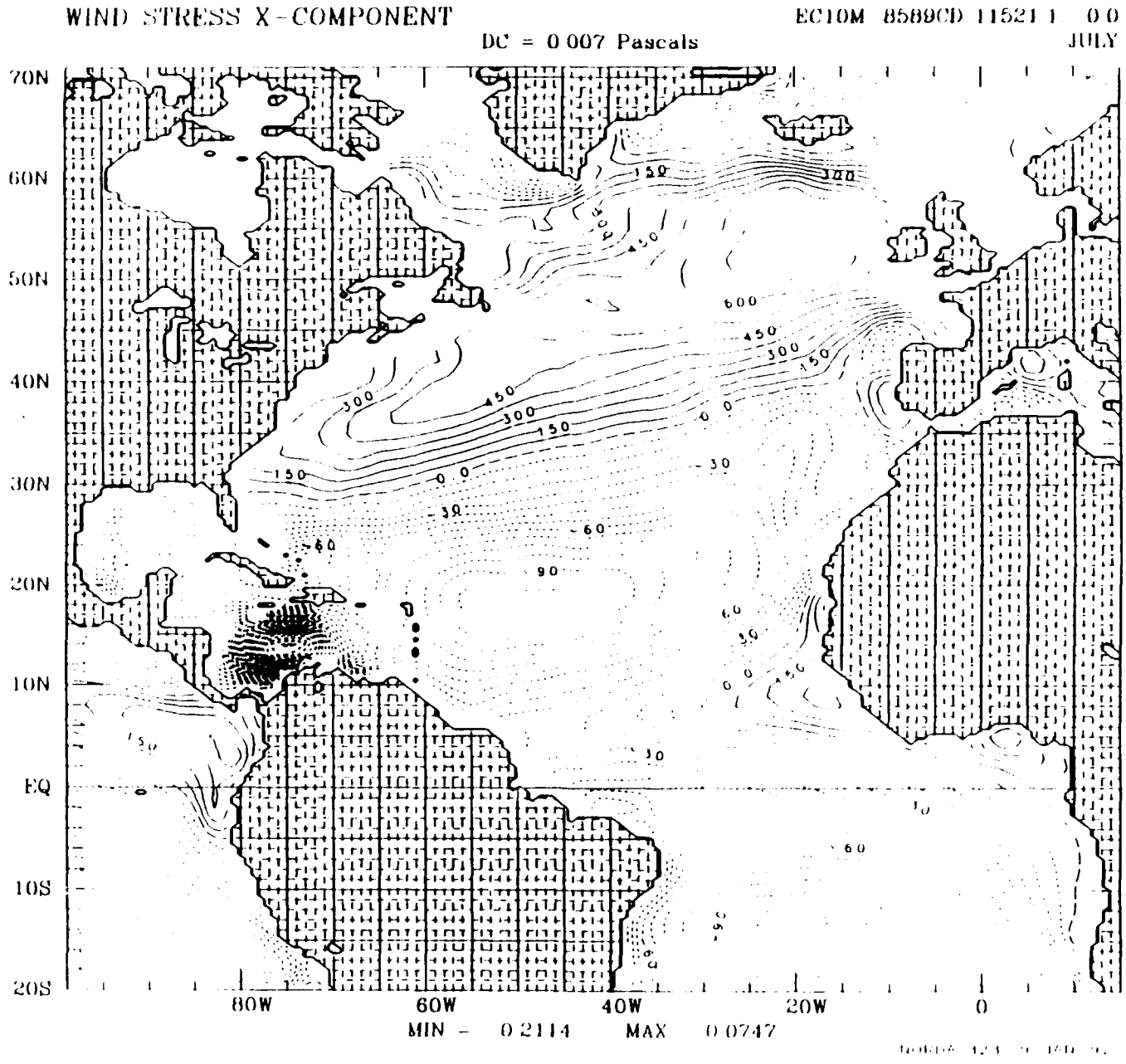

Fig. 13c Same as Fig. 13a but for July.

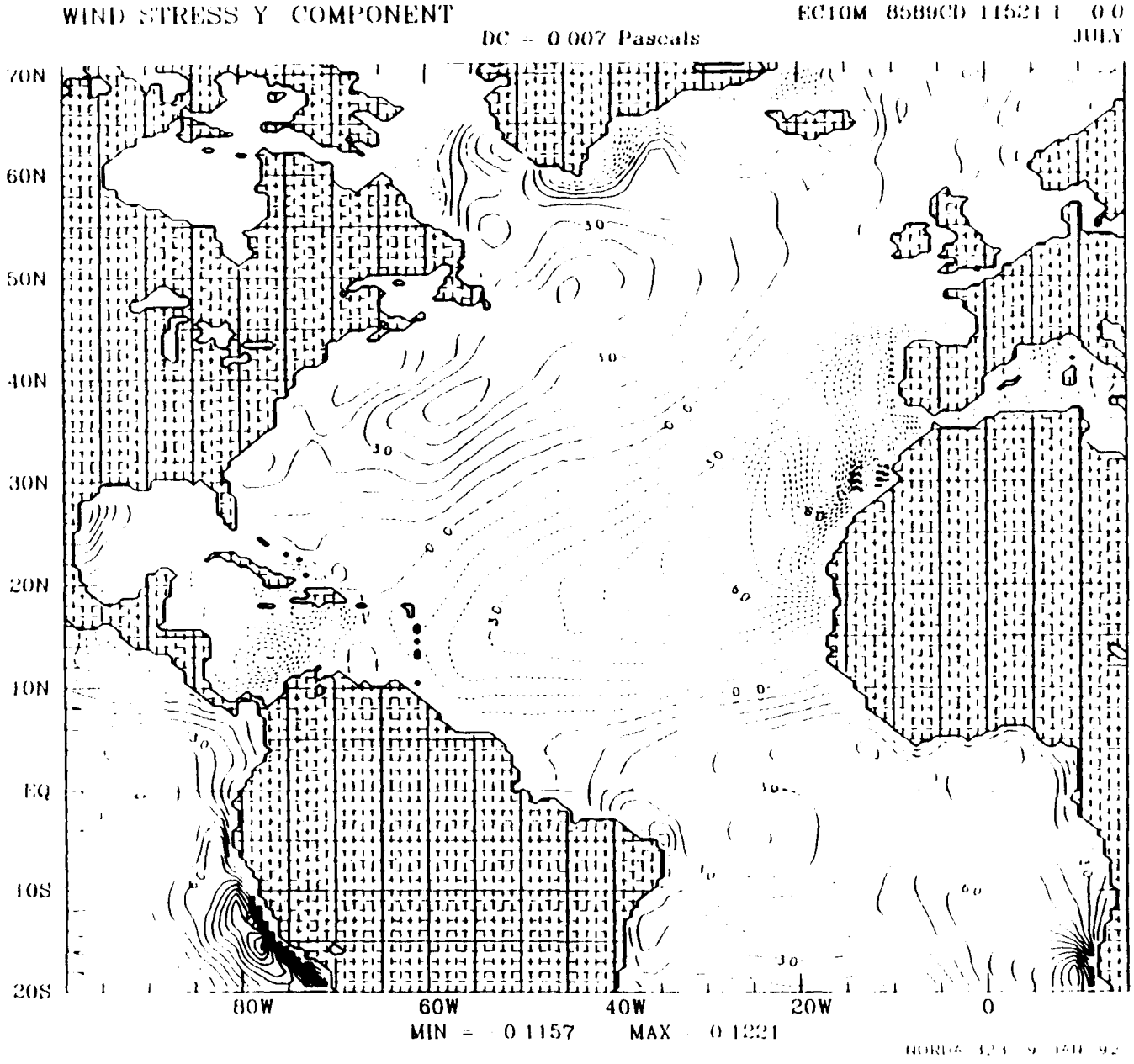

Fig. 13d Same as Fig. 13b but for July.

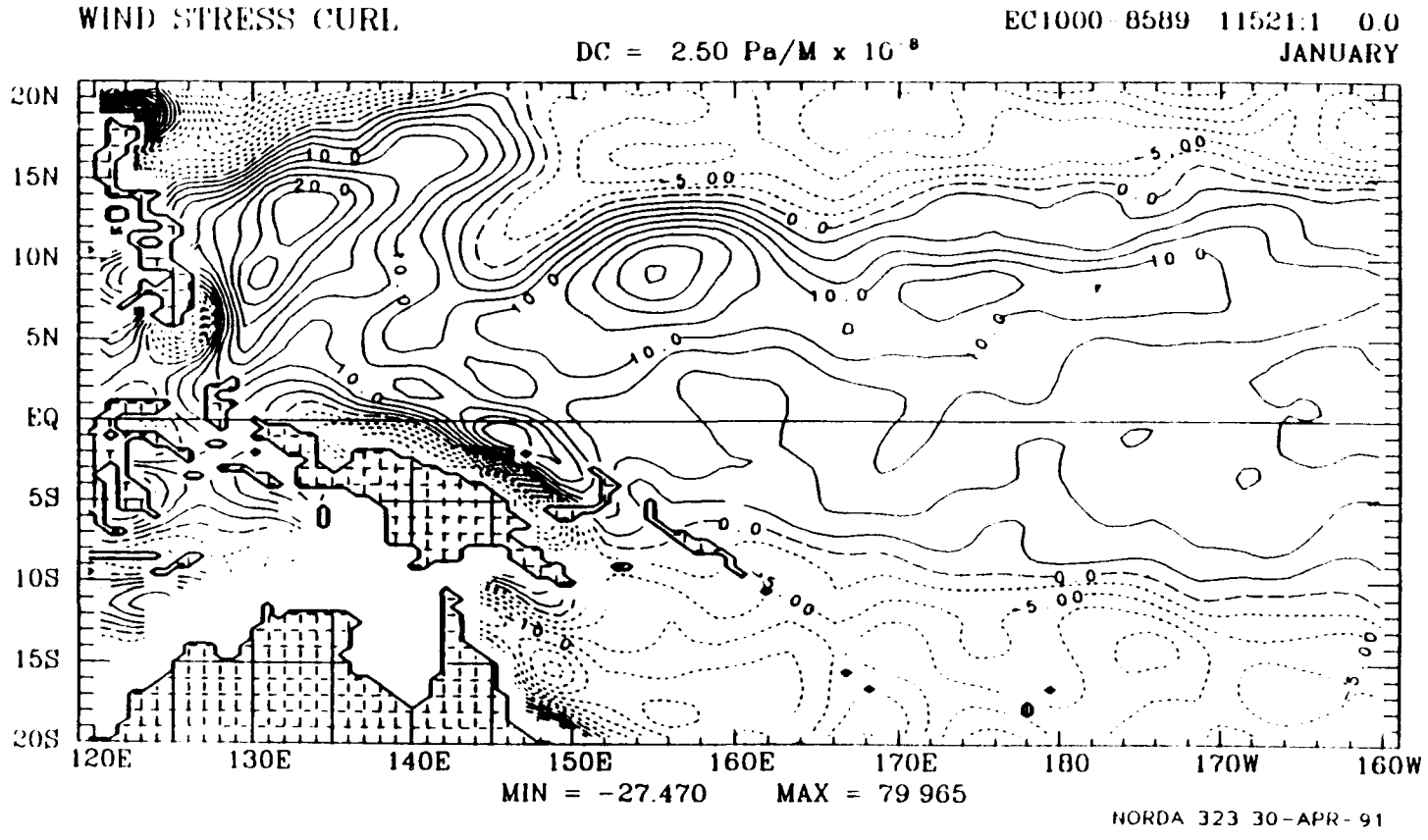

Fig. 14a Five-year January mean curl of the 1000 *mb* wind stress over WEP. The LCD is used. The contour interval is 25 $\times 10^{-8} dyn\ cm^{-3}$. The positive (negative) values are solid (dashed).

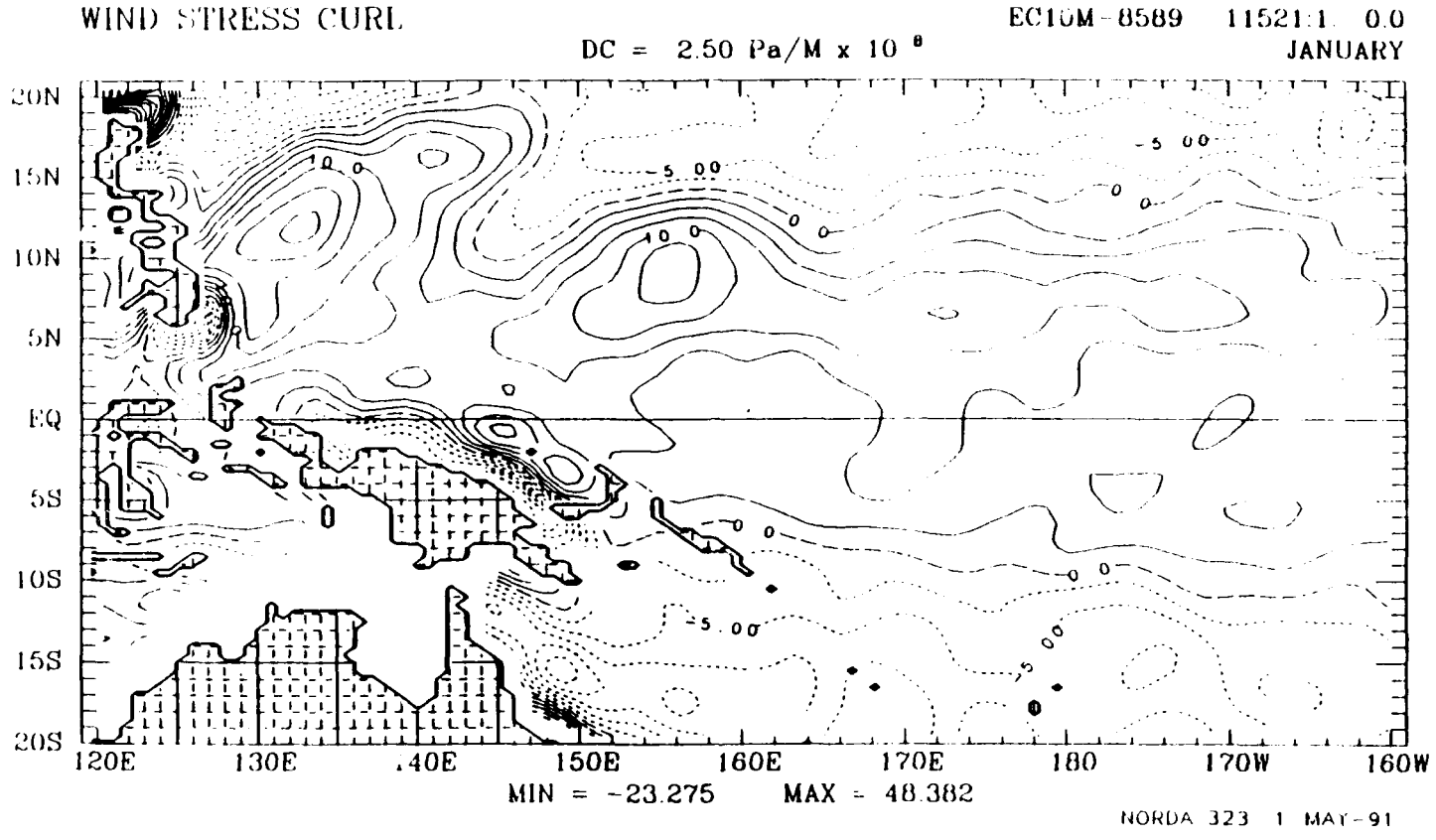

Fig. 14b Same as Fig. 14a but for 10 *m* height wind stress.

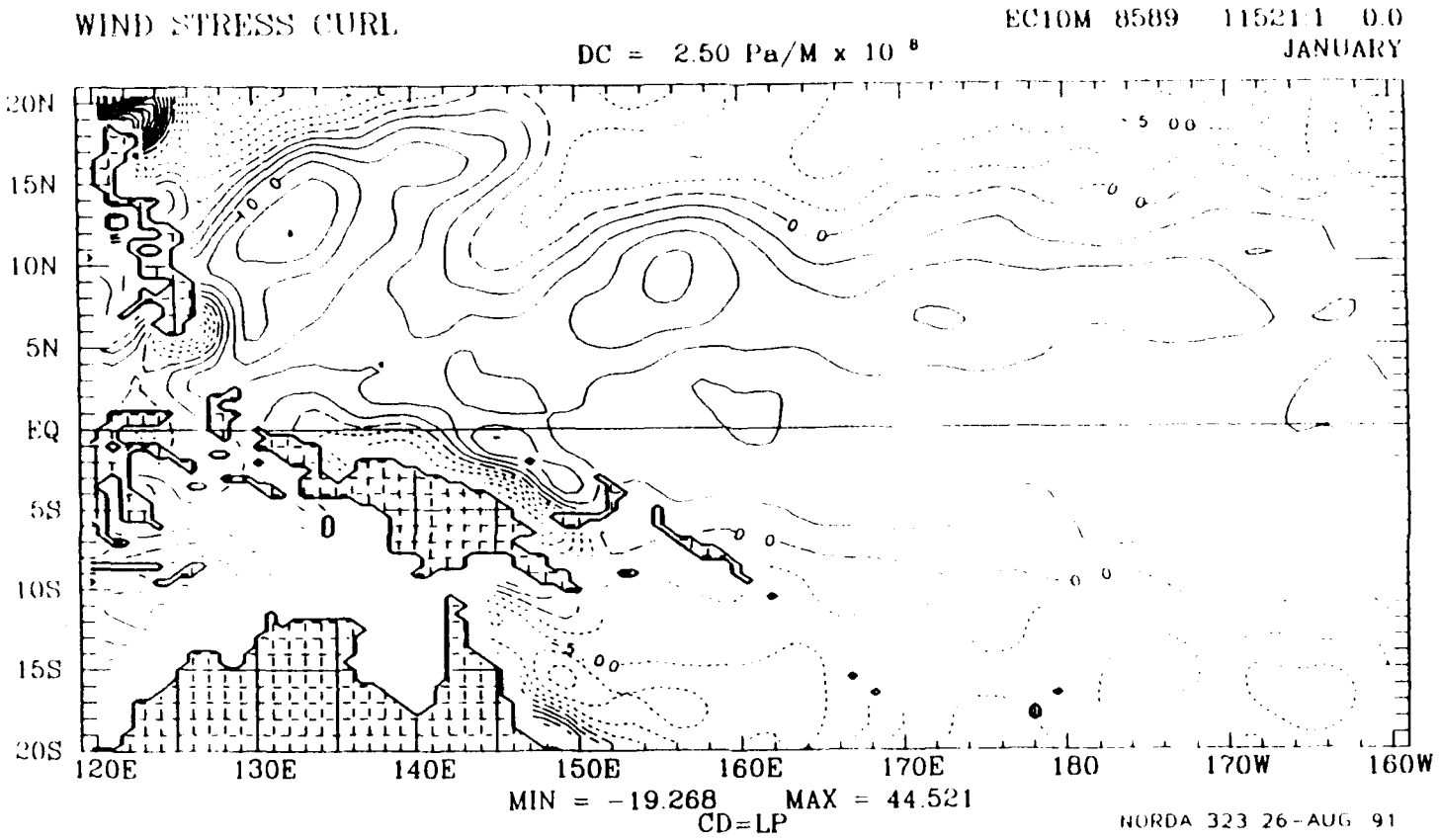

Fig. 14c Same as Fig. 14b but LPCD is used.

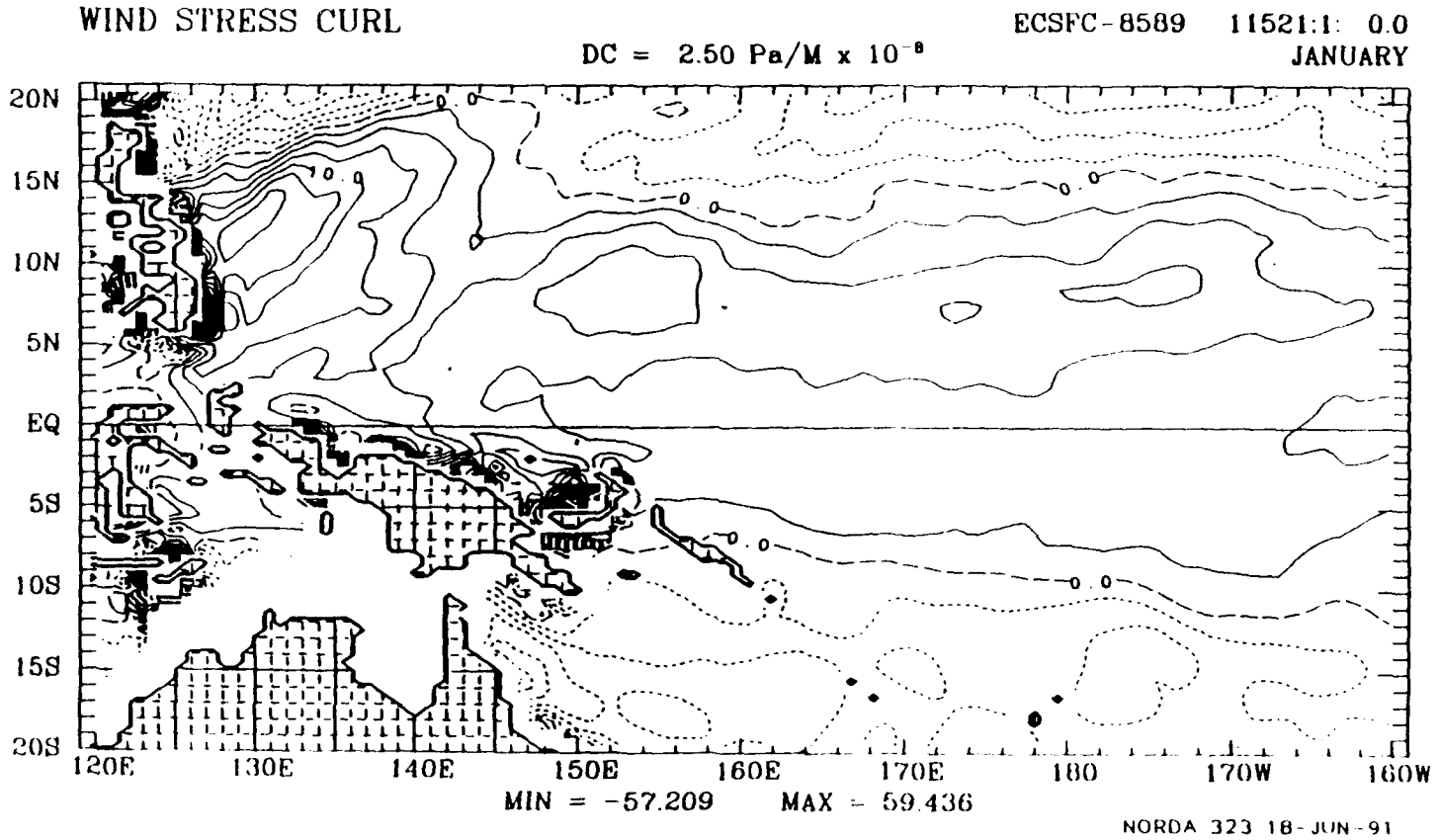

Fig. 14d Same as Fig. 14a but for the direct surface stress.

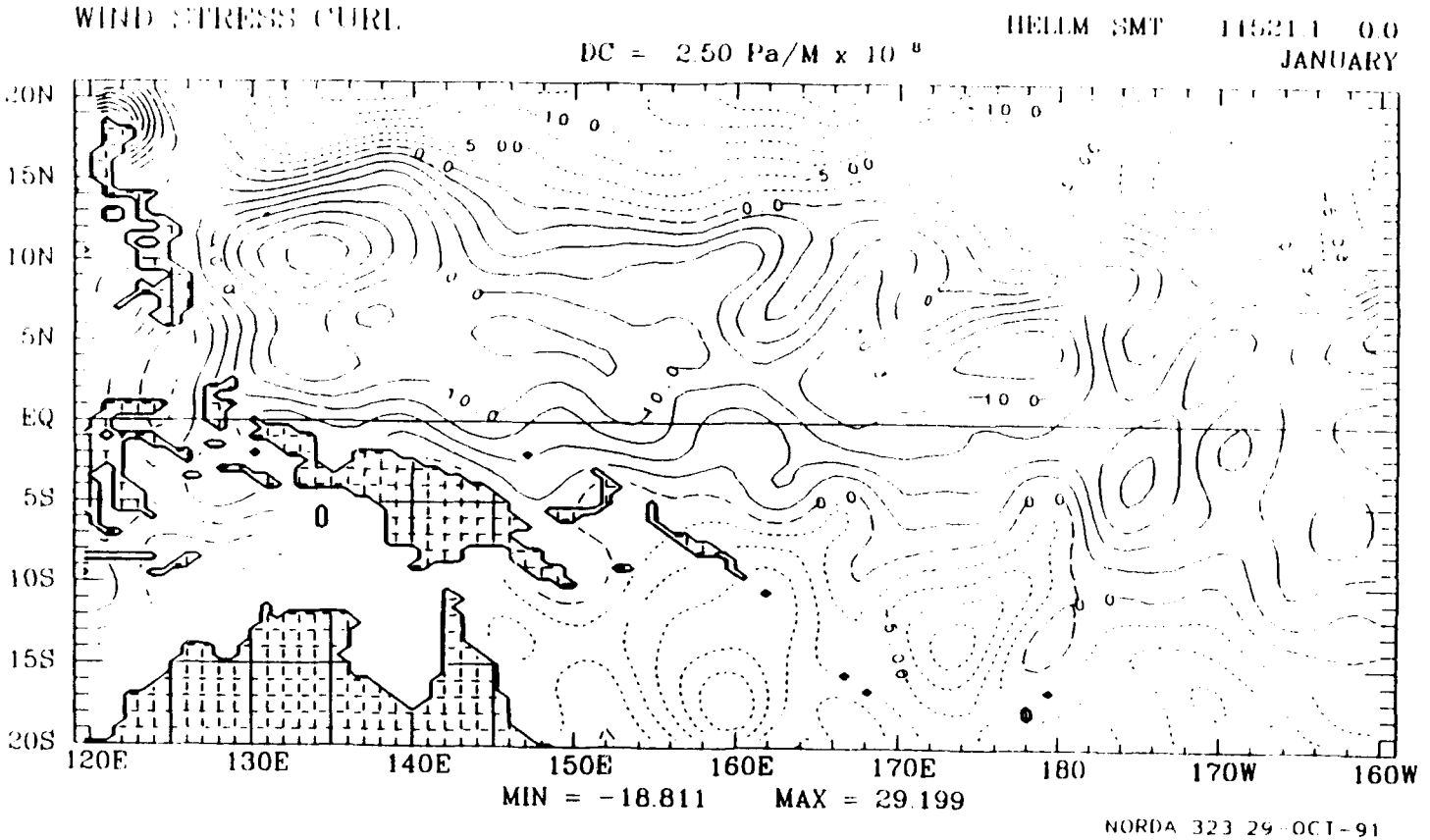

Fig. 14e Same as Fig. 14a but for HR wind stress.

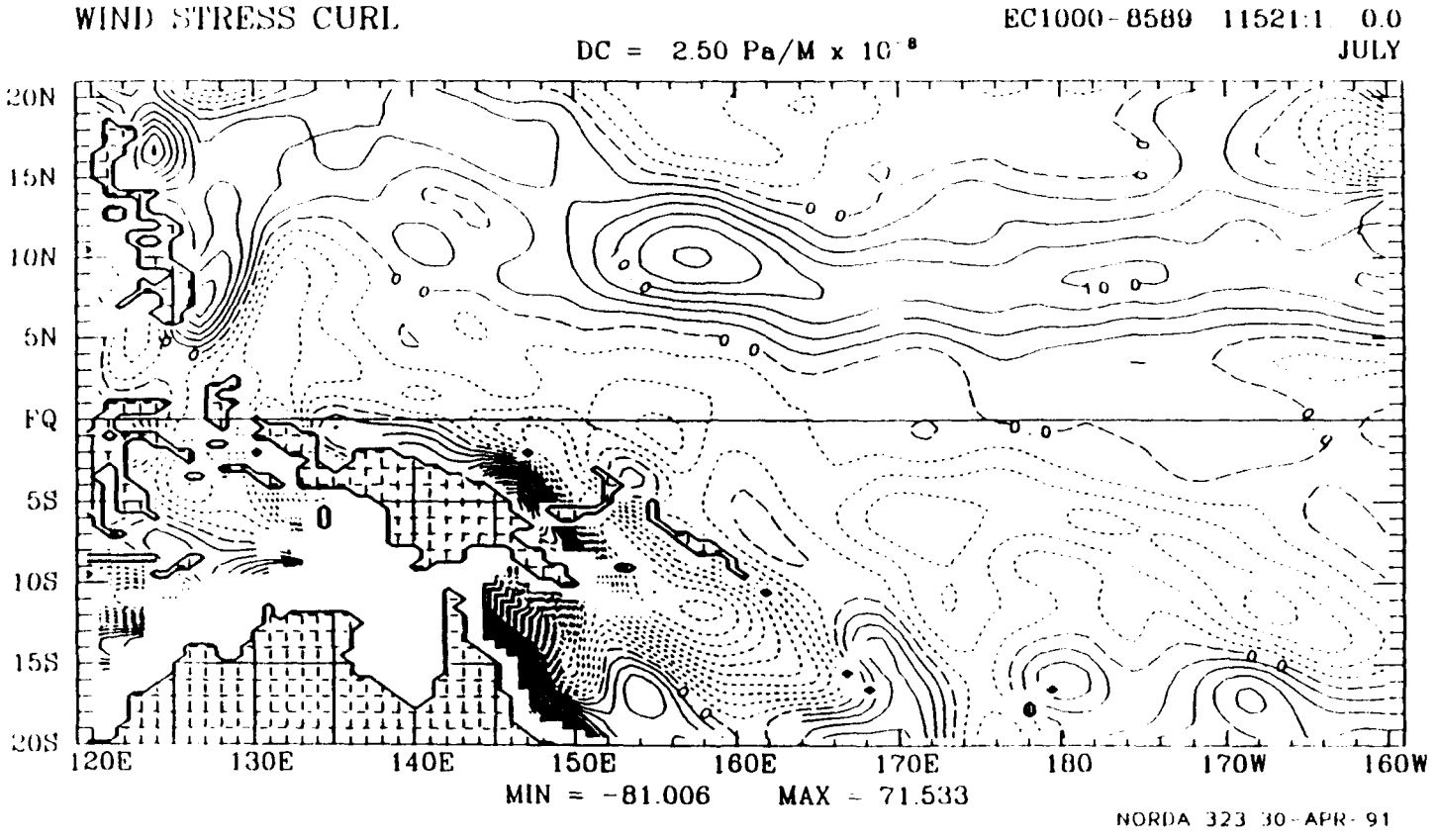

Fig. 15a Five-year July mean curl of the 1000 *mb* wind stress over WEP. The LCD is used. The contour interval is 25 $\times 10^{-8} dyn\ cm^{-3}$. The positive (negative) values are solid (dashed).

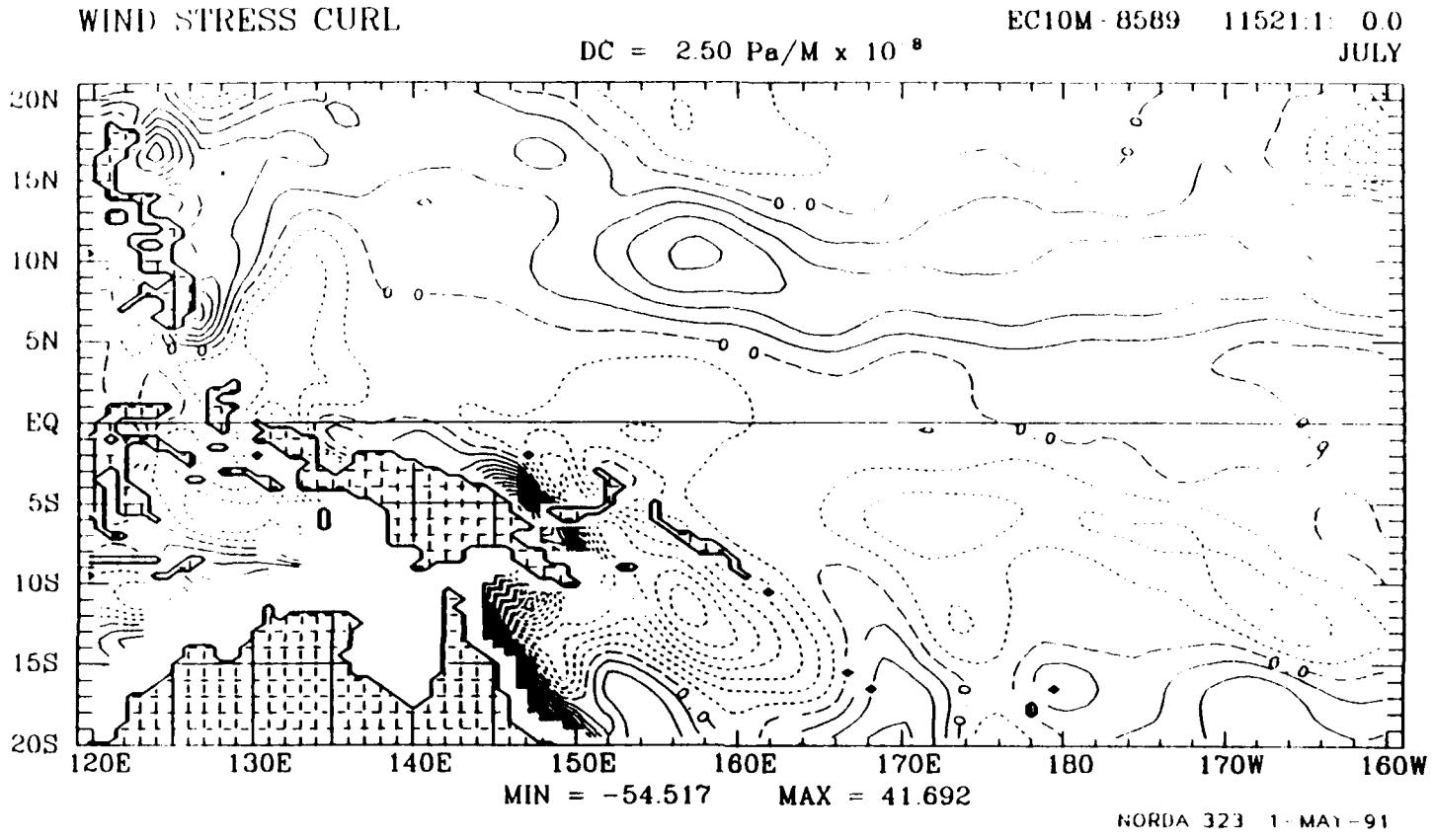

Fig. 15b Same as Fig. 15a but for the curl of the 10 m height wind stress.

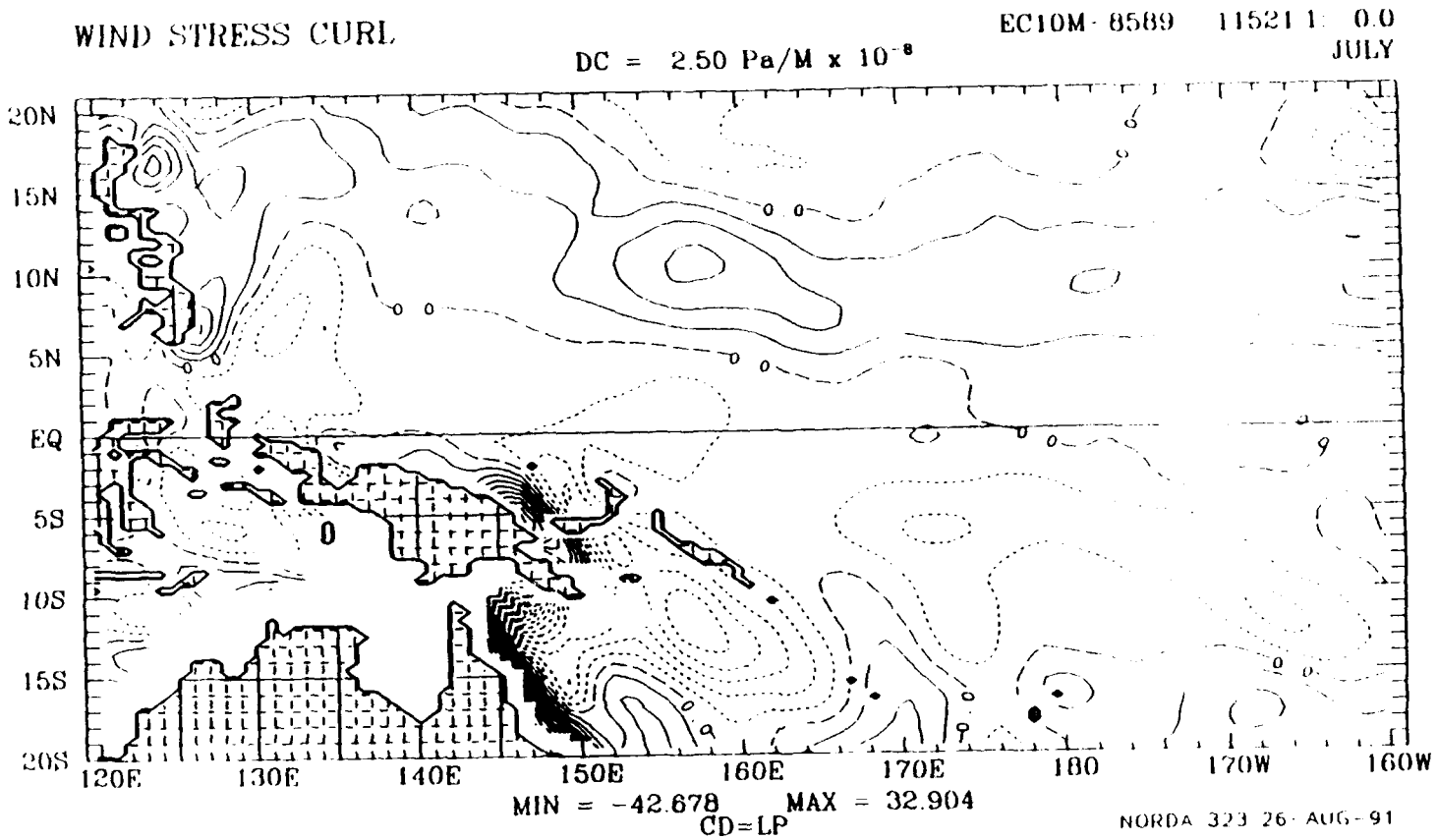

Fig. 15c Same as Fig. 15b but LPCD is used.

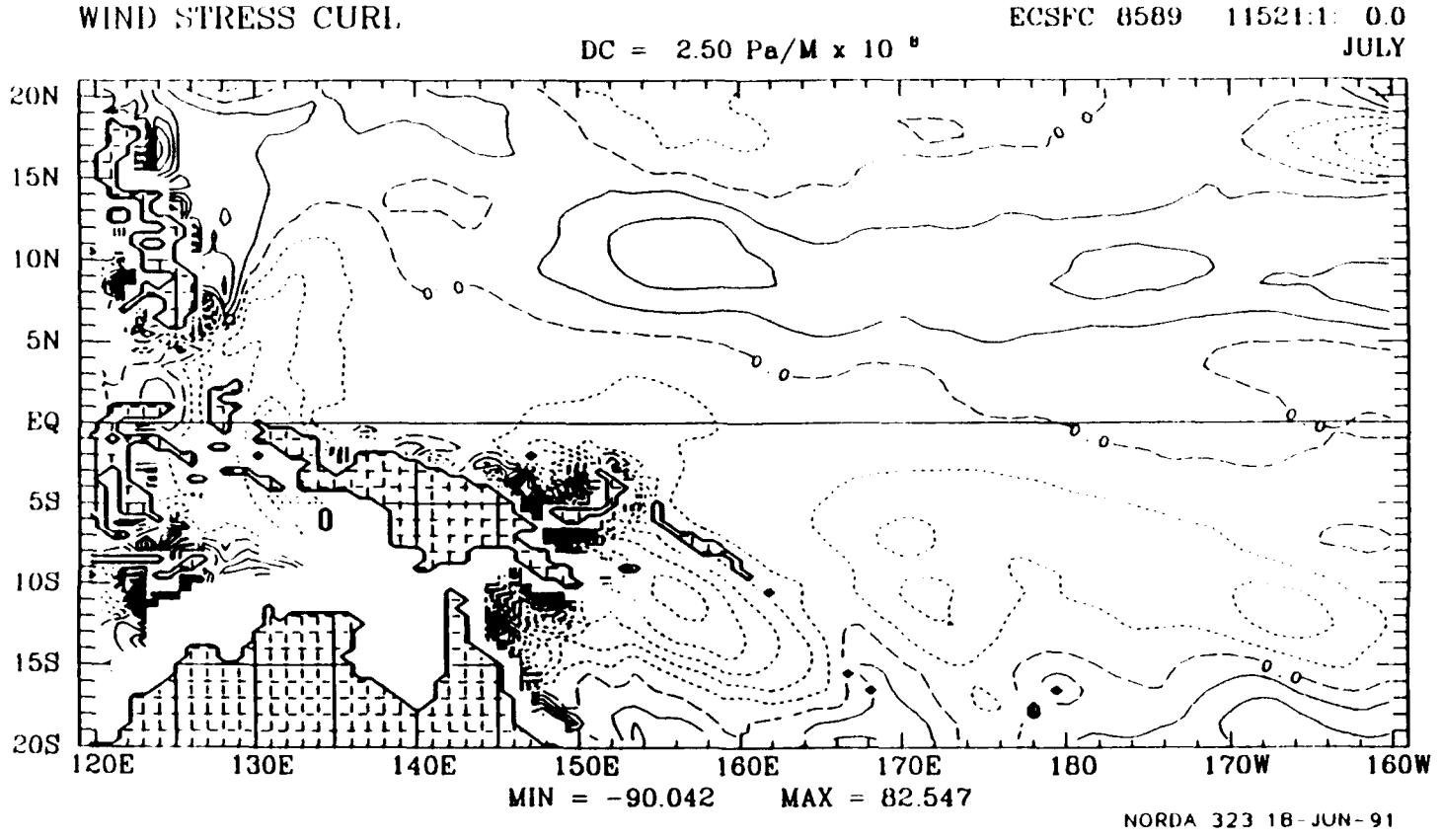

Fig. 15d Same as Fig. 15a but for curl of the direct surface stress.

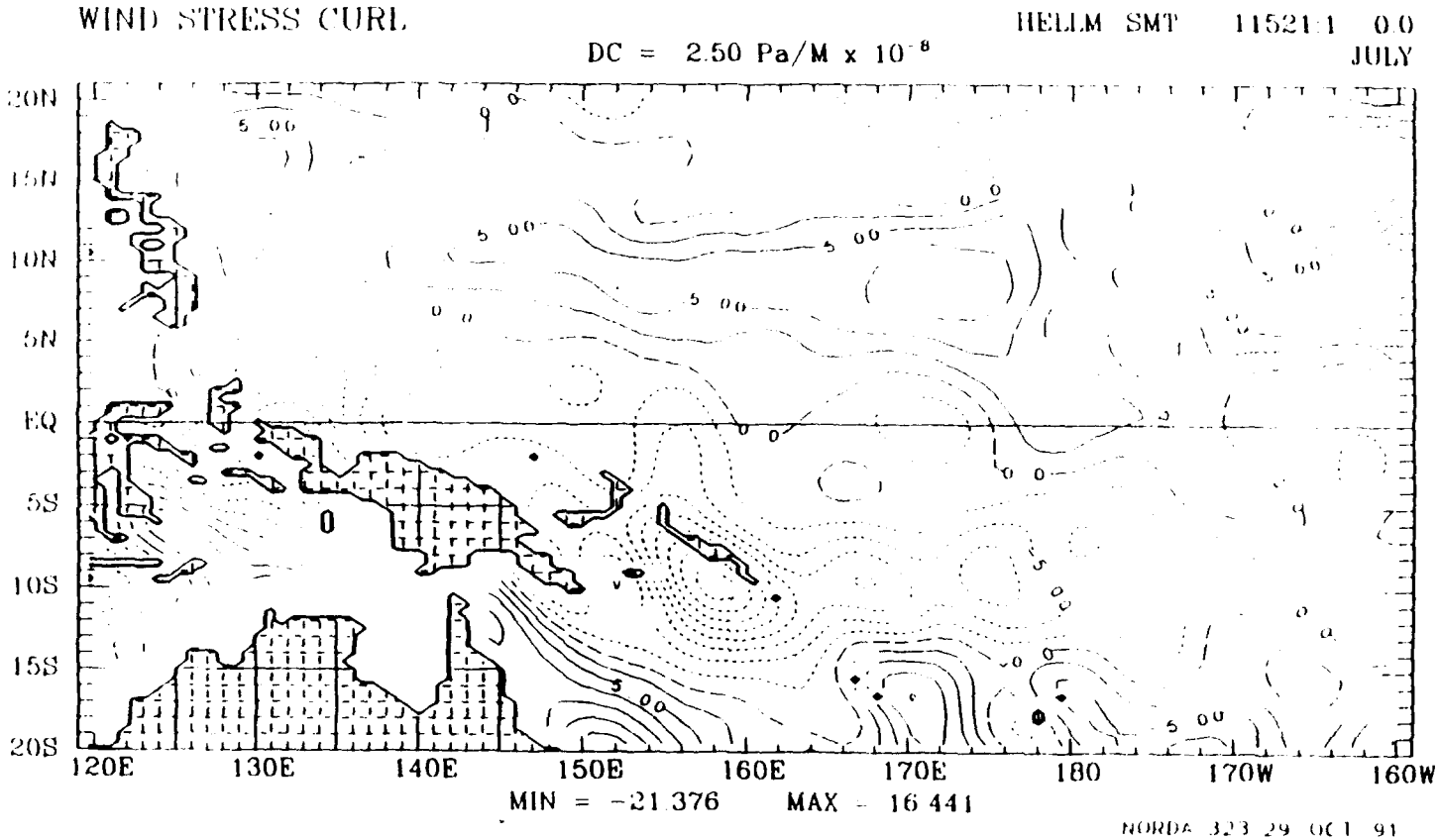

Fig. 15e Same as Fig. 15a but for curl of the HR wind stress.

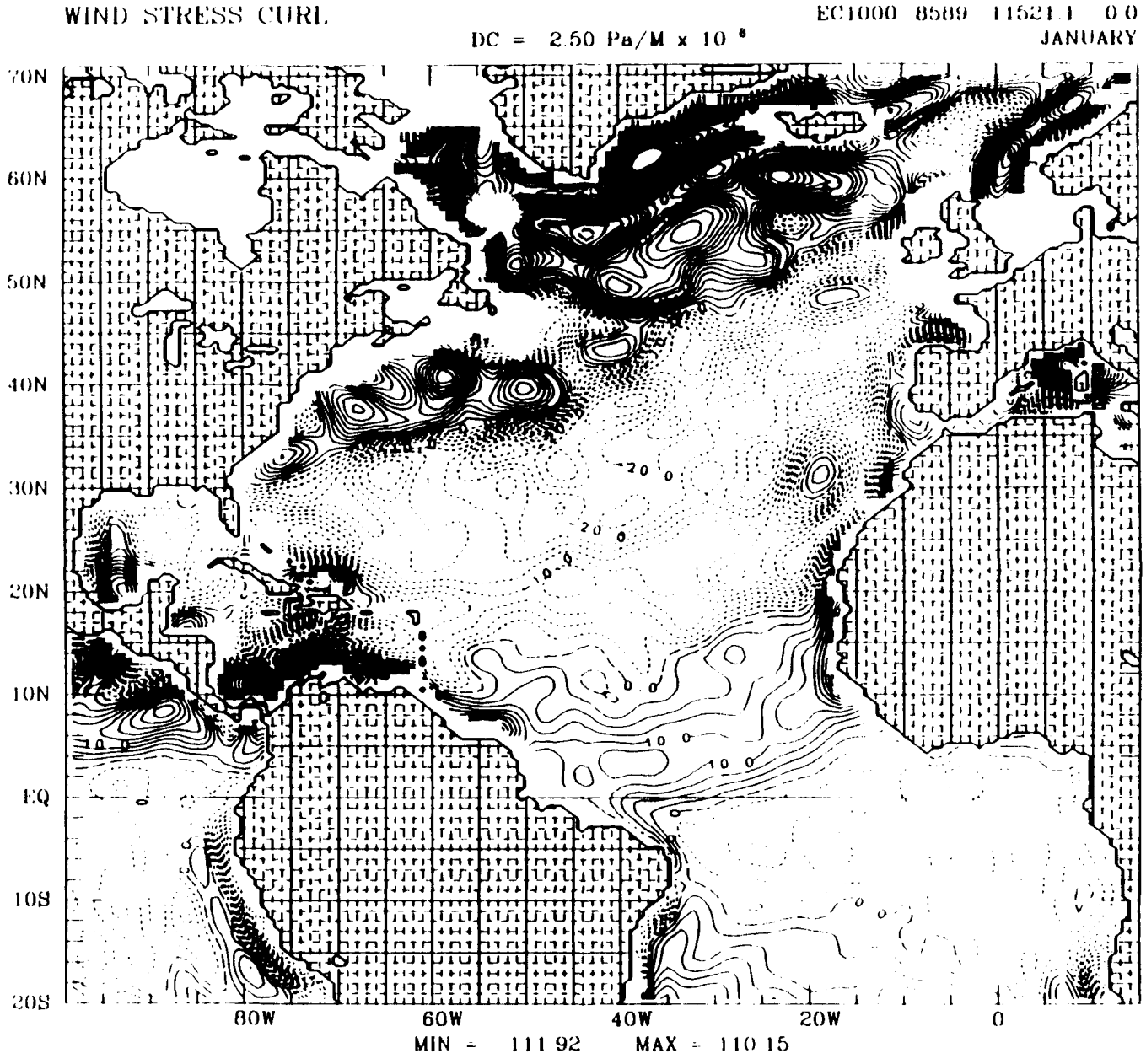

Fig. 16a Five-year January mean curl of the 1000 *mb* wind stress over NAB. The LCD is used. The contour interval is 25 $\times 10^{-8} dyn\ cm^{-3}$. The positive (negative) values are solid (dashed).

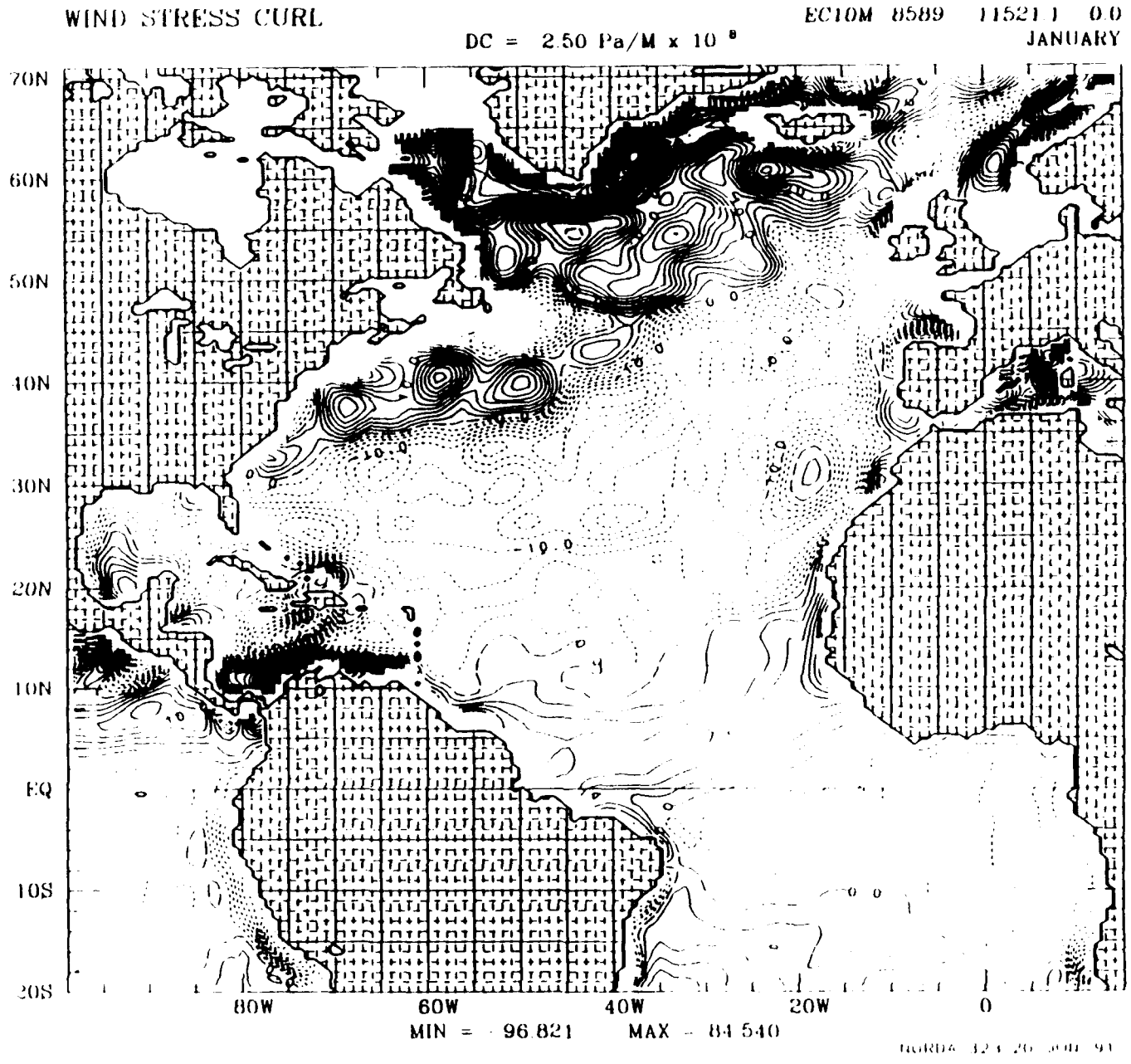

Fig. 16b Same as Fig. 16a but for curl of the 10 *m* height wind stress.

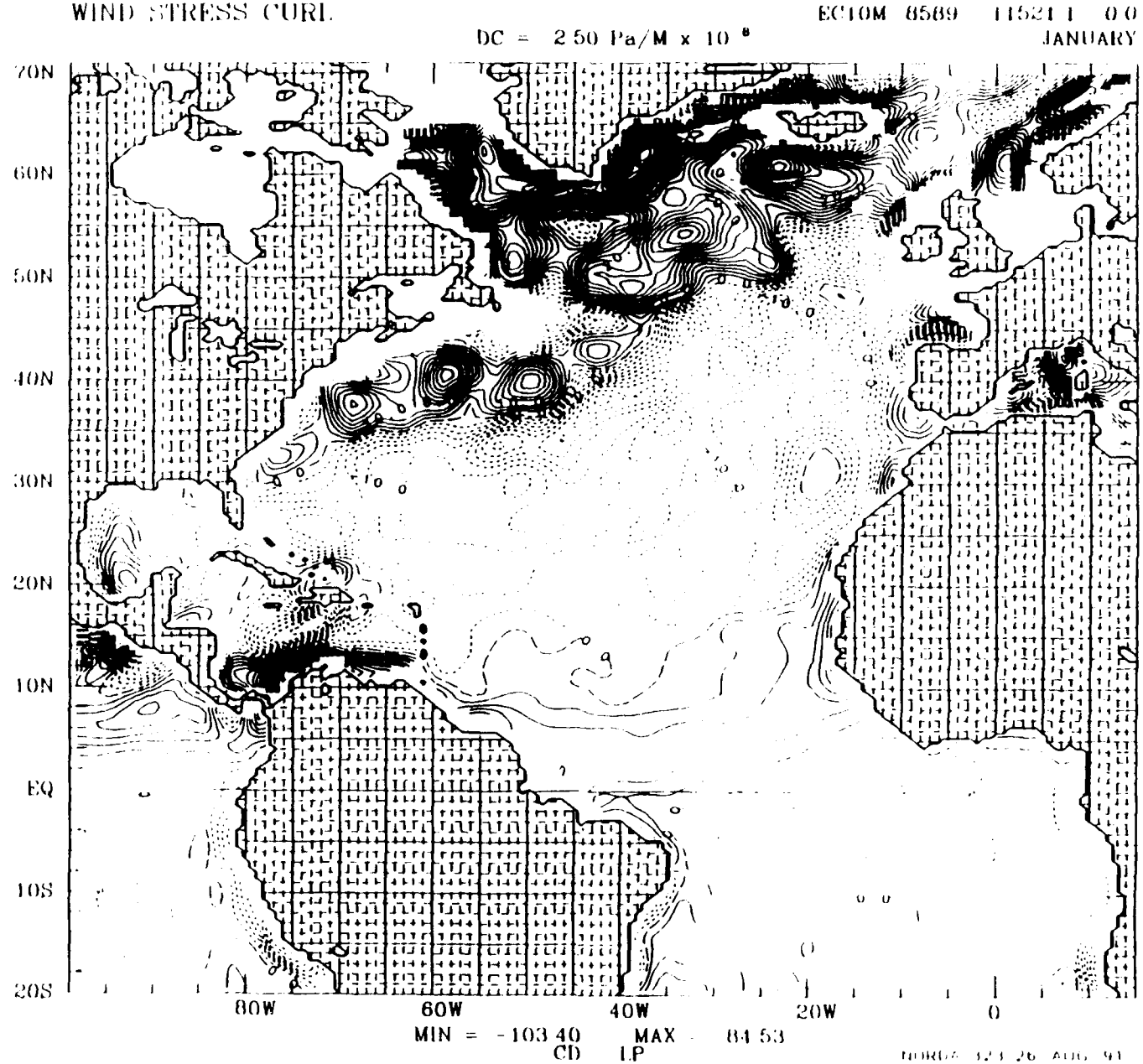

Fig. 16c Same as Fig. 16b but LPCD is used.

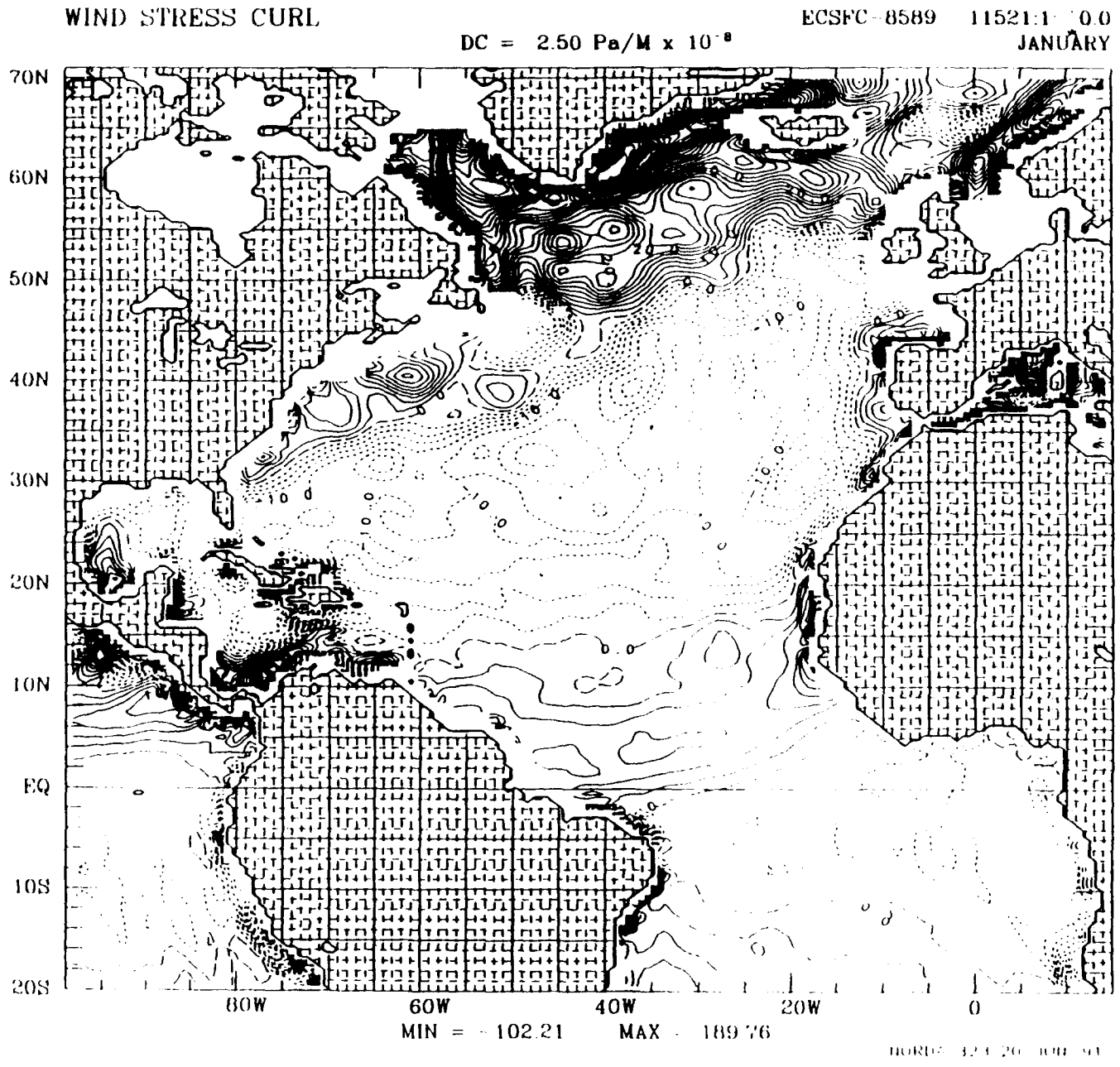

Fig. 16d Same as Fig. 16a but for curl of the direct surface stress.

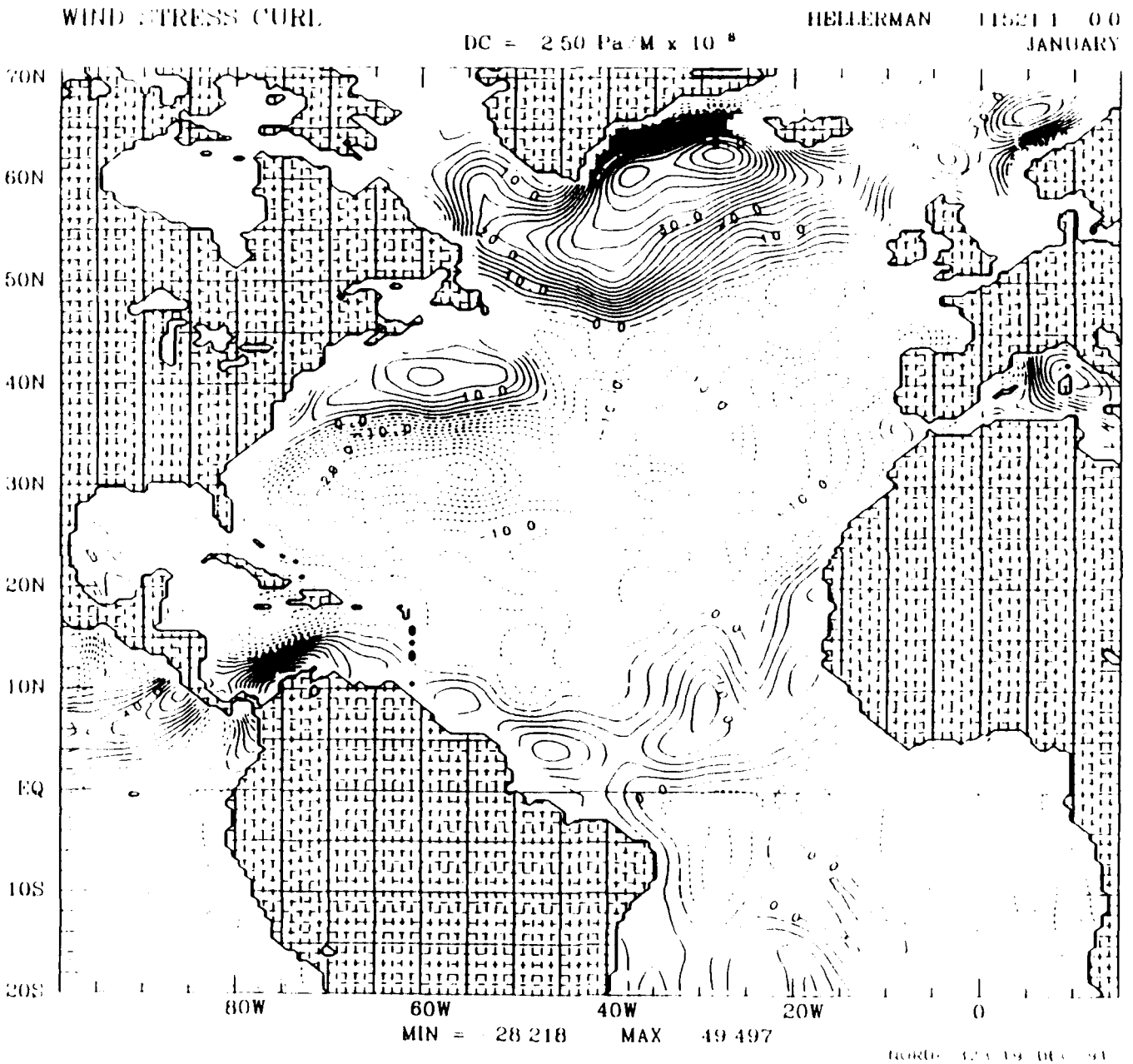

Fig. 16e Same as Fig. 16a but for curl of the HR wind stress.

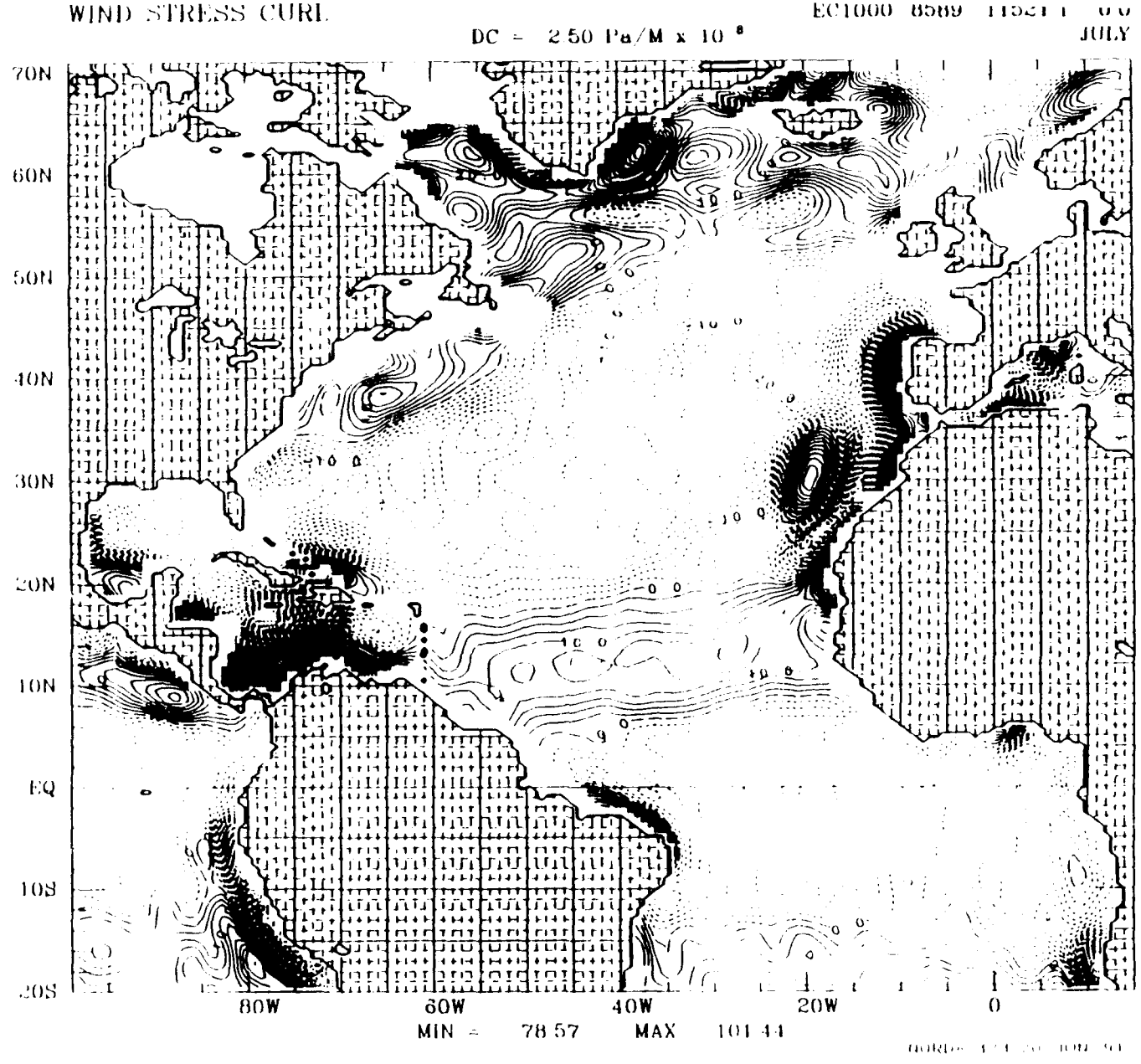

Fig. 17a Five-year July mean curl of the 1000 *mb* wind stress over NAB. The LCD is used. The contour interval is 25 $\times 10^{-8} dyn\ cm^{-3}$. The positive (negative) values are solid (dashed).

AD-A257 147 WIND STRESS ANALYSIS OVER THE WESTERN EQUATORIAL PACIFIC AND NORTH ATLANT..(U) INSTITUTE FOR NAVAL OCEANOGRAPHY STENNIS SPACE CENTER MS L H LY ET AL.

UNCLASSIFIED AUG 92 INO-TR-3 XB-NRL NL

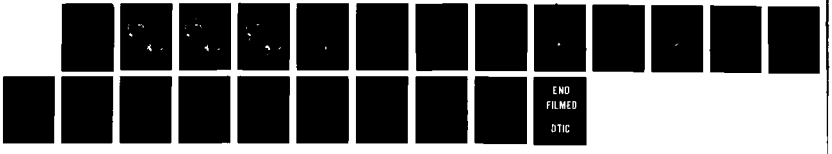

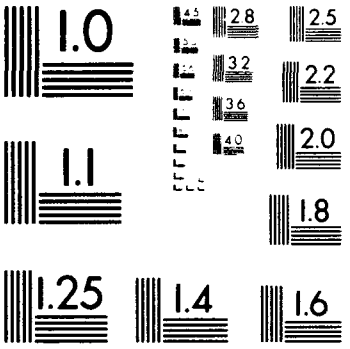
1.0
1.1
1.25
1.4
1.6
1.8
2.0
2.2
2.5
2.8
3.2
3.6
4.0
4.5

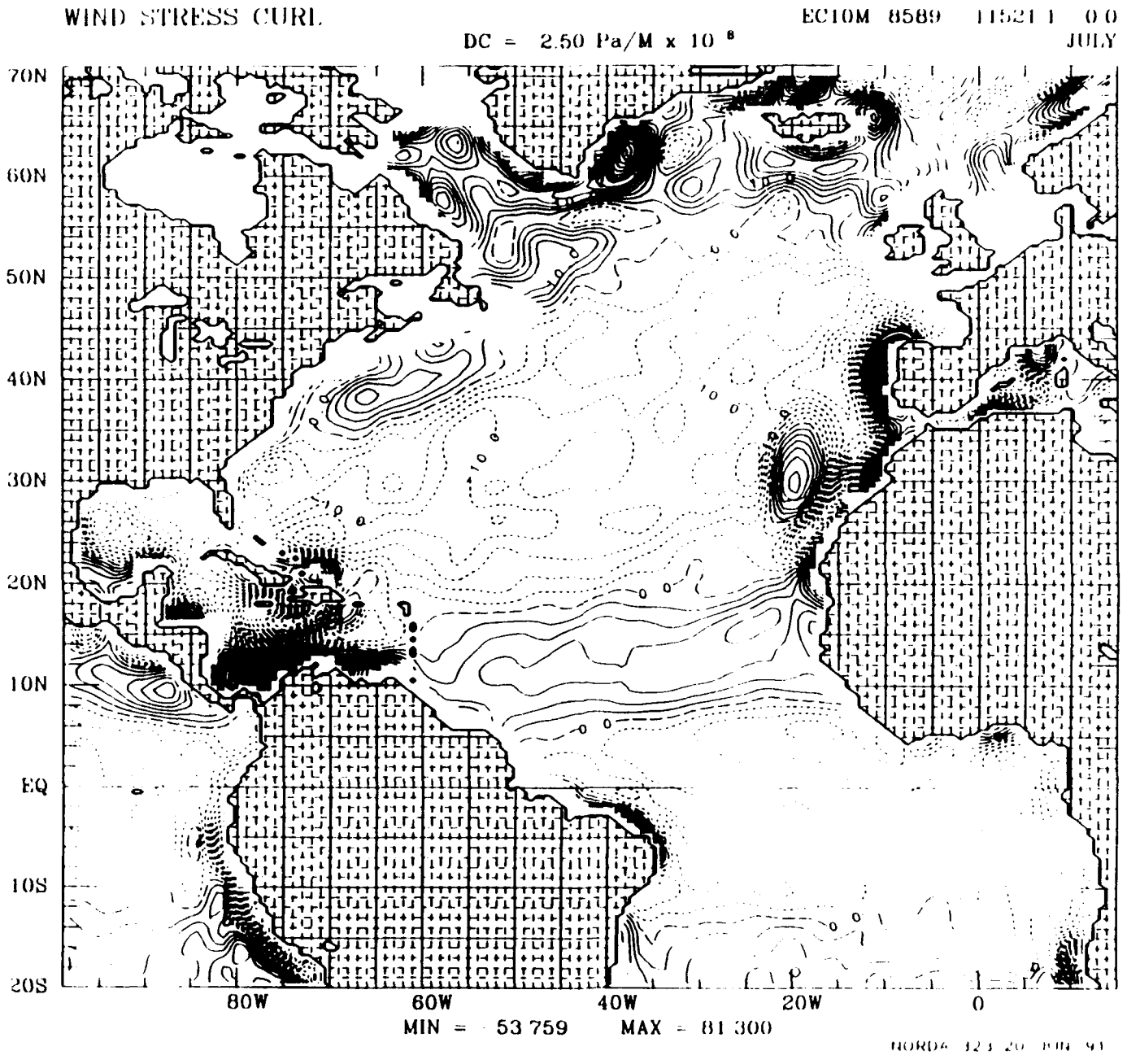

Fig. 17b Same as Fig. 17a but for curl of the 10 m height wind stress.

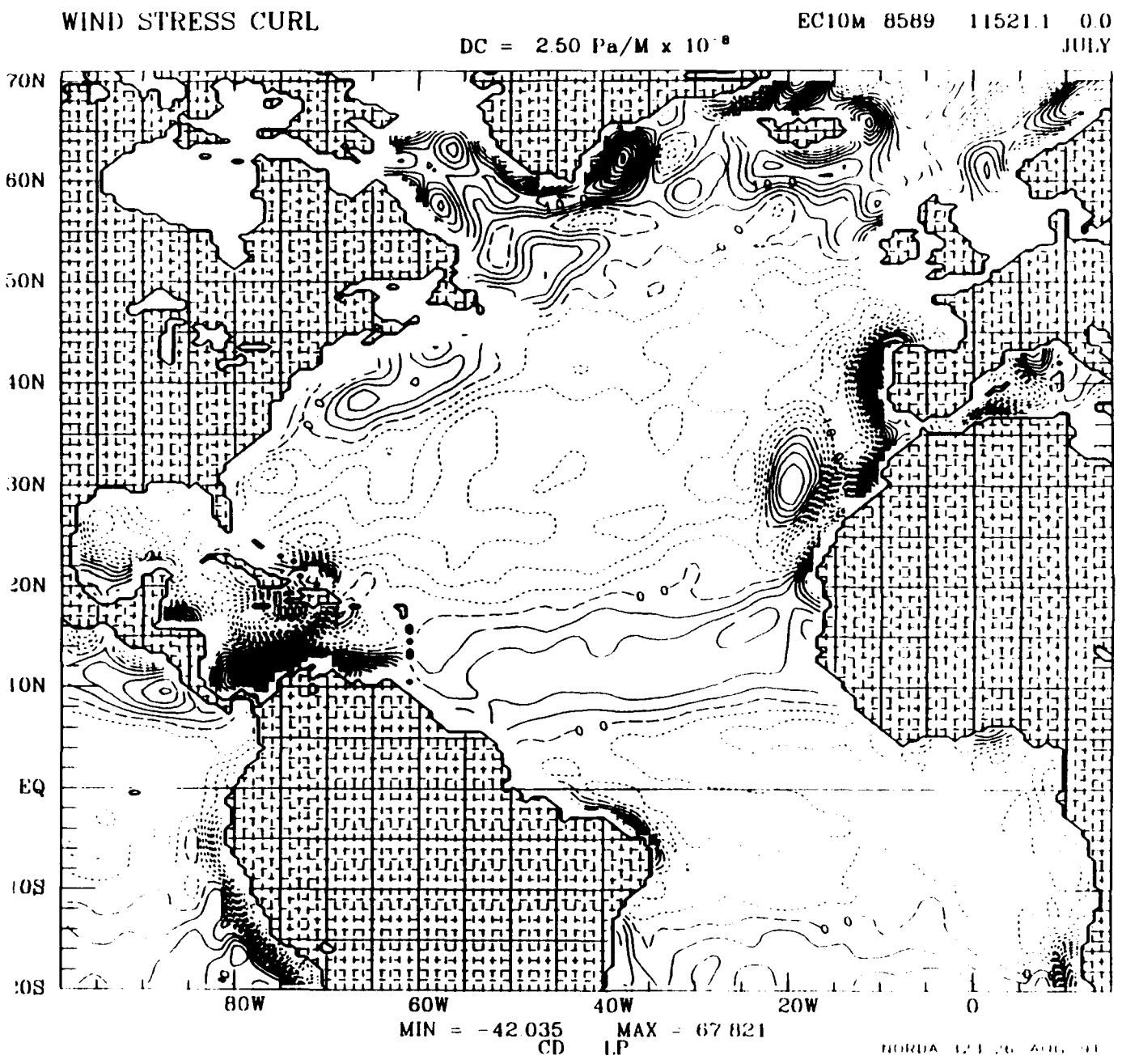

Fig. 17c Same as Fig. 17b but LPCD is used.

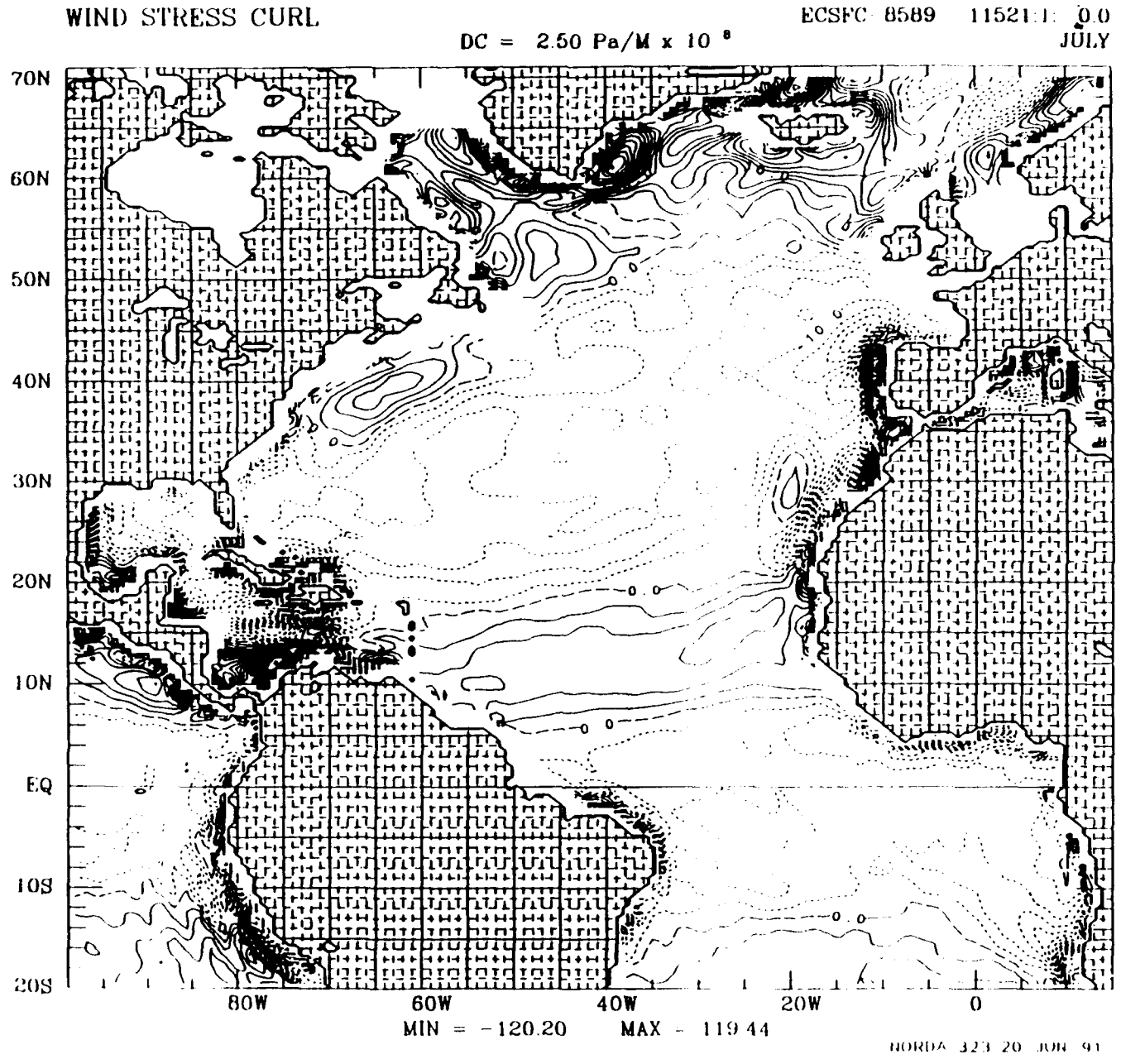

Fig. 17d Same as Fig. 17a but for curl of the direct surface stress.

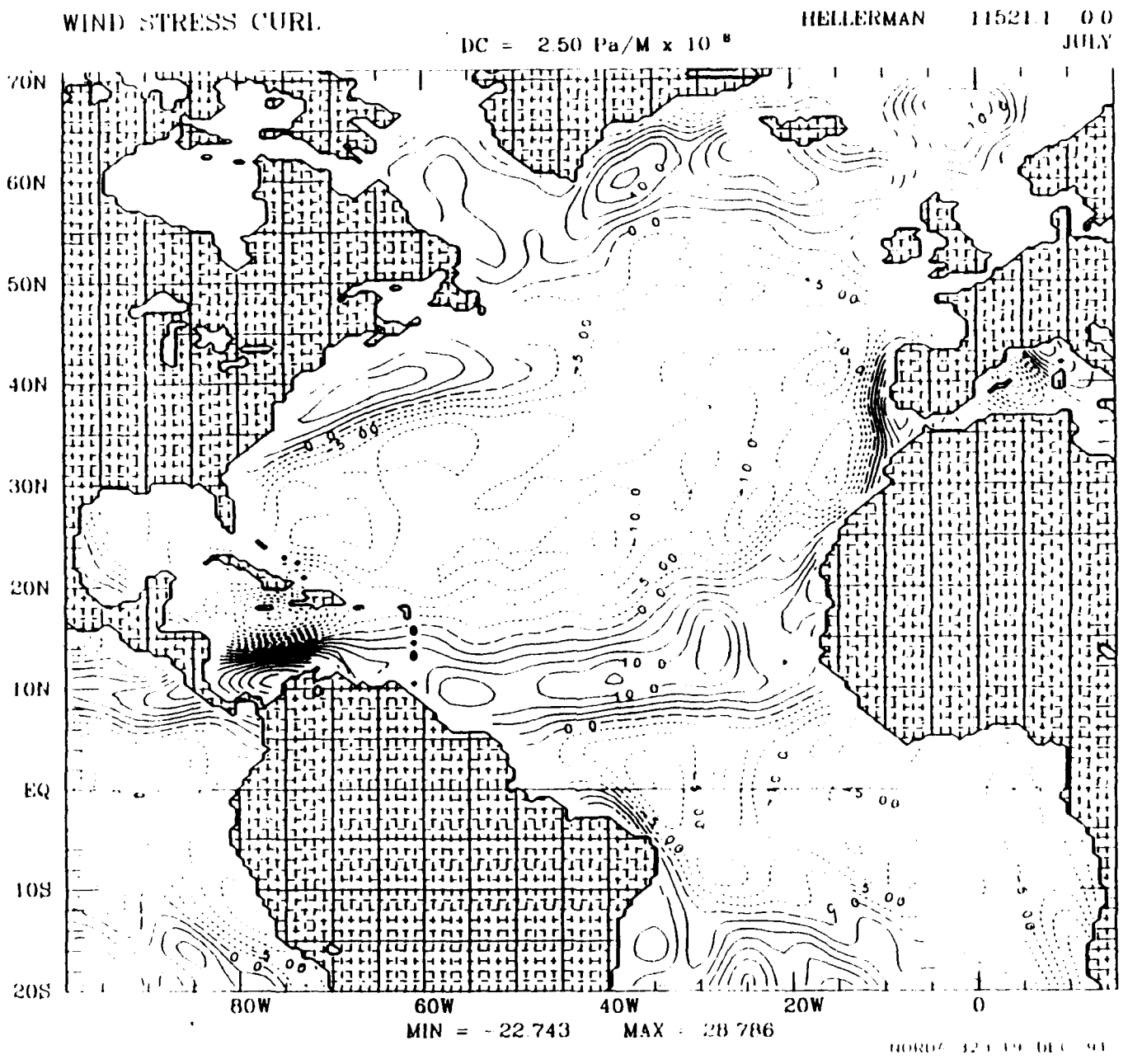

Fig. 17e Same as Fig. 17a but for curl of the HR wind stress.

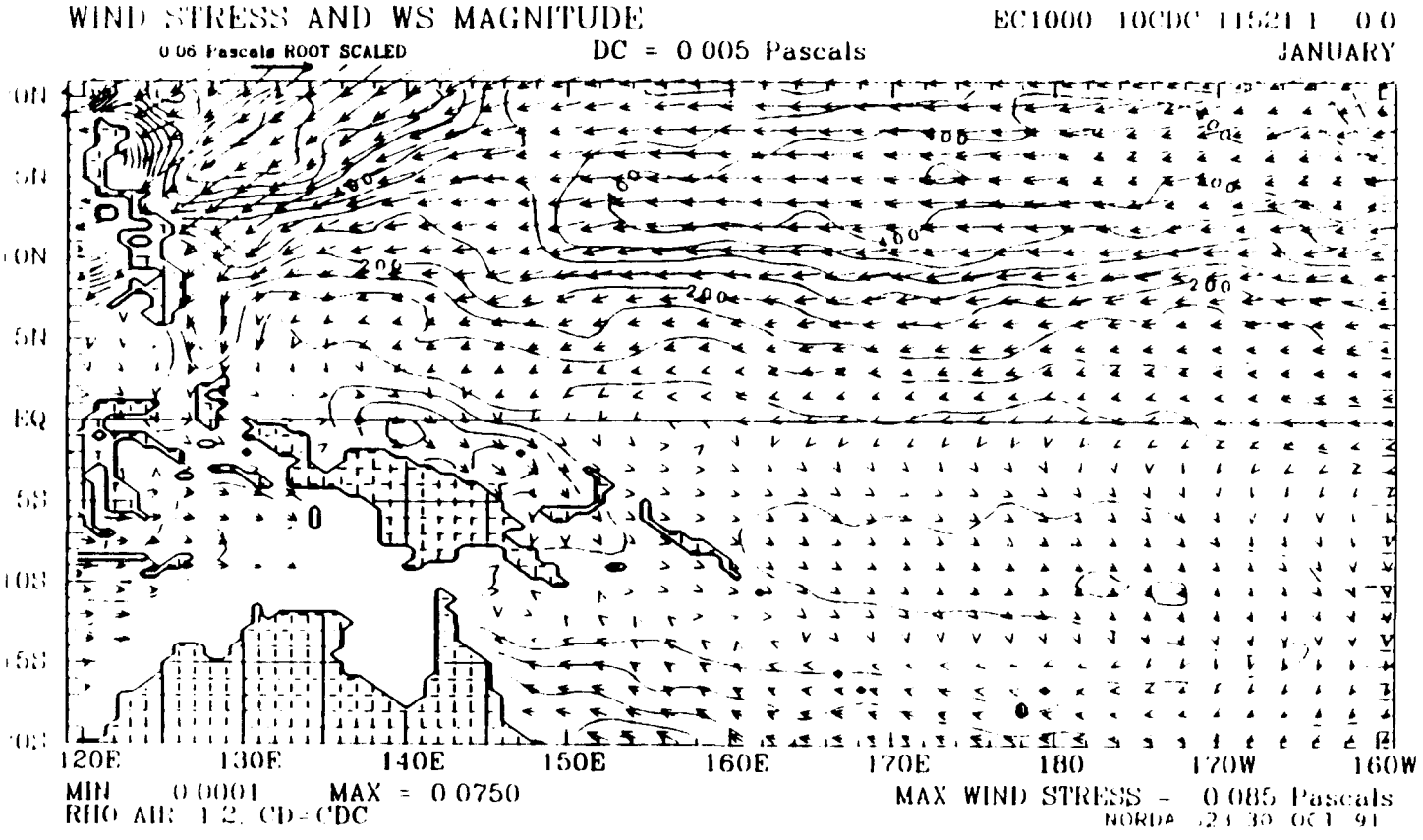

Fig. 18a Differences in the January mean wind stress vectors and magnitudes over WEP between 1000 *mb* and 10 *m* height wind stresses. The LCD is used for both wind stresses. The contour interval is 0.05 $dyn\ cm^{-2}$. The arrow at top left corresponds to 0.625 $dyn\ cm^{-2}$.

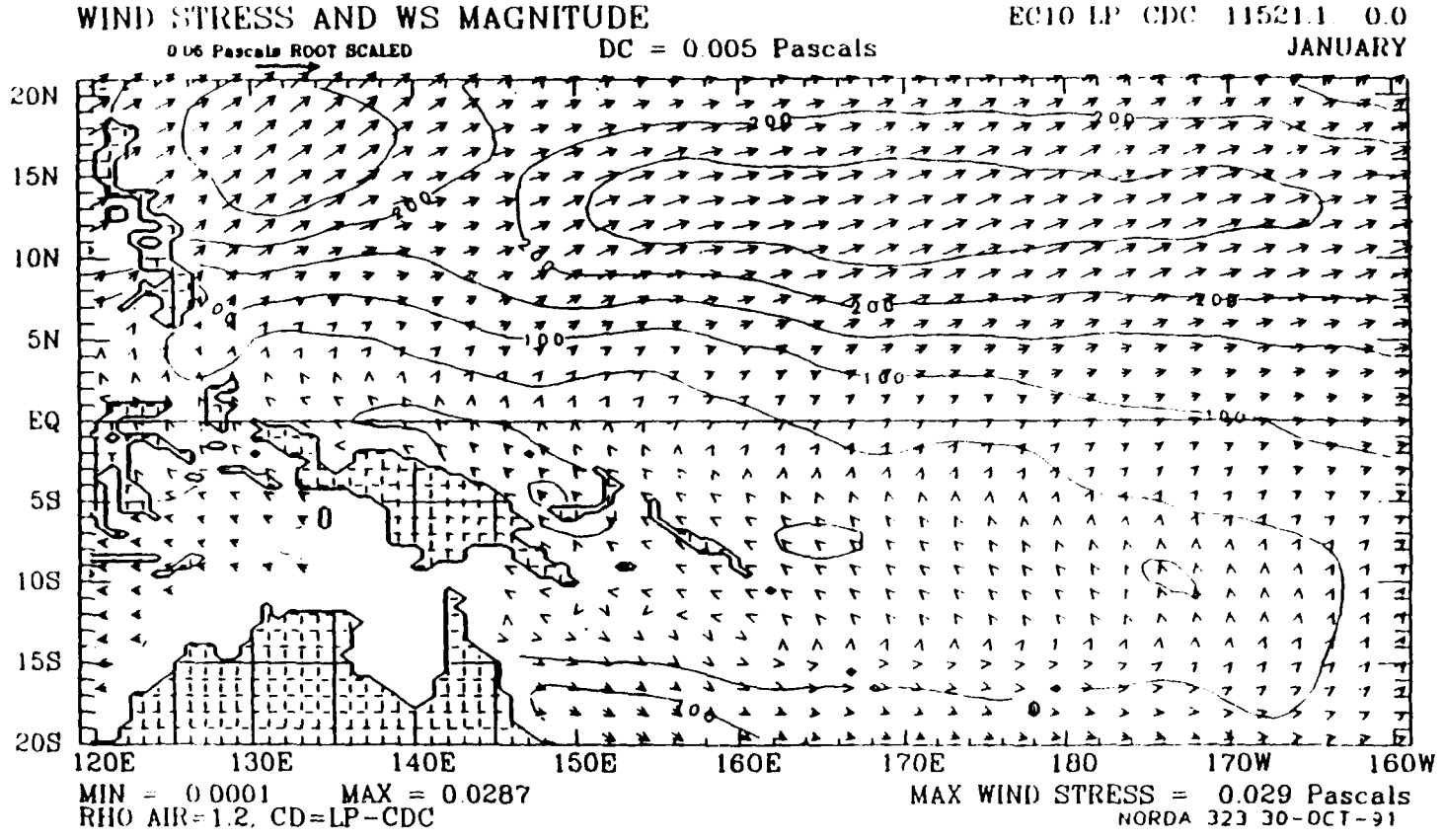

Fig. 18b Same as Fig. 18a but for 10 m height wind stresses using LPCD and LCD.

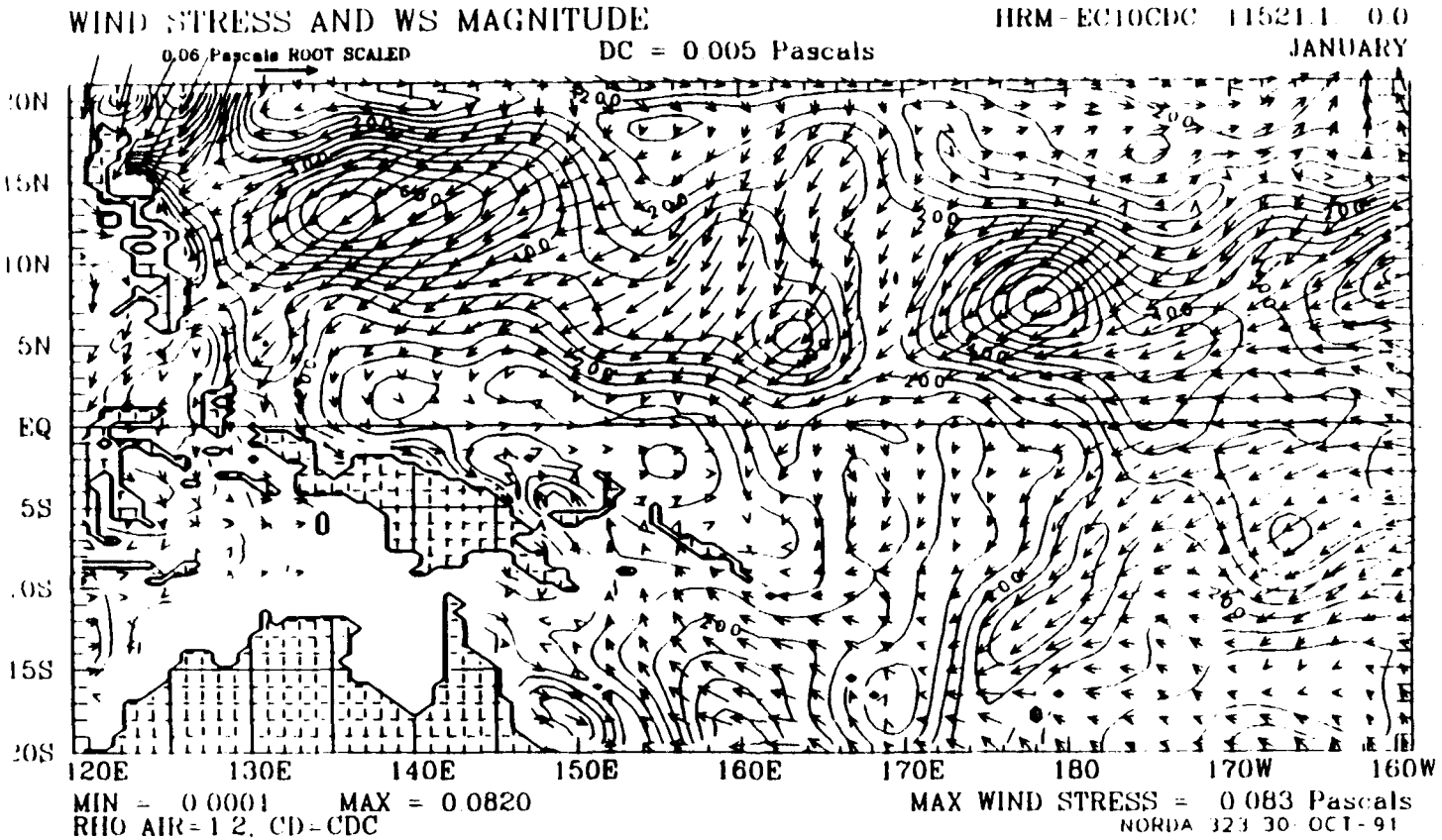

Fig. 18c Same as Fig. 18a but for HR and 10 m height wind stresses. The LCD is used for 10 m height wind stress.

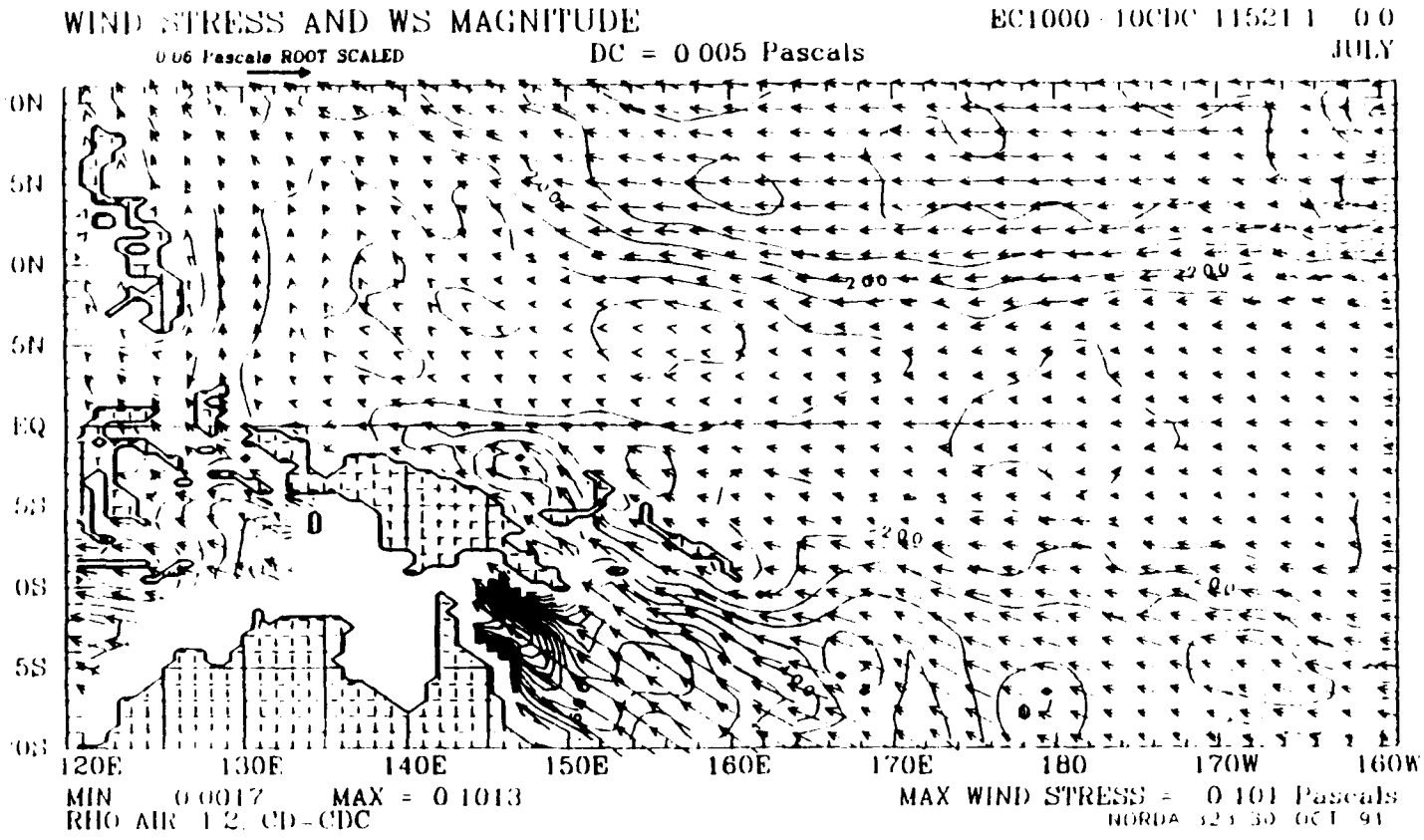

Fig. 19a Differences in the July mean wind stress vectors and magnitudes over WEP between 1000 mb and 10 m height wind stresses. The LCD is used for both wind stresses. The contour interval is 0.05 $dyn\ cm^{-2}$. The arrow at top left corresponds to 0.625 $dyn\ cm^{-2}$.

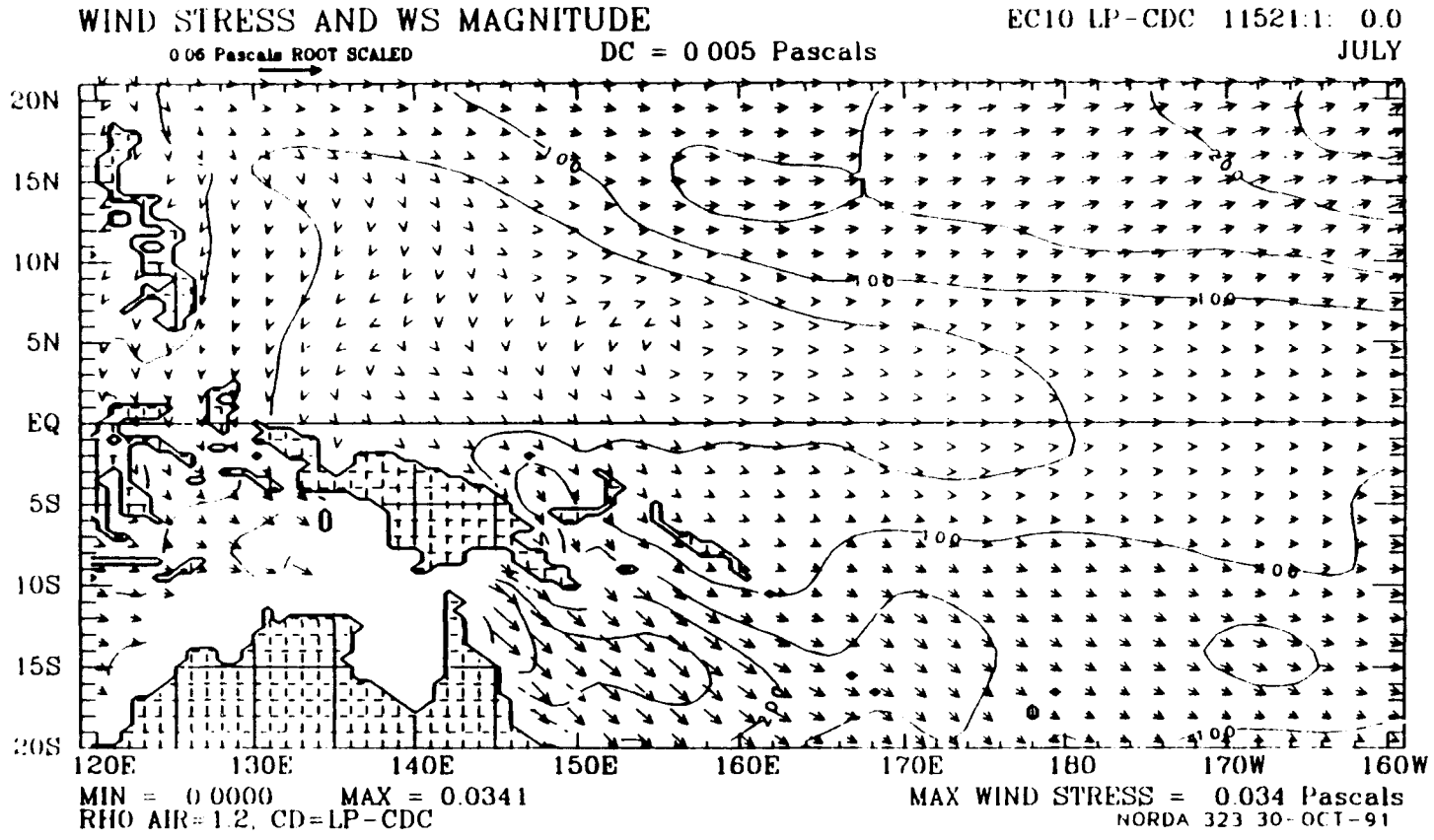

Fig. 19b Same as Fig. 19a but for 10 m height wind stresses using LPCD and LCD.

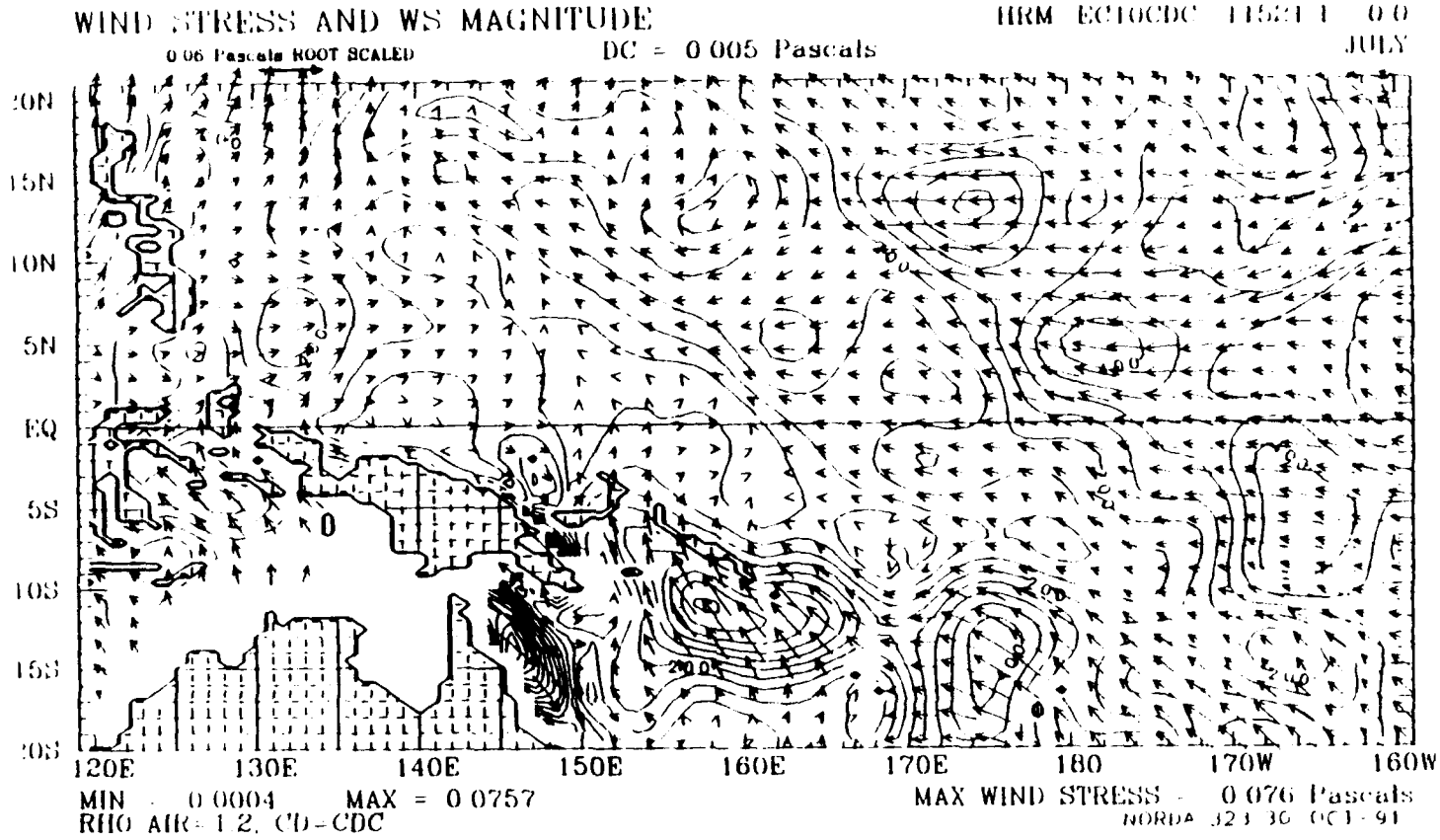

Fig. 19c Same as Fig. 19a but for HR and 10 m height wind stresses. The LCD is used for 10 m height wind stress.

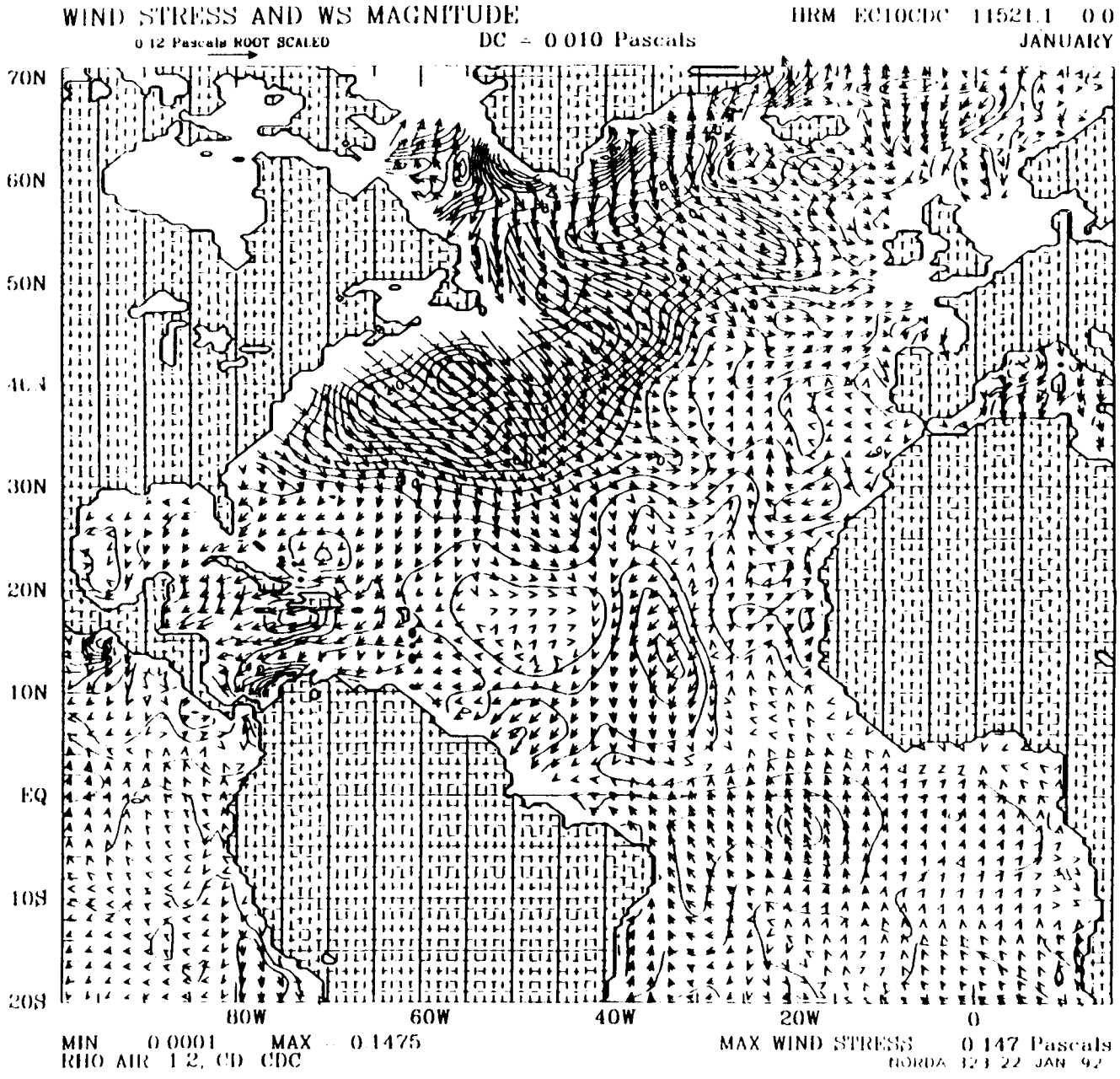

Fig. 20a Differences in the January mean wind stress vectors and magnitudes over NAB between HR and 10 *m* height wind stresses. The LCD is used for 10 *m* height wind stress. The contour interval is 0.1 $dyn\ cm^{-2}$. The arrow at top left corresponds to 1.25 $dyn\ cm^{-2}$.

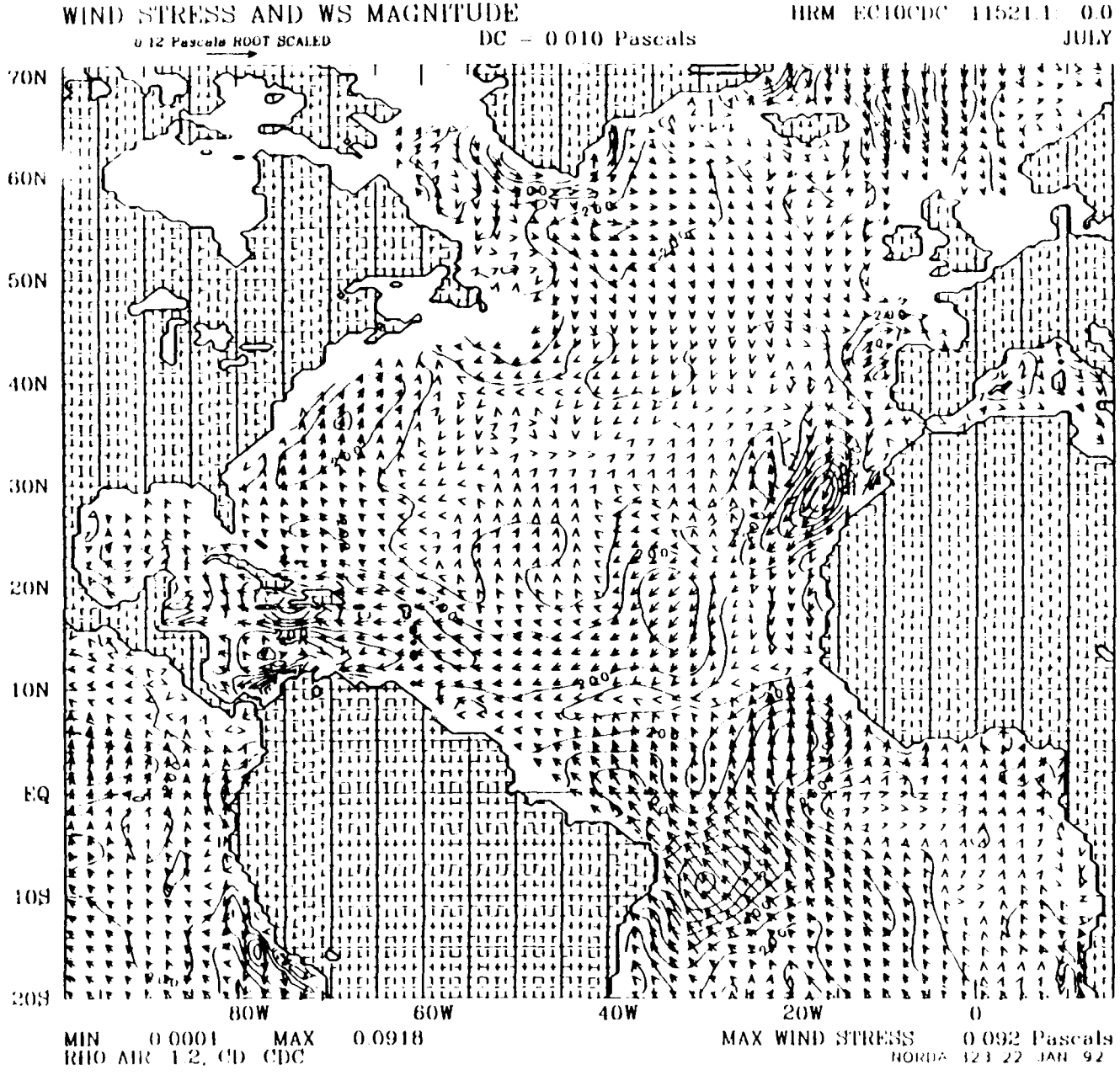

Fig. 20b Same as Fig. 20a but for July.

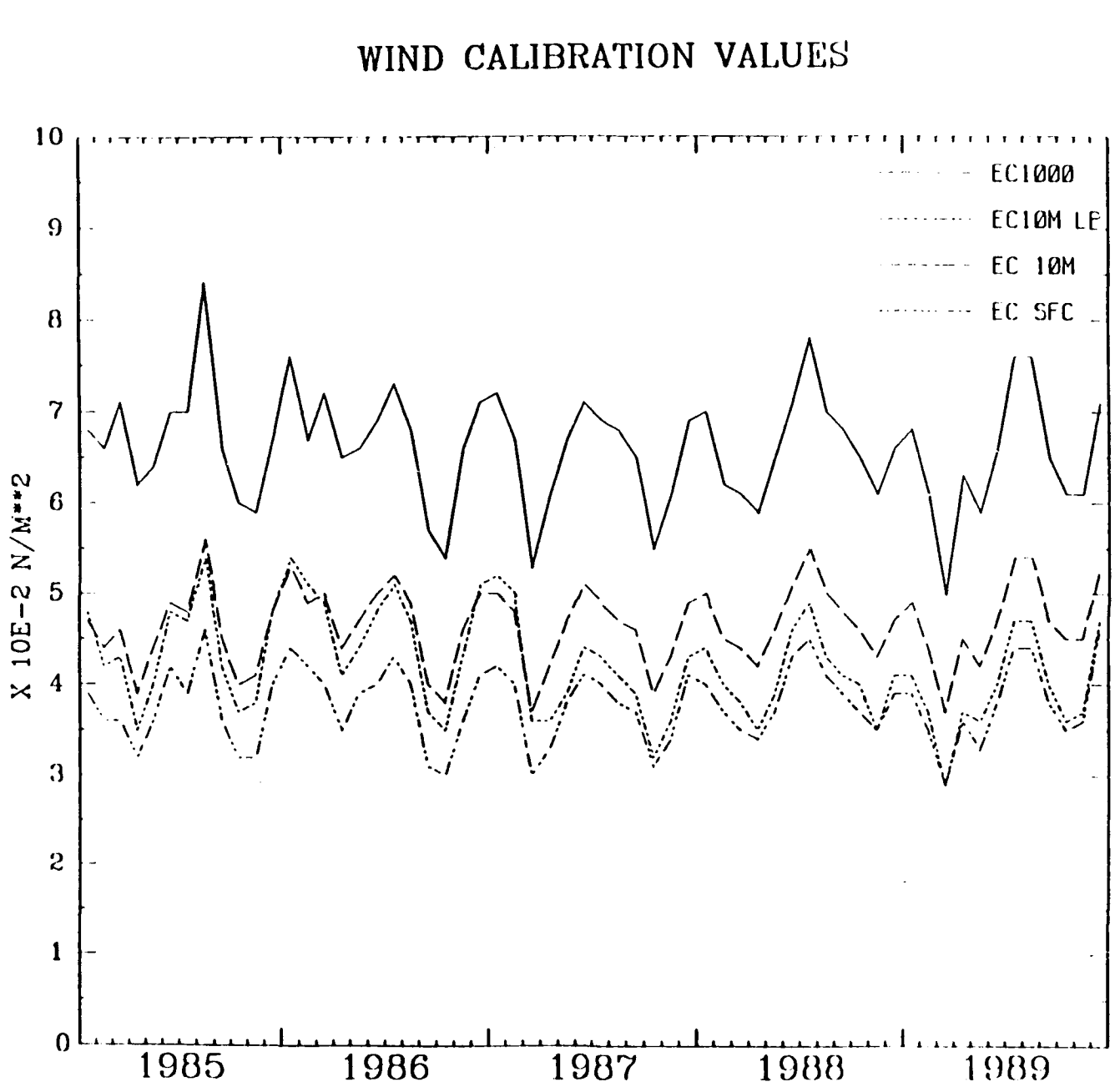

Fig. 21 Monthly mean of global average of wind stresses from 40°*N* to 40°*S* of 1000 *mb*, 10 *m* with LCD and LPCD, and direct surface stress.

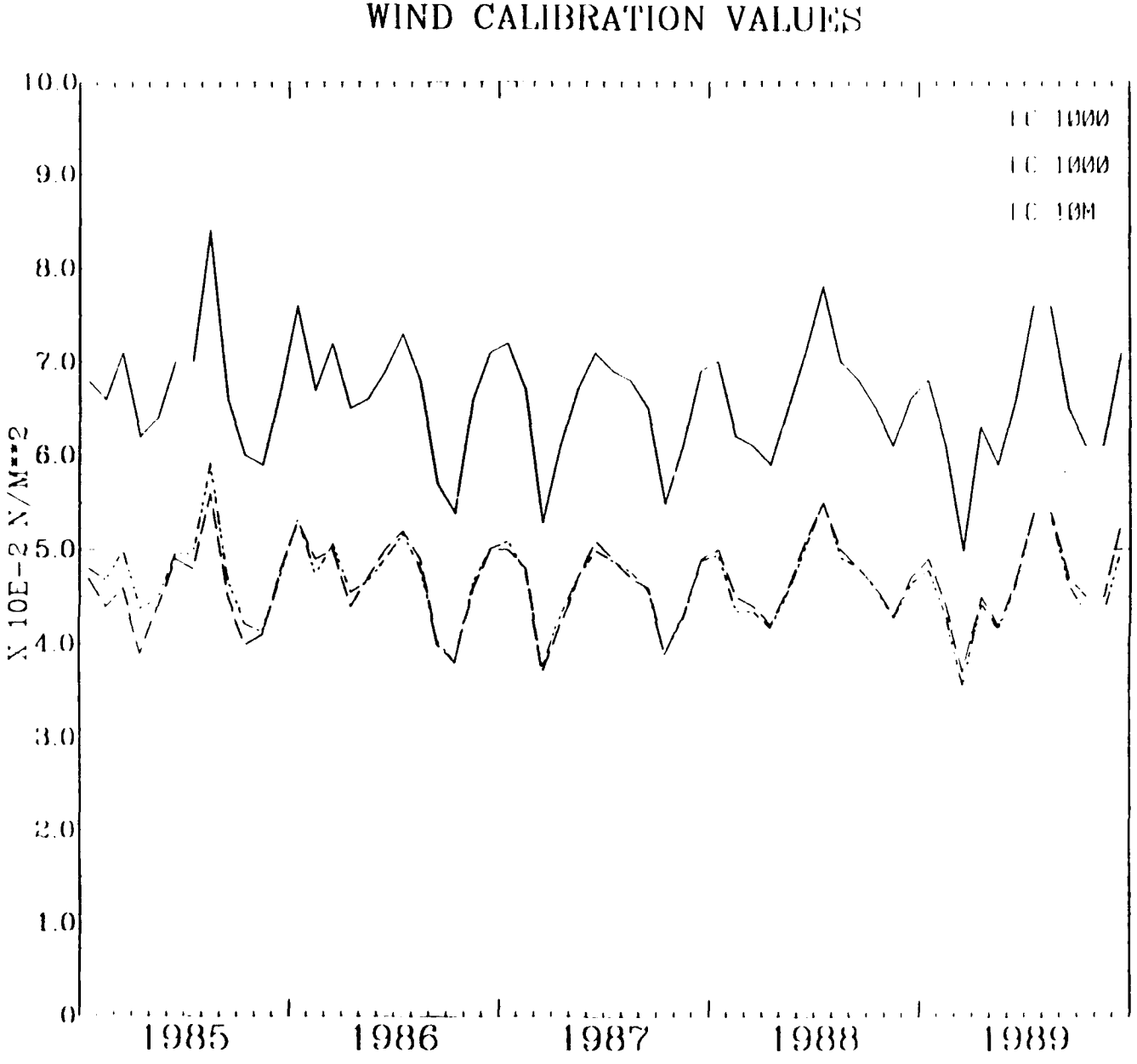

Fig. 22 Wind stress calibration values of 1000 *mb*, 10 *m* height wind with LCD, and a normalized 1000 *mb* with $C_D = 1.06 \times 10^{-3}$.

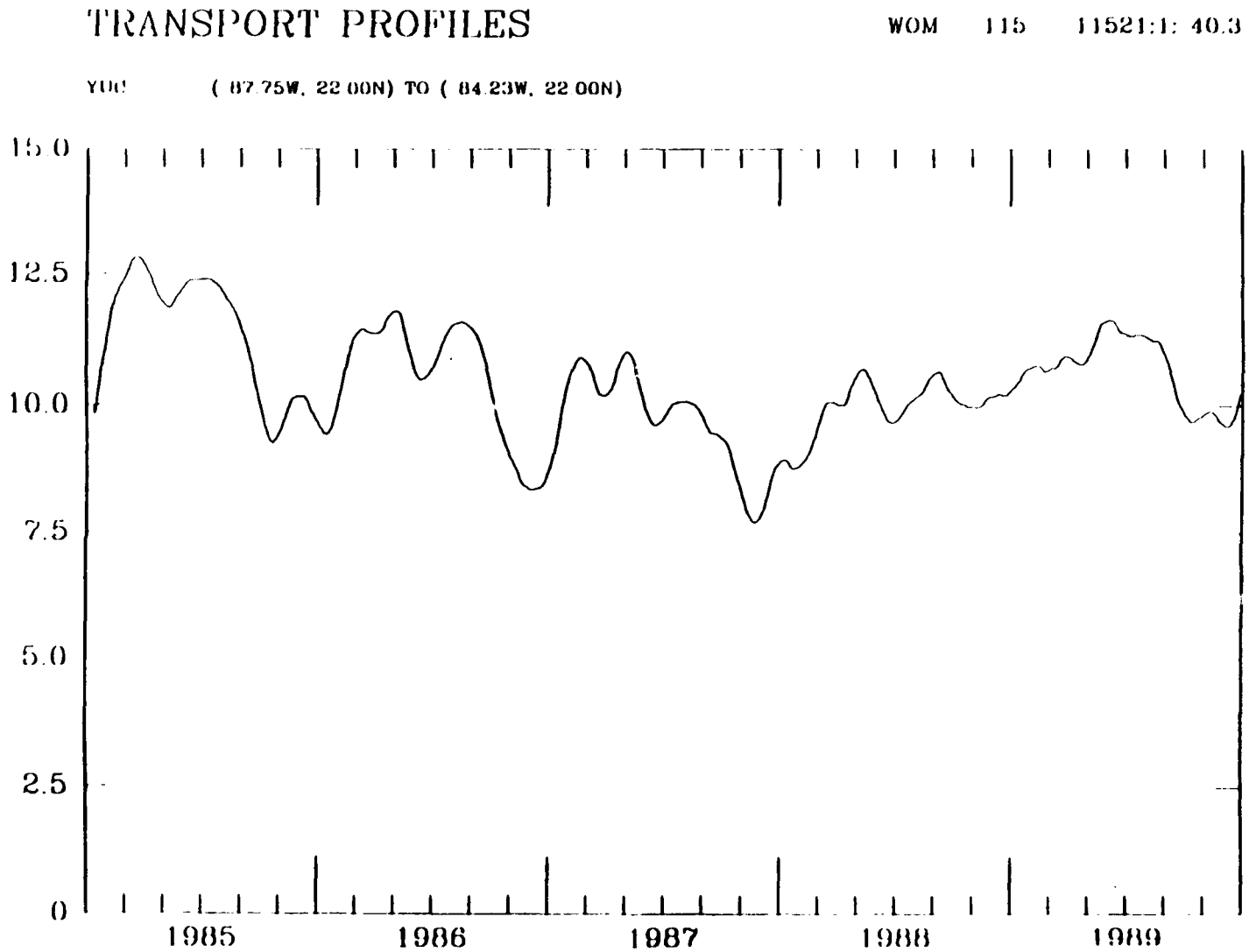

Fig. 23a The model transport variations through the Yucatan Straits from 1985 1989 with the normalized 1000 *mb* wind stress as forcing.

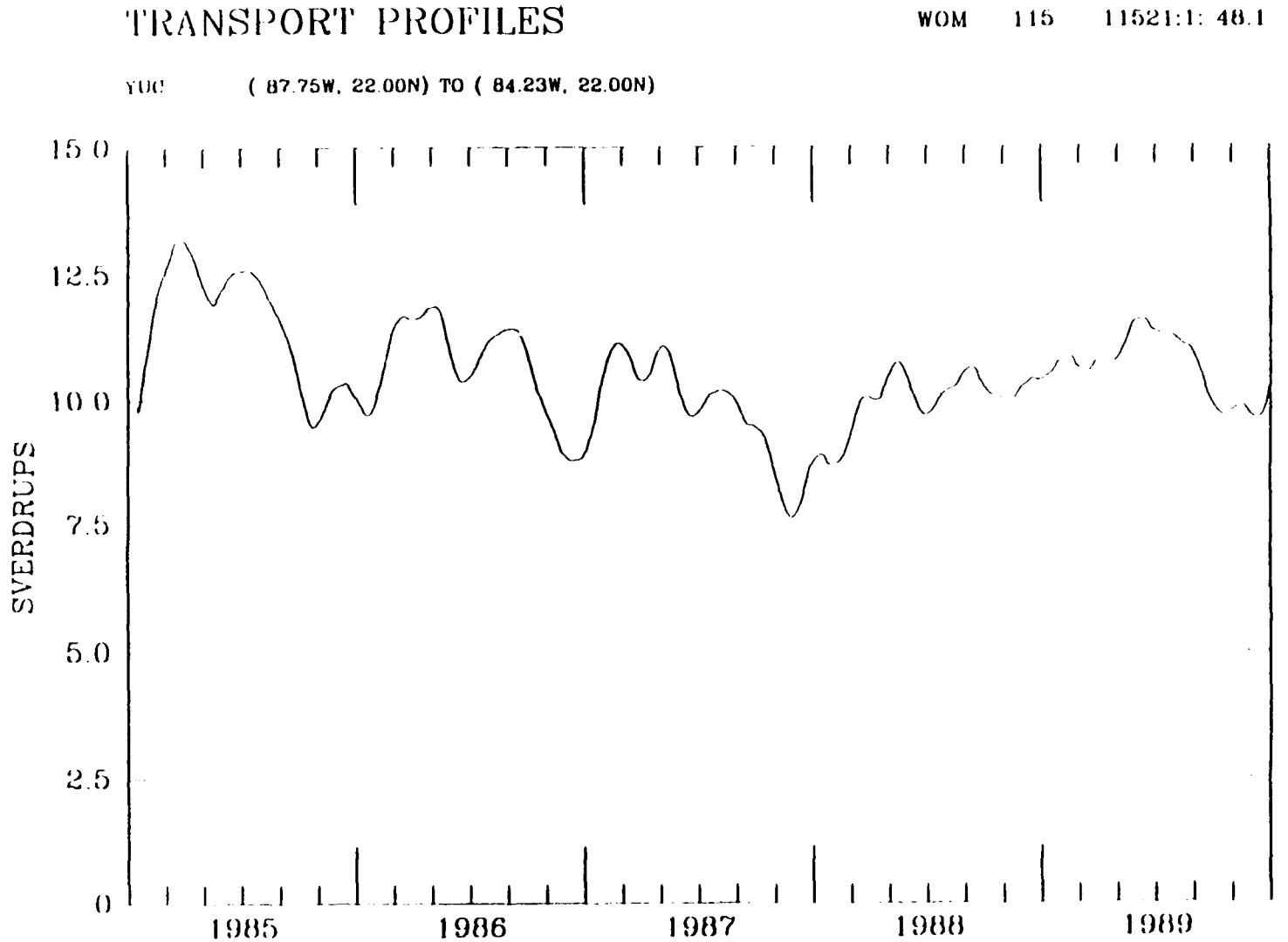

Fig. 23b Same as Fig. 23a but 10 m height wind stress as forcing.

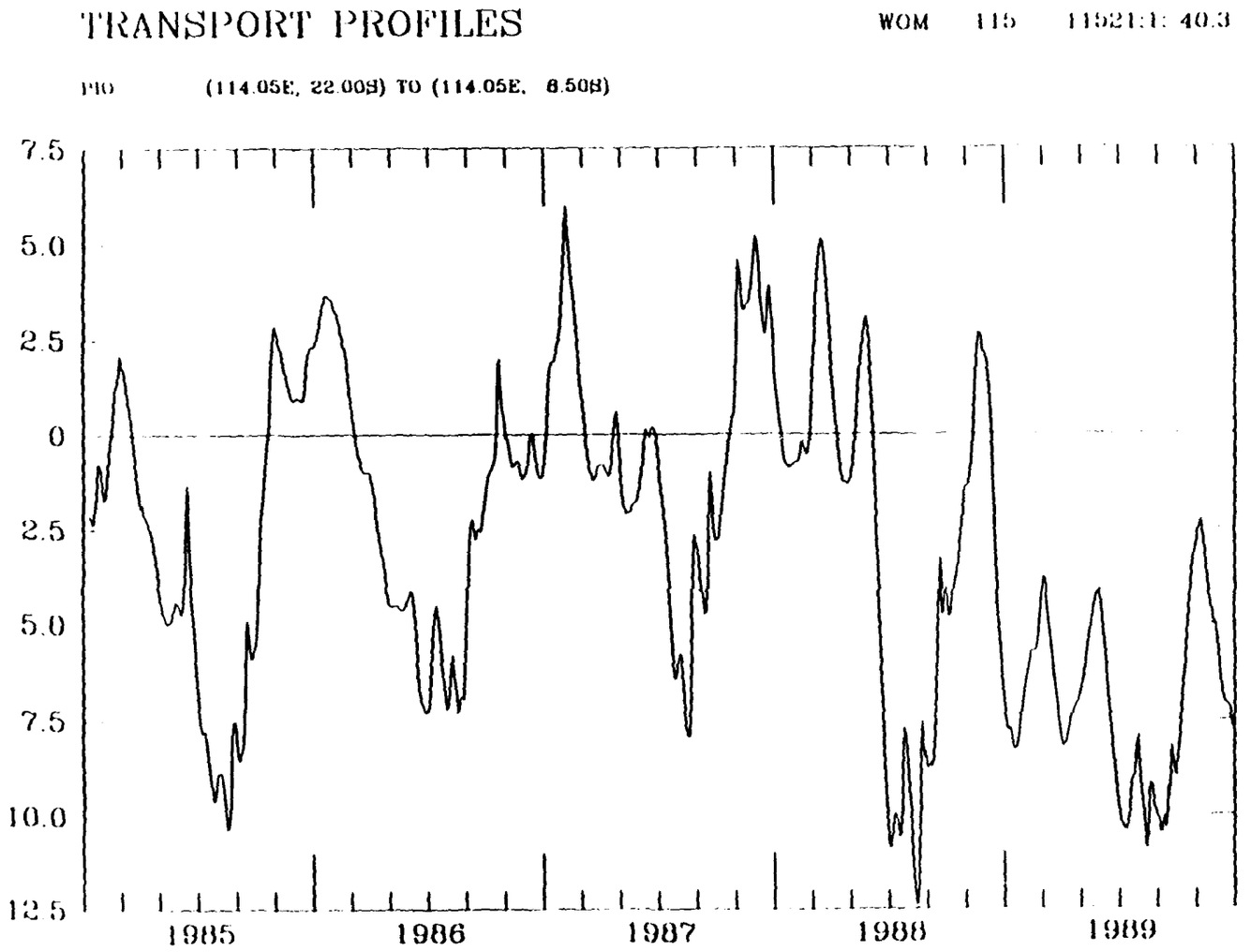

Fig. 24a Same as Fig. 23a but for the model transports between the Pacific and Indian Oceans.

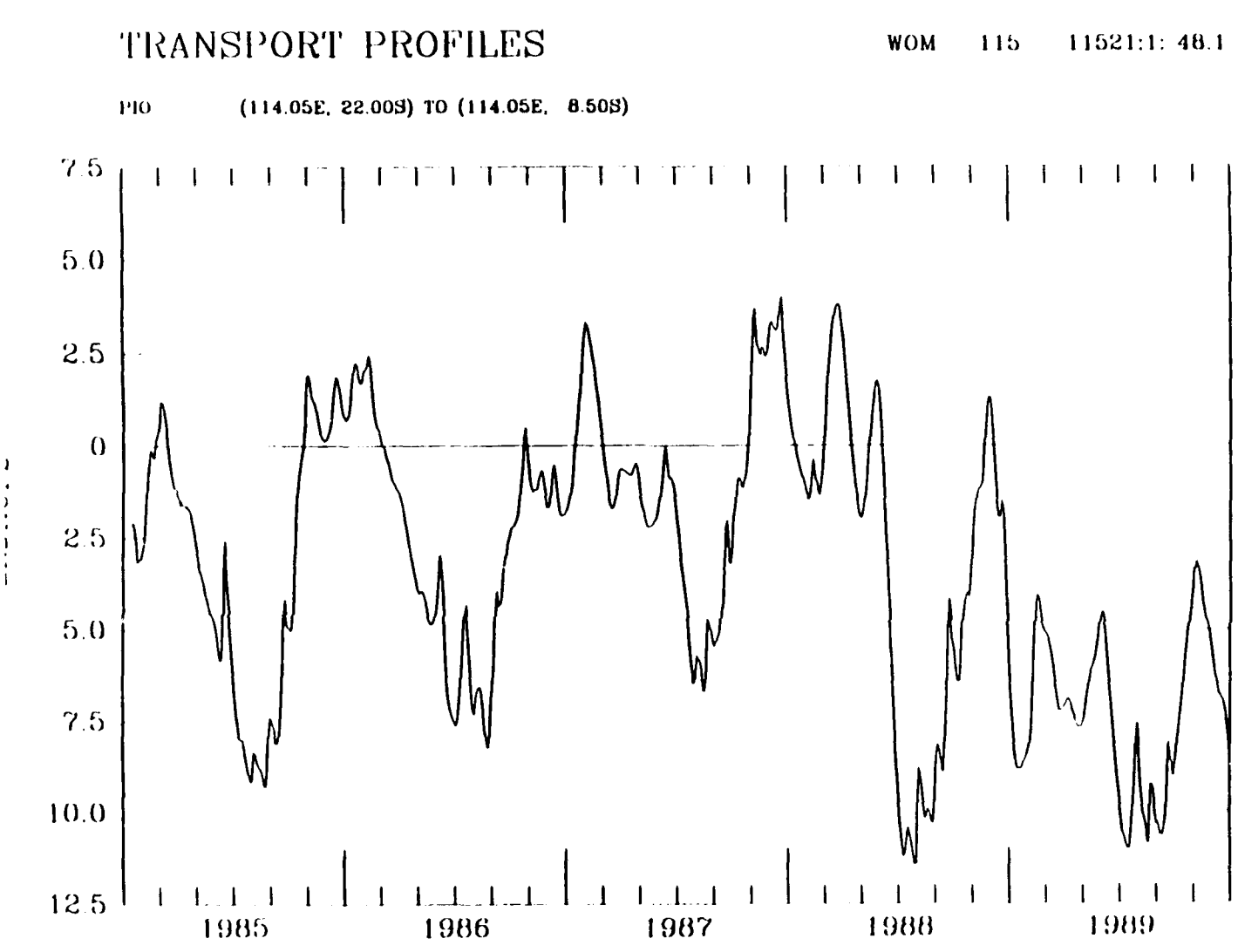

Fig. 24b Same as Fig. 23b but for the model transports between the Pacific and Indian Oceans.

DISTRIBUTION LIST

1. Office of Naval Research
   Code 1242 (10 copies)
   800 North Quincy Street
   Arlington, VA 22217-5000

2. Director, Atmospheric Sciences Directorate
   NRL West (Code 400)
   Monterey, CA 93943-5000

3. Commanding Officer
   Fleet Numerical Oceanography Office
   Monterey, CA 93943-5000

4. Commanding Officer
   Naval Oceanographic Office
   Stennis Space Center, MS 39529

5. Technical Director
   CNOC (Code OOT)
   Stennis Space Center, MS 39529

6. Officer In Charge
   NRL (Code 100)
   Stennis Space Center, MS 39529

7. Technical Director
   NRL (Code 110)
   Stennis Space Center, MS 39529

8. Director, Ocean Sciences Directorate
   NRL (Code 300)
   Stennis Space Center, MS 39529

9. Dr. A. D. Kirwan, Jr.
   College of Sciences
   Dept. of Oceanography
   Old Dominion University
   Norfolk, VA 23529-0276

10. Head, Ocean Sensing and Prediction Division
    NRL (Code 320)
    Stennis Space Center, MS 39529

11. Library (3 copies)
    NRL (Code 125)
    Stennis Space Center, MS 39529

12. Dr. William Holland
    National Center for Atmospheric Research
    P.O. Box 3000
    Boulder, CO 80307

13. UCAR Library
    P.O. Box 3000
    Boulder, CO 80307

14. Dr. Albert W. Green, Jr.
    NRL, Code 330
    Building 1105
    Stennis Space Center, MS 39529

15. Professor George L. Mellor
    Princeton University
    P.O. Box CN710, Sayre Hall
    Princeton, NJ 08544-0710

16. Dr. John R. Apel
    Applied Physics Laboratory
    Johns Hopkins University
    Laurel, MD 20723

17. Dr. J. Dana Thompson
    NRL, Code 320
    Stennis Space Center, MS 39529

18. Dr. William J. Schmitz
Dept. of Physical Oceanography
Woods Hole Oceanographic
Institution
Woods Hole, MA 02543

19. Dr. Edward L. Barker
NRL, Code 440
Monterey, CA 93943-5006

20. Professor Otis B. Brown
Division of Meteorology &
Physical Oceanography
RSMAS, University of Miami
4600 Rickenbacker Causeway
Miami, FL 33149

21. Dr. Richard W. Miksad, Chairman
Dept. of Aerospace Engineering
and Engineering Mechanics
The University of Texas at Austin
Austin, TX 78712-1085

22. Professor Allan R. Robinson
Center for Earth &
Planetary Physics
Harvard University, Pierce Hall
29 Oxford Street, Room 100D
Cambridge, MA 02138

23. Dr. Ron McPherson, Director
National Meteorological Center
World Weather Building
5200 Auth Road
Camp Springs, MD 20746

REPORT DOCUMENTATION PAGE

Form Approved
OMB No. 0704-0188

1. Agency Use Only *(Leave blank).*	2. Report Date.	3. Report Type and Dates Covered.
	AUGUST 1992	TECHNICAL REPORT

4. Title and Subtitle.
Wind Stress Analysis Over the Western Equatorial Pacific and North Atlantic Oceans Based on ECMWF Operational Wind Products 1985-1989

5. Funding Numbers.
Program Element No. 61153N
Project No. R310300
Task No. 801
Accession No. DN250022

6. Author(s).
LE NGOC LY, JOHN C. KINDLE, J. DANA THOMPSON, AND WESLEY J. YOUTSEY

7. Performing Organization Name(s) and Address(es).
INSTITUTE FOR NAVAL OCEANOGRAPHY, BUILDING 1103, ROOM 233, STENNIS SPACE CENTER, MS 39529

8. Performing Organization Report Number.
TR-3

9. Sponsoring/Monitoring Agency Name(s) and Address(es).
NAVAL RESEARCH LABORATORY
STENNIS SPACE CENTER, MS 39529

10. Sponsoring/Monitoring Agency Report Number.

11. Supplementary Notes.

12a. Distribution/Availability Statement.
Approved for public release; distribution is unlimited.
Institute for Naval Oceanography, Stennis Space Center, MS 39529

12b. Distribution Code.

13. Abstract *(Maximum 200 words).*

The mean annual and monthly mean wind stress and wind stress curl over the ocean have been computed for 1985-1989 from European Centre for Medium-Range Weather Forecasting (ECMWF) 12-hourly operational 1000 mb, 10 m winds, and direct surface stresses. Both linear and non-linear drag coefficient formulations were employed. The analyses focused on wind stress and curl fields over the Western Equatorial Pacific and the North Atlantic Basin. The wind stress and curl fields of the various ECMWF and Hellerman and Rosenstein wind products are compared.

14. Subject Terms.
(U) INO (U) NAOPS (U) SPEM (U) PRINCETON (U) NOGUFS (U) MODEL (U) PREDICTION (U) HARVARD (U) DART

15. Number of Pages.
117

16. Price Code.

17. Security Classification of Report.	18. Security Classification of This Page.	19. Security Classification of Abstract.	20. Limitation of Abstract.
UNCLASSIFIED	UNCLASSIFIED	UNCLASSIFIED	SAR